

Московский институт электронной техники (МИЭТ)

На правах рукописи

УДК 519.6

Mikhail Evgenievich Lebedev

**Stationary Solutions of Gross–Pitaevskii Equation
with Periodically Modulated Nonlinearity**

05.13.18 – Математическое моделирование, численные методы и комплексы
программ

ДИССЕРТАЦИЯ
на соискание ученой степени
кандидата физико-математических наук

Научный руководитель
д. ф.-м. н., проф.
G. L. Alfimov

Moscow – 2021

Contents

Introduction	4
Chapter 1. General Propositions on Regular and Singular Solutions for Stationary States Equation $u_{xx} + Q(x)u + P(x)u^3 = 0$	5
1.1. Objectives	5
1.2. Absence of the Singular Solutions: $P(x) \geq P_0 > 0$	6
1.3. Asymptotic Behaviour at a Collapse Point: $P(x_0) < 0$	8
1.4. All Solutions Are Singular: $P(x) \leq P_0 < 0, Q(x) \leq Q_0 < 0$	12
1.5. Summary	14
Chapter 2. Stationary States Classification Within Symbolic Dynamics Framework	16
2.1. Objectives	16
2.2. Geometry of the Poincaré Map	17
2.3. Poincaré Map Domains for Piecewise Periodic Pseudopotential	25
2.4. Symbolic Dynamics: Coding of Solutions	39
2.5. Summary	51
Chapter 3. Localized Solutions of Gross-Pitaevskii Equation with Periodic Pseudopotential	53
3.1. Objectives	53
3.2. Coding of Solutions	54
3.3. Analysis of Stability	61
3.4. Summary	67
Chapter 4.	69
Appendix A. Lemma on Bounded Solutions	70

Appendix B. Solutions of Duffing equations	74
Appendix C. Strips Mapping Theorems	75
Bibliography	84

Itroduction

One dimensional Gross–Pitaevskii equation (describes “cigar-shaped” condensate) takes form:

$$i\Psi_t + \Psi_{xx} + U(x)\Psi + P(x)|\Psi|^2\Psi = 0. \quad (1)$$

Here $\Psi(t, x)$ is the macroscopic wave function of the condensate, $U(x)$ corresponds to the potential of the trap holding the condensate, and $P(x)$ describes characteristic length of the atomic interactions. Function $P(x)$ is called as *pseudopotential* which is induced by spatial periodic modulation. This can be achieved in BEC by means of the Feshbach resonance controlled by magnetic or optical field [1–3]. In the nonlinear optics spatial modulation of the Kerr coefficient can be induced by inhomogeneous density of resonant nonlinearity-enhancing dopants implanted into the waveguide [4].

...

Chapter 1

General Propositions on Regular and Singular Solutions for Stationary States Equation

$$u_{xx} + Q(x)u + P(x)u^3 = 0$$

1.1. Objectives

In this chapter our main goal is to formulate general propositions about singular and regular solutions for the general form of the stationary states equation.

$$u_{xx} + Q(x)u + P(x)u^3 = 0. \quad (1.1)$$

As it was shown previously this equation follows from the original Gross–Pitaevskii equation by the the substitution

$$\Psi(t, x) = u(x)e^{-i\omega t}, \quad (1.2)$$

where the corresponding localization conditions allow us to consider $u(x)$ as a real-valued function.

We suppose that functions $Q(x), P(x) \in C^1(\mathbb{R})$ and will put additional restrictions further when it's needed. Mainly we are interested in two main cases: (A) when do exist regular solutions; and (B) what are the conditions on function $Q(x)$ and $P(x)$ which can guarantee the existence of the singular solutions for the equation (2.1), and what is the behaviour of the collapsing solutions near the collapse point. In this chapter partial answer to question (A) is given by the Propositions 1 and 2. On the other hand Proposition 3 gives a partial answer to the question (B). It states that if the function $P(x)$ less then zero at least at one point $x = x_0$ then there exist two one-parametric families of solutions collapsing at x_0 .

1.2. Absence of the Singular Solutions: $P(x) \geq P_0 > 0$

This section contains a sufficient condition for absence of singular solutions of the equation (2.1). It's given by the following proposition.

Proposition 1. *Let $\forall x$ functions $Q(x), P(x) \in C^1(\mathbb{R})$, moreover:*

$$(a) \quad P(x) \geq P_0 > 0, |P'(x)| \leq \tilde{P};$$

$$(b) \quad Q(x) \geq Q_0, |Q'(x)| \leq \tilde{Q};$$

then solution of the Cauchy problem for the equation (2.1) with arbitrary initial conditions $u(x_0) = u_0, u_x(x_0) = u'_0$ can be continued to the whole real axis \mathbb{R} .

Proof. By the existence and uniqueness theorem for ODE there exists an interval $[x_0; x_1)$ such that a solution of the Cauchy problem $u(x)$ for the equation (2.1) with initial conditions $u(x_0) = u_0, u_x(x_0) = u'_0$ exists and is unique on the interval, $u(x) \in C^2[x_0; x_1)$. Suppose that $[x_0; x_1)$ is the maximum interval of existence for the the solution $u(x)$. It means that solution of the Cauchy problem $u(x)$ cannot be continued beyond the point x_1 . Multiply the original equation by $4u_x(x)$ and then integrate it over $[x_0, x)$, $x < x_1$, we have the following relationship:

$$\begin{aligned} 2u_x^2(x)) + 2Q(x)u^2(x) - 2 \int_{x_0}^x Q'(\xi)u^2(\xi)d\xi + P(x)u^4(x) - \int_{x_0}^x P'(\xi)u^4(\xi)d\xi = \\ = 2(u'_0)^2 + 2Q(x_0)u_0^2 + P(x_0)u_0^4 \equiv C. \end{aligned} \tag{1.3}$$

We can omit term $u_x^2(x) \geq 0$ in the left-hand side of the equality, and take into account the lower limits for $Q(x), P(x)$ functions, so we come to the following inequality:

$$2Q_0u^2(x) + P_0u^4(x) \leq C + 2 \int_{x_0}^x Q'(\xi)u^2(\xi)d\xi + \int_{x_0}^x P'(\xi)u^4(\xi)d\xi. \tag{1.4}$$

Further we can replace the derivatives $Q'(\xi)$ and $P'(\xi)$ with their upper bounds: $Q'(\xi) \leq \tilde{Q}, P'(\xi) \leq \tilde{P}$, where $\tilde{Q} \geq 0, \tilde{P} \geq 0$. With multiplying both sides of the

inequality by P_0 , we have

$$2Q_0P_0u^2(x) + P_0^2u^4(x) \leq P_0C + 2P_0\tilde{Q} \int_{x_0}^x u^2(\xi)d\xi + P_0\tilde{P} \int_{x_0}^x u^4(\xi)d\xi. \quad (1.5)$$

Let $v(x) = (P_0u^2(x) + Q_0)^2$, $v(x) \geq 0$, substituting this into (1.5) gives

$$v(x) \leq \tilde{C} + \frac{\tilde{P}}{P_0} \int_{x_0}^x w(v(\xi))d\xi. \quad (1.6)$$

Here $\tilde{C} = P_0C + Q_0^2 \geq 0$, $\alpha = 2\tilde{Q}P_0/\tilde{P} \geq 0$, and $w(v)$ is defined by

$$w(v) \equiv \alpha(\sqrt{v} - Q_0) + (\sqrt{v} - Q_0)^2. \quad (1.7)$$

Consider the following function

$$G(s) = \int_{s_0}^s \frac{dv}{w(v)}. \quad (1.8)$$

Here $s_0 > Q_0^2$ is an arbitrary constant, $s \geq s_0$. Since $w(v)$ is a positive and monotonically decreasing function, and the integral

$$\int_{s_0}^{+\infty} \frac{dv}{w(v)} \quad (1.9)$$

diverges, one can conclude that $G(s)$ is a positive, monotonically increasing, and unbounded function. It means that an inverse function $G^{-1}(r)$ is well-defined for $r \geq 0$, increases monotonically, and is unbounded. The above-mentioned statements allow as to apply *Bihary* inequality [5, theorem 2.3.1] to (1.6) which allows us to conclude that:

$$v(x) \leq G^{-1} \left(G(\tilde{C}) + \frac{\tilde{P}}{P_0} \int_{x_0}^x d\xi \right) = G^{-1} \left(G(\tilde{C}) \frac{\tilde{P}}{P_0} (x - x_0) \right) < \infty. \quad (1.10)$$

Inequality (1.10) is valid for all $x \in [x_0; x_1]$. It follows from (1.10) that function $v(x)$ is bounded on the whole segment $[x_0; x_1]$:

$$v(x) \leq M = G^{-1} \left(G(\tilde{C}) + \frac{\tilde{P}}{P_0} (x_1 - x_0) \right). \quad (1.11)$$

We observe that $\tilde{C} \geq Q_0^2$, moreover $\tilde{C} = Q_0^2$ only if $u_0 = u'_0 = 0$. It means that $G(s)$ is well-defined for each constant \tilde{C} corresponding to any non-zero solution $u(x)$. The boundedness of $v(x)$ yields that solution $u(x)$ is also bounded on the segment $[x_0; x_1]$:

$$|u(x)| \leq \sqrt{\frac{\sqrt{M} - Q_0}{P_0}}, \quad x \in [x_0; x_1]. \quad (1.12)$$

Substitution of the estimate (1.12) into the identity (1.3) gives the upper bound for the derivative $u_x(x)$ on the interval $x \in [x_0; x_1]$. Since functions $u(x)$ and $u_x(x)$ are continuous and bounded on $[x_0; x_1]$, the values $u(x_1) = u_1$ and $u_x(x_1) = u'_1$ are finite. Hence there exists a continuation of the solution to the Cauchy problem with the initial conditions $u(x_0) = u_0$, $u_x(x_0) = u'_0$ on a larger interval beyond the initial $[x_0; x_1]$. It contradicts to the original assumption.

Thus we have proven the possibility of continuation of the solution to the half-line $x > x_0$. In order to prove the same statement for $x < x_0$, one can make a substitution $x \rightarrow -x$ and repeat the above-mentioned proof. \square

One trivial corollary simply follows from this proposition.

Corollary 1. *If the conditions (a) and (b) are satisfied not on the whole real axis \mathbb{R} , but only on some segment $[x_1; x_2]$, then a solution of the Cauchy problem for the equation (2.1) with arbitrary initial conditions does not collapse at any point of the segment $[x_1; x_2]$.*

1.3. Asymptotic Behaviour at a Collapse Point: $P(x_0) < 0$

1.3.1. Asymptotic Expansions

If $P(x)$ is negative at least at one point $x_0 \in \mathbb{R}$, formal asymptotic expansions predict existence of two one-parametric families of the solutions for the equation (2.1) collapsing at this point.

Let us construct these asymptotic expansions. We suppose that $P(x_0) = -1$ (this condition can be achieved by a simple renormalisation of the independent

variable), denote by $\eta = x - x_0$, and assume that in the vicinity of the point $x = x_0$, the following expansions are valid:

$$Q(x) = Q_0 + Q_1\eta + Q_2\eta^2 \dots, \quad P(x) = -1 + P_1\eta + P_2\eta^2 + \dots \quad (1.13)$$

Substituting these expansions into (2.1), we have

$$u_{\eta\eta} + (Q_0 + Q_1\eta + Q_2\eta^2 \dots)u + (-1 + P_1\eta + P_2\eta^2 + \dots)u^3 = 0. \quad (1.14)$$

If a solution of the equation (1.14) collapses at the point $x = x_0$ then it satisfies the following condition, $u(\eta) \rightarrow \pm\infty$, when $\eta \rightarrow 0$. Let η approaches to zero *from the right*, $\eta > 0$. We make the following variable changes $v(\eta) = \eta u(\eta)$, $\eta = e^{-t}$. It gives

$$v_{tt} + 3v_t + 2v + e^{-2t}Q(t)v + P(t)v^3 = 0. \quad (1.15)$$

Let's determine the main term of the expansion by balancing $2v$ and $-v^3$ terms, we have

$$V_0(t) = \pm\sqrt{2}. \quad (1.16)$$

Now let's define the first order term $V_1(t)$, $v(t) = \pm\sqrt{2} + V_1(t) + o(V_1(t))$. Substituting the last expression into the (1.15), considering expansion for the functions $Q(t)$, $P(t)$, and omitting the terms of order higher than e^{-t} , we obtain

$$V_{1,tt} + 3V_{1,t} - 4V_1 = \mp 2\sqrt{2}e^{-t}, \quad (1.17)$$

that gives $V_1(t) = \pm\frac{\sqrt{2}}{3}e^{-t}$. Second, third, and forth order terms V_n , $n = 2, 3, 4$, can be found in a similar manner. For each term the corresponding equation takes form:

$$V_{n,tt} + 3V_{n,t} - 4V_n = C_n e^{-nt}. \quad (1.18)$$

However, for $n = 2, 3$ solutions of the equation (1.18) are of the form $V_n \sim e^{-nt}$, but in the case $n = 4$, the exponent term in the right hand side coincides with one of the roots of the characteristic polynomial for the differential operator in the left-hand side. In this case solution of the equation (1.18) must be chosen in the

form $Ce^{-4t} - A_3te^{-4t}$. Here C is an arbitrary constant, while A_3 can be determined uniquely from the coefficients of the series expansions for $Q(t)$, $P(t)$. If constant C is fixed, at the further steps of this procedure the corresponding equations are uniquely solvable. One can note that the replacement of $+$ to $-$ in the expression (1.16) leads to the corresponding replacement of the signs for all coefficients A_n , $n = 0, 1, \dots$, that is natural due to the invariance of the equation (2.1) with regard to the change $u \rightarrow -u$. We have

$$\pm v(t) = \sqrt{2} + A_0 e^{-t} + A_1 e^{-2t} + A_2 e^{-3t} + A_3 \cdot (-t) \cdot e^{-4t} + C e^{-4t} + \dots \quad (1.19)$$

Explicit expressions for the A_0, \dots, A_3 are:

$$A_0 = \frac{\sqrt{2}}{3} P_1; \quad (1.20)$$

$$A_1 = \frac{\sqrt{2}}{3} P_2 + \frac{\sqrt{2}}{6} Q_0 + \frac{2\sqrt{2}}{9} P_1^2; \quad (1.21)$$

$$A_2 = \frac{2\sqrt{2}}{3} P_2 P_1 + \frac{7\sqrt{2}}{27} P_1^3 + \frac{\sqrt{2}}{6} Q_0 P_1 + \frac{\sqrt{2}}{4} Q_1 + \frac{\sqrt{2}}{2} P_3; \quad (1.22)$$

$$A_3 = -\frac{\sqrt{2}}{6} Q_1 P_1 - \frac{\sqrt{2}}{5} Q_2 - \frac{32\sqrt{2}}{45} P_2 P_1^2 - \frac{3\sqrt{2}}{5} P_3 P_1 - \quad (1.23)$$

$$-\frac{2\sqrt{2}}{15} P_2 Q_0 - \frac{2\sqrt{2}}{15} Q_0 P_1^2 - \frac{2\sqrt{2}}{5} P_4 - \frac{28\sqrt{2}}{135} P_1^4 - \frac{4\sqrt{2}}{15} P_2^2. \quad (1.24)$$

In the other case when $\eta \rightarrow 0$ *from the left*, $\eta < 0$, to construct similar expansions one should make the variable changes $v(\eta) = \eta u(\eta)$, $\eta = -e^{-t}$. Expressions for the coefficient A_n remain the same as for $\eta > 0$.

Finally we get an asymptotic expansion for the original solution $u(x)$ for $x \rightarrow x_0 \pm 0$:

$$\pm u(x) = \frac{\sqrt{2}}{\eta} + A_0 + A_1 \eta + A_2 \eta^2 + A_3 \eta^3 \ln |\eta| + C \eta^3 + A_4 \eta^4 \ln |\eta| + \dots \quad (1.25)$$

here $\eta = x - x_0$, A_0, \dots, A_3 are determined by the equations (1.20)-(1.24), and all other coefficients A_n , $n > 3$ can be expressed with Q_n , P_n and arbitrary constant C .

Summarizing all above mentioned, one can say that asymptotic expansion (1.25) *predicts the existence* of two one-parametric families of solutions collapsing

at the point x_0 . These families are connected by the symmetry $u \rightarrow -u$. When $x \rightarrow x_0$, the solutions from one of these families tends to $+\infty$, while solutions from another family tends to $-\infty$ correspondingly.

1.3.2. Existence of One-Parametric Families of Collapsing Solutions

The possibility of constructing asymptotic expansions (1.25) itself does not prove the existence of one-parametric families of solutions collapsing at point x_0 . But at the same time, the following rigorous statement is true.

Proposition 2. *Let Ω be a neighbourhood of the point x_0 , $Q(x) \in C^3(\Omega)$ and $P(x) \in C^4(\Omega)$, then there exist two C^1 -smooth one-parametric families of solutions for the equation (2.1) corresponding to the expansions (1.25), collapsing at the point $x = x_0$ (while approaching from the left, $x < x_0$), and connected by a symmetry $u \rightarrow -u$. Each of these families can be parametrized by a free variable $C \in \mathbb{R}$ from the expansions (1.25).*

Proof. By the initial statement the following expansions are valid:

$$Q(x) = Q_0 + Q_1\eta + Q_2\eta^2 + \tilde{Q}(\eta)\eta^3; \quad (1.26)$$

$$P(x) = -1 + P_1\eta + P_2\eta^2 + P_3\eta^3 + P_4\eta^4 + \tilde{P}(\eta)\eta^5. \quad (1.27)$$

Here $\eta = x - x_0$, and $\tilde{Q}, \tilde{P} \in C(\Omega)$. To prove existence of the family that corresponds to the $+$ sign in (1.25) we make a variable change:

$$u(x) = \frac{\sqrt{2}}{\eta} + A_0 + A_1\eta + A_2\eta^2 + A_3\eta^3 \ln(-\eta) + z(\eta)\eta^3, \quad (1.28)$$

where $z(\eta)$ is a new unknown function. Coefficients A_0, \dots, A_3 are chosen accordingly to the expressions (1.20)-(1.24), so the coefficients at the terms η^{-2} , η^{-1} , η^0 , and η are vanish. It's easy to check that direct substitution of the (1.28) into (2.1) shows that for such choice of A_0, \dots, A_3 the following equation for z takes place:

$$z_{\eta\eta} + \frac{6}{\eta}z_\eta + g(\eta, z) = 0, \quad (1.29)$$

where $g(\eta, z)$ is a third order polynomial with respect to z , and $g(\eta, z) \sim \frac{\ln(-\eta)}{\eta}$ when $\eta \rightarrow -0$ and z is fixed. Variable change $\eta = -e^{-t}$ map the point $\eta = 0$ into $t = +\infty$, and turn equation (1.29) into

$$z_{tt} - 5z_t - f(t, z) = 0. \quad (1.30)$$

Here $f(t, z) \sim te^{-t}$ while $t \rightarrow +\infty$. Properties of the function $f(t, z)$ allows us to apply *Lemma on Bounded Solutions* from Appendix A to the equation (1.30). This lemma states that for $t \rightarrow +\infty$ all bounded solutions of the equation (1.30) tend to some constant C when $t \rightarrow +\infty$, moreover for each $C \in \mathbb{R}$ there exists unique solution that approaches to that constant asymptotically while $t \rightarrow +\infty$. Furthermore these solutions form a C^1 -smooth family. Finally we can move to the previous equation (1.29), and then to the (2.1) to get the initial statement of the proposition. The existence of the second family of solutions corresponding to the sign “−” in (1.25) follows from the invariance of equation (2.1) under the replacement $u \rightarrow -u$. \square

Similar one-parametric families of collapsing solutions exist from the right side of the point $x = x_0$. The corresponding proof can be performed in the same way.

1.4. All Solutions Are Singular: $P(x) \leq P_0 < 0$, $Q(x) \leq Q_0 < 0$

It turns out that under some assumptions all non-trivial solutions of the equation (2.1) are singular.

Proposition 3. *Let for all $x \in \mathbb{R}$ conditions $P(x) \leq P_0 < 0$, $Q(x) \leq Q_0 < 0$ take place, then all solutions of the equation (2.1) are singular except for the zero one.*

To prove this proposition we prove the following auxiliary lemma first.

Lemma 1. *Let $p, q > 0$ are real constants, then all solutions of equation*

$$v_{xx} - qv - pv^3 = 0, \quad (1.31)$$

are singular except for the zero one.

Proof. Solution to the Cauchy problem for the equation (1.31) with initial conditions $v(x_0) = v_0$, $v_x(x_0) = v'_0$ can be written in an implicit way as:

$$\pm \int_{v_0}^v \frac{d\xi}{\sqrt{C + q\xi^2 + \frac{p}{2}\xi^4}} = x - x_0; \quad C \equiv (v'_0)^2 - qv_0^2 - \frac{p}{2}v_0^4. \quad (1.32)$$

Choice of the sign in the left hand-side depends on the initial conditions and the value of x . Integral in the left hand-side of the equality (1.32) converges when $v \rightarrow \infty$, and hence there exist a value x^* , defined as

$$x^* = x_0 \int_{v_0}^{\infty} \frac{d\xi}{\sqrt{C + q\xi^2 + \frac{p}{2}\xi^4}}, \quad (1.33)$$

and $v(x)$ goes to infinity while x approaches to the x^* . So a solution $v(x)$ with arbitrary non-zero initial conditions is singular, lemma is proven. \square

Now we can prove the Proposition 3.

Proof of the Proposition 3. We use a so-called *Comparison Lemma* from [6, Appendix C]. Consider the equation

$$v_{xx} + Q_0v + P_0v^3 = 0. \quad (1.34)$$

We introduce the denotations

$$g(x, \xi) = -Q(x)\xi - P(x)\xi^3; \quad (1.35)$$

$$f(x, \xi) = f(\xi) = -Q_0\xi - P_0\xi^3. \quad (1.36)$$

Now we apply Comparison Lemma to the following pair of equations:

$$u_{xx} = g(x, u); \quad (1.37)$$

$$v_{xx} = f(x, v). \quad (1.38)$$

In the domain $D_+ = \{x \in \mathbb{R}, \xi \in (0; +\infty)\}$ we have $f(x, \xi) \leq g(x, \xi)$. Let $\tilde{u}(x)$ be a solution to the Cauchy problem for the equation (1.37) with initial conditions

$u(x_0) = u_0$, $u_x(x_0) = u'_0$. Choose the initial conditions for the Cauchy problem for the equation (1.38) as follows: $v(x_0) = u(x_0) = u_0$, $v_x(x_0) = u_x(x_0) = u'_0$; let $\tilde{v}(x)$ is a solution for that second problem. Let $u_0 > 0$, then one of the two cases takes place.

- (i) $u'_0 \geq 0$. Function $\tilde{v}(x)$ increases monotonically; this fact can be easily established from the phase portrait of the equation (1.38). Solution $\tilde{u}(x)$ limits solution $\tilde{v}(x)$ from above, which is singular. It follows from the Comparison Lemma that solution $\tilde{u}(x)$ is also singular.
- (ii) $u'_0 < 0$. We make a variable change $= -x$. In that case solution $\tilde{v}(\tilde{x})$ also increases monotonically, and since $\tilde{u}(\tilde{x})$ limits $\tilde{v}(\tilde{x})$ from above, $\tilde{u}(\tilde{x})$ is singular by the Comparison Lemma, hence $\tilde{u}(x)$ is also singular.

Similarly in the domain $D_- = \{x \in \mathbb{R}, \xi \in (-\infty; 0)\}$, the inequality $f(x, \xi) \geq g(x, \xi)$ holds. One can prove in the same manner that in the domain D_- solution $u(x)$ is also singular. □

1.5. Summary

Our main findings on regular and singular solutions for the stationary states equation (2.1) are summarised within Table 1.1. All these results were published by us in [7]. Our further findings are focused on the case when $P(x)$ changes its sign along the x . In the next chapter we describe a so-called *singular solution elimination method* which allow us under some additional assumptions classify all regular stationary states solution for the equation (2.1) within the symbolic dynamics framework.

$P(x)$	$Q(x)$	
$P(x) > 0$	—	All the solutions can be continued to the whole real line, singular solutions are absent (Proposition 1).
$P(x) < 0$ at least at one point $x = x_0$	—	There exists a pair of one-parametrical family of solutions collapsing at point $x = x_0$ and related by the symmetry $u \rightarrow -u$ (Proposition 2).
$P(x) < 0$	$Q(x) < 0$	All solutions are singular except for the zero one (Proposition 3).
$P(x)$ changes sign along \mathbb{R}	—	Singularity is a common behaviour of solutions. That fact allows us under some additional assumption apply so-called <i>singular solution elimination method</i> and classify all remaining regular solutions in terms of symbolic dynamics. We reveal this method and its application in the Chapter 2.

Table 1.1. Summary of the results for the Chapter 1.

Chapter 2

Stationary States Classification Within Symbolic Dynamics Framework

2.1. Objectives

In this chapter we describe an approach that will be used in what follows to classify the stationary states of one-dimensional GPE that are described by the equation,

$$u_{xx} + Q(x)u + P(x)u^3 = 0. \quad (2.1)$$

Here and in what follows we assume $Q(x)$, $P(x)$ to be periodic functions of the same period L : $Q(x+L) = Q(x)$, $P(x+L) = P(x)$. We also assume functions $Q(x)$, $P(x)$ to be piecewise continuously differentiable. That allows us to split the whole real axis \mathbb{R} into separate intervals where the corresponding Cauchy problem is correctly defined and a solution exists and is unique for any initial conditions within each such interval.

Our classification approach is based on the technique proposed in the paper [8]. In [8] authors show that presence of a large number of families of singular solutions allows to classify all remaining bounded (i.e. non-singular) solutions within a symbolic dynamics framework. That leads us to another important requirement: function $P(x)$ must *changes its sign along the period L* . As we saw in the previous chapter such fact guarantees the existence of singular solution families that in its turn is a base of the technique and makes the announced approach even possible.

The goal of this chapter is to provide a framework for stationary states classification and point out restrictions for its application. The main idea is the following. We define a Poincaré map \mathcal{P} for equation (2.1). Since function $P(x)$ changes its sing, Poincaré map \mathcal{P} and an inverse map \mathcal{P}^{-1} cannot be defined on the whole plane of initial data, instead they are defined on some subset of initial data plane. Studying

the domains of maps \mathcal{P} , \mathcal{P}^{-1} is crucial for the proposed approach. We determine conditions which allow to conclude that Poincaré map is a kind of the *horseshoe map* [9, Chapter 5]. If these conditions are met we can conclude that there exists one-to-one correspondence between all bounded solution of equation (2.1) and the points of fractal set that is invariant with respect to action of \mathcal{P} . That is what we call *singular solution elimination method*.

The presence of the horseshoe map structure allows us to relate uniquely each bounded solution with a bi-infinite sequence of symbols of some alphabet (finite or even infinite). This correspondence is bijective. We refer to the resulting bi-infinite sequence as a *solution code* and the overall process as the *coding of solutions*. Such coding, if possible, may provide a complete picture of the bounded solutions for equation (2.1) that can be highly demanded in different physical applications which involve Gross–Pitaevskii equation with both periodic potential and periodic pseudopotential.

2.2. Geometry of the Poincaré Map

First of all let's introduce several definitions.

2.2.1. Poincaré Map

Since we consider functions $Q(x)$, $P(x)$ to be L -periodic let's introduce the Poincaré map associated with the period L of the equation (2.1). Define the Poincaré map $\mathcal{P} : \mathbb{R}^2 \rightarrow \mathbb{R}^2$ in the following manner:

$$\mathcal{P} \begin{pmatrix} u_0 \\ u'_0 \end{pmatrix} = \begin{pmatrix} u_L \\ u'_L \end{pmatrix}, \quad (2.2)$$

where $u_L = u(L)$, $u'_L = u'(L)$, and $u(x)$ is a solution of equation (2.1) with initial conditions $u(0) = u_0$, $u'(0) = u'_0$. In the plane (u, u') Poincaré map is an *area-preserving diffeomorphism*. Due to presence of singular solutions, Poincaré map \mathcal{P}

and its inverse \mathcal{P}^{-1} may be defined not on the whole plane (u, u') . Denote by \mathcal{U}_L^+ the domain of the map \mathcal{P} , and denote by \mathcal{U}_L^- the domain of the map \mathcal{P}^{-1} correspondingly. Also define a set \mathcal{U}_L as an intersection of the two above mentioned sets: $\mathcal{U}_L = \mathcal{U}_L^+ \cap \mathcal{U}_L^-$.

It follows from the definitions of \mathcal{U}_L^\pm that $\mathcal{P}(\mathcal{U}_L^+) = \mathcal{U}_L^-$. Indeed any point $\mathbf{p} \in \mathcal{U}_L^+$ has \mathcal{P} -image \mathbf{q} . Then \mathbf{q} has \mathcal{P} -pre-image, therefore $\mathbf{q} \in \mathcal{U}_L^-$. On the other hand if $\mathbf{q} \in \mathcal{U}_L^-$ then \mathbf{q} has \mathcal{P} -pre-image \mathbf{p} . Therefore \mathbf{p} has \mathcal{P} -image and hence $\mathbf{p} \in \mathcal{U}_L^+$. Inverse statement $\mathcal{P}^{-1}(\mathcal{U}_L^-) = \mathcal{U}_L^+$ is also valid.

We also note here that symmetry in equation (2.1) naturally produces symmetry in \mathcal{U}_L^\pm sets. For example we can prove the following important statement.

Proposition 4. *Let functions $Q(x)$, $P(x)$ are even, then*

$$\mathcal{P}(\mathcal{U}_L^+) = I(\mathcal{U}_L^+); \quad (2.3)$$

$$\mathcal{P}^{-1}(\mathcal{U}_L^-) = I(\mathcal{U}_L^-), \quad (2.4)$$

where map I is a reflection with respect to the u' axis.

Proof. Let's prove statement (2.3). Consider a point $\mathbf{q} \in \mathcal{P}(\mathcal{U}_L^+)$. By definition of \mathcal{U}_L^+ , there is a point $\mathbf{p} = (u_0, u'_0) \in \mathcal{U}_L^+$, such that there exists a solution $u(x)$ of (2.1) with initial conditions $u(0) = u_0$, $u'(0) = u'_0$, and $\mathbf{q} = (u(L), u'(L))$. Denote by $\tilde{\mathbf{p}}$ a reflection $I(\mathbf{p})$, $\tilde{\mathbf{p}} = (-u_0, u'_0)$. Since functions $Q(x)$, $P(x)$ are even, Eq. (2.1) is invariant with respect to the transformation $\tilde{u} = -u$, $\tilde{x} = -x$. It means that $\tilde{u}(\tilde{x}) = -u(-x)$ is also a solution of (2.1) with initial conditions $\tilde{u}(0) = -u_0$, $\tilde{u}'(0) = u'_0$. Then $\tilde{u}(-L) = -u(L) = -u_L$ and $\tilde{u}'(-L) = u'(L) = u'_L$. Denote $\tilde{\mathbf{q}} = (\tilde{u}(-L), \tilde{u}'(-L))$. By definition of \mathcal{P} map, $\tilde{\mathbf{q}} = \mathcal{P}^{-1}(\tilde{\mathbf{p}})$ and hence $\tilde{\mathbf{q}} \in \mathcal{U}_L^+$. On the other hand $\tilde{\mathbf{q}} = (-u_L, u'_L) = I(\mathbf{q})$. Finally from $I(\mathbf{q}) \in \mathcal{U}_L^+$ we get $\mathbf{q} \in I(\mathcal{U}_L^+)$. It's also straightforward to check the inverse statement $\mathbf{q} \in I(\mathcal{U}_L^+) \Rightarrow \mathbf{q} \in \mathcal{P}(\mathcal{U}_L^+)$ and prove the equality (2.3). Statement (2.4) can be proven in an identical manner. \square

If the conditions of Proposition 4 are met one can conclude that $I(\mathcal{U}_L^+) = \mathcal{U}_L^-$ and $I(\mathcal{U}_L^-) = \mathcal{U}_L^+$, so the above mentioned sets are connected with each other with

a reflection with respect to the u' axis.

Definition 1. Define an **orbit** as a sequence of points $\{\mathbf{p}_n\}$, $\mathbf{p}_n \in \mathbb{R}^2$ such that $\mathcal{P}(\mathbf{p}_n) = \mathbf{p}_{n+1}$.

Let \mathbf{p}_0 be a starting point. Since \mathcal{P} is defined only on the \mathcal{U}_L^+ set, the next point \mathbf{p}_1 of the orbit exists only if $\mathbf{p}_0 \in \mathcal{U}_L^+$. Moreover for $n > 0$ points \mathbf{p}_n are consecutive \mathcal{P} -iterations of the initial point \mathbf{p}_0 . If at k -th iteration $\mathcal{P}^k(\mathbf{p}_0)$ leaves \mathcal{U}_L^+ then the orbit cannot be defined for $n > k$. Similarly for $n < 0$ points \mathbf{p}_n are consecutive \mathcal{P}^{-1} -iterations of \mathbf{p}_0 . Since the \mathcal{P}^{-1} map defined only on \mathcal{U}_L^- the iterations may stop after a finite number of steps. As a consequence not all orbits are bi-infinite. But bi-infinite orbits exist. For example one can easily specify the bi-infinite orbit of zero points that trivially satisfies the equation (2.1) and corresponds to its zero solution $u(x) \equiv 0$.

Another interesting observation comes from Proposition 1. If the function $P(x) > 0$ for all $x \in \mathbb{R}$ then all the orbits for the equation (2.1) are bi-infinite. From that point of view the case when $P(x)$ changes its sign becomes interesting. According to Proposition 2 points x where $P(x) < 0$ originate families of collapsing solutions. Such families at their turn sift the set of bi-infinite orbits.

2.2.2. Island Set

Definition 2. Let $\gamma > 0$ be fixed. A continuous function $f(x) : \Delta \rightarrow \mathbb{R}^2$, $\Delta = [a, b]$ is called a **γ -Lipschitz function** if $\forall x_1, x_2 \in \Delta$ the following inequality holds:

$$|f(x_1) - f(x_2)| \leq \gamma|x_1 - x_2|. \quad (2.5)$$

Definition 3. We call **island** an open curvilinear quadrangle $D \subset \mathbb{R}^2$ on the plane (u, u') formed by two pairs of nonintersecting monotonic curves α^\pm, β^\pm , moreover:

- curves α^\pm are graphs of monotonic γ -Lipschitz functions $u' = h_\pm(u)$, and a solution of equation (2.1) with initial conditions $(u_0, u'_0) \in \alpha^\pm$ collapses at the point $x = -L$;

- curves β^\pm are graphs of monotonic γ -Lipschitz functions $u = v_\pm(u')$, and a solution of equation (2.1) with initial conditions $(u_0, u'_0) \in \beta^\pm$ collapses at the point $x = +L$;
- if the functions $h_\pm(u)$ are increasing then $v_\pm(u')$ are decreasing, and vice versa, if functions $h_\pm(u)$ are decreasing then $v_\pm(u')$ are increasing respectively.

Remark 1. For convenience hereinafter by monotonically increasing / decreasing function we mean a function that satisfy non-strict inequalities. We call function $f(x)$ monotonically increasing if for $x_1 < x_2$, $f(x_1) \leq f(x_2)$, and monotonically decreasing if $f(x_1) \geq f(x_2)$. We also say that monotonicity type coincides for functions $f(x)$ and $g(x)$ if both $f(x)$ and $g(x)$ are increasing or decreasing functions simultaneously.

To emphasise the fact that Lipschitz constant γ must be predefined we also refer to the island as **γ -island**. We also say that points from the island boundaries are mapped to infinity by \mathcal{P} (β^\pm boundaries) or \mathcal{P}^{-1} (α^\pm boundaries), since the corresponding solution to the Cauchy problem with initial conditions in that points collapse exactly in the points $x = \pm L$.

Remark 2. If D is a γ_1 -island and $\gamma_2 > \gamma_1$ then D also is a γ_2 -island.

In our definition of island we explicitly specify its connection with initial equation (2.1) and collapses of its solutions. Further we'll see that such connection naturally comes from the dynamics of the \mathcal{P} map for equation of such type.

Remark 3. Solution of Cauchy problem for the initial conditions at the intersections of the α^\pm , β^\pm curves collapse both at $x = +L$ and $x = -L$ points.

Definition 4. Let S be a finite or a countable set of indices. Define **island set** as a set $\mathcal{D} = \bigcup_{i \in S} D_i$ that is finite or countable union of disjoint islands.

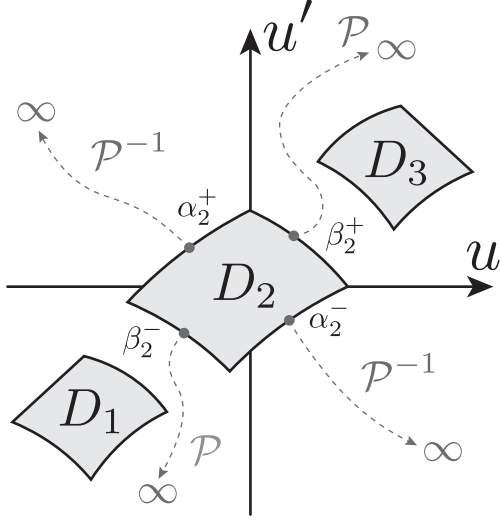


Figure 2.1. Hypothetical example of an island set $\mathcal{D} = \bigcup_{i \in \{1,2,3\}} D_i$ on a plane of initial conditions for equation (2.1). Boundaries of each component are mapped to the infinity by the \mathcal{P} and \mathcal{P}^{-1} maps (i.e. the corresponding solution of Cauchy problem collapses at $x = L$ and $x = -L$ respectively).

2.2.3. Curves and Strips

Move on to the definition of h,v-curves and h,v-strips.

Definition 5. Let D be an island bounded by curves α^\pm, β^\pm . Consider a curve α that connects the opposite sides β^\pm of the island D . We call such curve as **h-curve** (or h_γ -curve) if it represents a graph of a monotonic γ -Lipschitz function $u' = h(u)$ and its monotonicity type coincides with the functions $u' = h_\pm(u)$ that correspond to the α^\pm boundaries of the island D . We also call **h-strip** (or h_γ -strip) an open subset of the island D bounded by two h_γ -curves.

Definition 6. Similarly consider a curve β that connects opposite sides α^\pm of an island D . We call it as **v-curve** (or v_γ -curve) if it represents a graph of a monotonic γ -Lipschitz function $u = v(u')$ and its monotonicity type coincide with the functions $u = v_\pm(u')$ that correspond to the β^\pm boundaries of the island D . Also we call **v-strip** (or v_γ -strip) an open subset of the island D bounded by two v_γ -curves.

Remark 4. Island by itself represents a limit case of the h and v strips simultaneously.

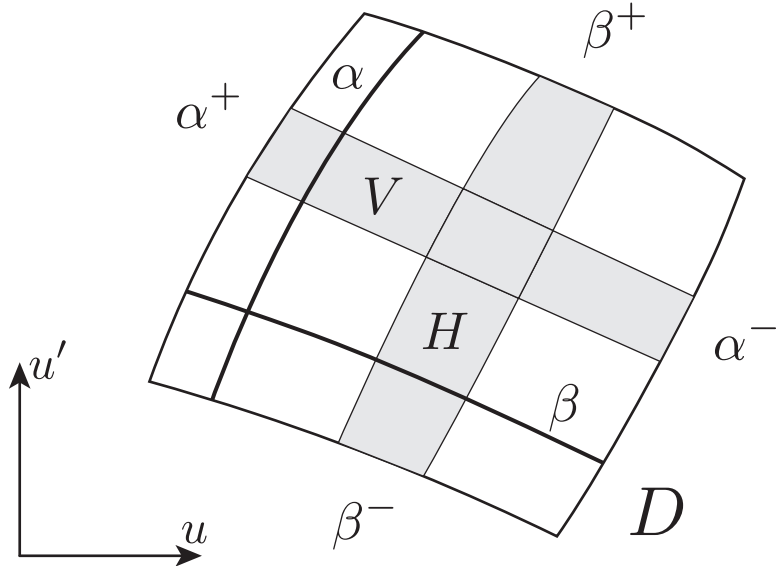


Figure 2.2. An island D bounded by curves α^\pm, β^\pm ; h-curve α , v-curve β , and two strips: h-strip H and v-strip V .

All the above introduced definitions are illustrated in Figures 2.1 and 2.2. At last let's define one additional property of island set along with \mathcal{P} , \mathcal{P}^{-1} maps.

Definition 7. Let \mathcal{D} be an island set that is a domain for both \mathcal{P} and \mathcal{P}^{-1} maps. Consider two islands $D_1, D_2 \in \mathcal{D}$. We call the island D_2 **forward-reachable** from the island D_1 if for any h-curve $\alpha \in D_1$ with endpoints lying on the opposite boundaries β_1^\pm of the island D_1 the intersection $\mathcal{P}(\alpha) \cap D_2$ is not empty. On the other hand we call the island D_2 **backward-reachable** from the island D_1 if for any v-curve $\beta \in D_1$ with endpoints lying on the opposite boundaries α_1^\pm of the island D_1 the intersection $\mathcal{P}^{-1}(\beta) \cap D_2$ is not empty. Finally we call the island D_2 **reachable** from the D_1 if it satisfies both forward and backward reachability.

Remark 5. If an island D_2 is forward-reachable from D_1 then D_1 is backward-reachable from D_2 and vice versa.

Definition 8. We call an island set $\mathcal{D} = \bigcup_{i \in S} D_i$ **complete** if for any i, j island D_i is reachable from D_j .

2.2.4. Thickness of Strips

Next we'll also need a definition of the strips thickness. Let an h-strip H lie inside an island D and is bounded by h-curves α^+ and α^- . Consider graphs of these curves as functions of u : $u' = h_{\pm}(u)$. By definition, $h_{\pm}(u)$ are γ -Lipschitz functions. Denote their domains by Δ^{\pm} . Due to the geometric properties of an island, domains Δ^{\pm} do not coincide except the case when the opposite boundaries of the island D are vertical straight lines. Let $\Delta^+ = [u_0^+; u_1^+]$, $\Delta^- = [u_0^-; u_1^-]$, consider new domain $\Delta = \Delta^+ \cup \Delta^-$ and define functions $\tilde{h}_{\pm}(u)$ on Δ as follows:

$$\tilde{h}_{\pm}(u) = \begin{cases} h_{\pm}(u_0^{\pm}) & u < u_0^{\pm}; \\ h_{\pm}(u) & u \in \Delta^{\pm}; \\ h_{\pm}(u_1^{\pm}) & u > u_1^{\pm}. \end{cases} \quad (2.6)$$

Since h_{\pm} are γ -Lipschitz functions the new functions \tilde{h}_{\pm} are also γ -Lipschitz on the whole domain Δ . Denote by $\tilde{\alpha}^{\pm}$ the curves that are the graphs of $\tilde{h}_{\pm}(u)$.

Definition 9. *By thickness of an h-strip H , denoted $d_h(H)$, we mean the distance between curves $\tilde{\alpha}^{\pm}$ in C-norm, i.e.*

$$d_h(H) = d(\tilde{\alpha}^+, \tilde{\alpha}^-) = \max_{u \in \Delta} |\tilde{h}_+(u) - \tilde{h}_-(u)|. \quad (2.7)$$

Remark 6. *For two h-strips H_1, H_2 the following statement is valid: $H_2 \subseteq H_1 \Rightarrow \Delta_2 \subseteq \Delta_1$ and $d_h(H_2) \leq d_h(H_1)$.*

Definition 10. *Let maximum of the expression (2.7) be reached at point u_* , i.e.*

$$u_* = \arg \max_{u \in \Delta} |\tilde{h}_+(u) - \tilde{h}_-(u)|. \quad (2.8)$$

We call h-strip H well-measurable if $u_ \in \Delta^+ \cap \Delta^-$.*

Proposition 5. *For h-strip H the following statement is valid:*

$$\Delta^+ \cap \Delta^- \neq \emptyset \Rightarrow u_* \in \Delta^+ \cap \Delta^-, \quad (2.9)$$

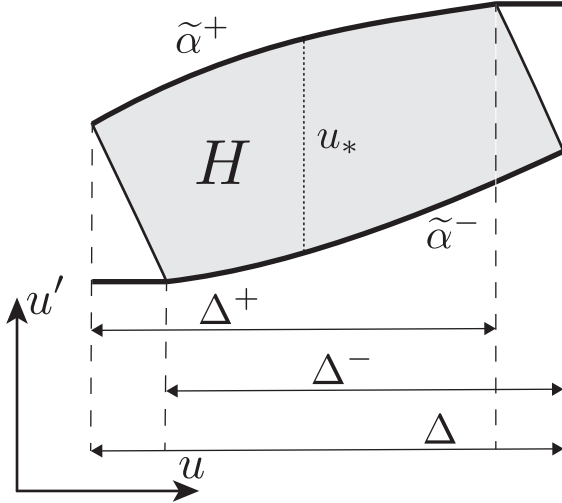


Figure 2.3. An illustration to the definition of an h-strip thickness. Strip H is *well-measurable* in a sense of Definition 10. Curves $\tilde{\alpha}^\pm$ are continuations of the initial h-strip borders to the whole Δ ; u_* is a point of maximum of the expression (2.7).

i.e. h-strip is well-measurable if domains of its border functions have at least one common point.

Proof. The statement immediately follows from the monotonicity of the h-strip borders α^+ and α^- . \square

In a similar way we define thickness of v-strips. Let an v-strip V lie inside an island D and is bounded by v-curves β^+ and β^- . Consider this curves as a functions of u' : $u = v_\pm(u')$. Denote domains of these functions by Δ^\pm . Continue functions $v_\pm(u')$ to the whole interval $\Delta = \Delta^+ \cap \Delta^-$ in the same way as for h-strips, see (2.6), and introduce new functions $\tilde{v}_\pm(u')$ and curves $\tilde{\beta}^\pm$.

Definition 11. By **thickness** of an v-strip V , denoted $d_v(V)$, we mean the distance between curves $\tilde{\beta}^\pm$ in C-norm, i.e.

$$d_v(V) = d(\tilde{\beta}^+, \tilde{\beta}^-) = \max_{u' \in \Delta} |\tilde{v}_+(u') - \tilde{v}_-(u')|. \quad (2.10)$$

The definition of *well-measurable* v-strip is introduced in a same way. Remark 6 and Proposition 5 can be also written for v-strips. Note that thickness of h-strip is measured in vertical direction, and thickness of v-strip is measured in horizontal

direction. If a strip is well-measurable then its thickness is measured in a direction along the straight line that connects points from the opposite side of the strip.

2.3. Poincaré Map Domains for Piecewise Periodic Pseudopotential

Let's demonstrate how the definitions introduced above work all together. For that purpose consider equation (2.1) with $Q(x) \equiv -1$ and periodic piecewise constant pseudopotential $P(x) = \eta(x)$, where $\eta(x)$ is a function of the period $L = L_* + L_0$, defined as

$$\eta(x) = \begin{cases} -1, & x \in [0; L_*); \\ +1, & x \in [L_*; L_* + L_0), \end{cases} \quad (2.11)$$

Function (2.11) is represented in Figure 2.4. Equation (2.1) takes form

$$u_{xx} - u + \eta(x)u^3 = 0. \quad (2.12)$$

Since pseudopotential is a piecewise constant function that has only two different

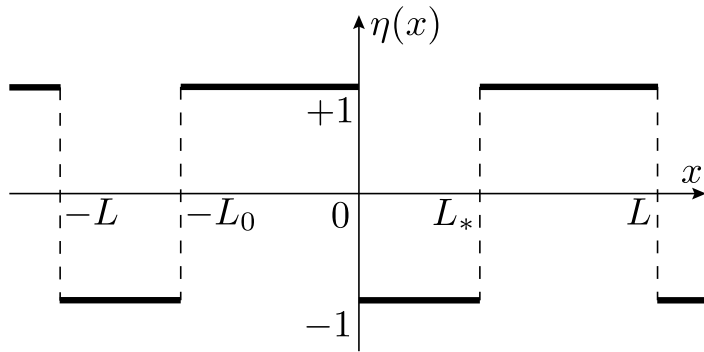


Figure 2.4. Plot of function $\eta(x)$ defined in (2.11).

values on the period L we can split the period into two intervals and consider two different cases for equation (2.12). In each region Eq. (2.12) has a form of conservative Duffing equation:

$$u_{xx} - u - u^3 = 0, \quad x \in [0; L_*]; \quad (2.13)$$

$$u_{xx} - u + u^3 = 0, \quad x \in [L_*; L_* + L_0]. \quad (2.14)$$

Each of equations (2.13), (2.14) can be solved explicitly through Jacobi elliptic functions. Exact solutions are given in Appendix B.

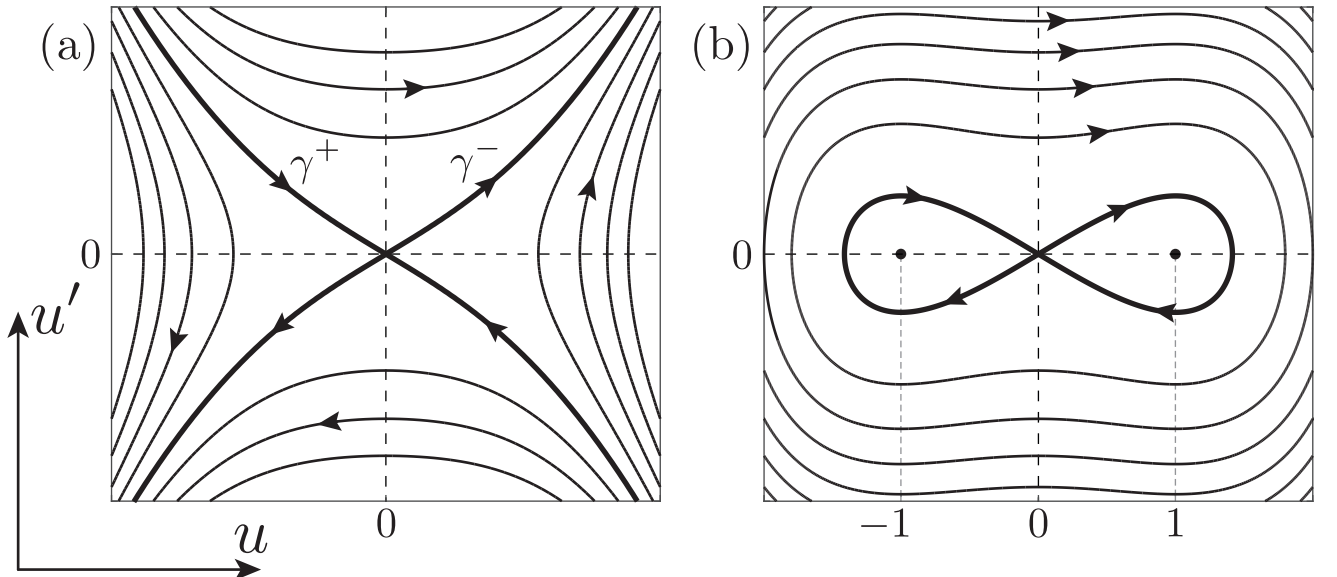


Figure 2.5. Phase portraits for different cases of equation (2.12) with piecewise pseudopotential (2.11). Panel (a) represents the phase portrait for equation (2.13), curves γ^\pm correspond to the separatrices which enter the equilibrium point $(0, 0)$ as x approaches $\pm\infty$. Panel (b) depicts the phase portrait for equation (2.14).

Equation (2.13) has a first integral of the form:

$$H_* = u_x^2 - u^2 - \frac{1}{2}u^4. \quad (2.15)$$

The phase portrait for equation (2.13) is presented in Figure 2.5 (a). Any trajectory on the phase plane corresponds to some value of H_* . Level $H_* = 0$ corresponds to the equilibrium state $(0, 0)$, and four separatrices related to it. Two of the separatrices $\gamma_{1,2}^+$ enter the zero equilibrium as x approaches $+\infty$. We denote them by curve γ^+ . Another two separatrices $\gamma_{1,2}^-$ enter the zero equilibrium as x approaches $-\infty$. We denote them by curve γ^- correspondingly. Resulting curves γ^\pm satisfy the equations

$$u' = \pm \frac{u}{\sqrt{2}} \sqrt{2 + u^2}. \quad (2.16)$$

It follows from the exact form of the solutions of equation (2.13) that all of them, except the zero one, are singular. It means that a solution for a Cauchy

problem with initial conditions $u(0) = u_0$, $u'(0) = u'_0$ (u_0 and u'_0 not equals zero simultaneously) tends to infinity while x approaches some finite point both to the left and to the right of $x = 0$. It means that a solution for equation (2.13) has a *finite domain* if $H_* \neq 0$.

The first integral of equation (2.14) is

$$H_0 = u_x^2 - u^2 + \frac{1}{2}u^4. \quad (2.17)$$

Phase portrait for equation (2.14) is given in Figure 2.5 (b). It has two center equilibrium points $(\pm 1, 0)$ and one hyperbolic equilibrium point $(0, 0)$. Separatrix loops correspond to the localized solutions

$$u(x) = \pm \frac{\sqrt{2}}{\cosh x}. \quad (2.18)$$

The area inside the separatrix loops is filled by closed orbits of periodic solutions with nonzero mean. All other orbits turn around the origin and correspond to solutions with zero mean. That's why we mark a corresponding period part L_0 with a symbol “0”, since it looks like a little curve circle.

2.3.1. General Propositions on the \mathcal{U}_L^\pm Sets for Piecewise Pseudopotential

Let's move on to the consideration of the \mathcal{U}_L^\pm sets for equation (2.12). We consider a decomposition of the Poincaré map $\mathcal{P} = \mathcal{P}_0 \mathcal{P}_*$, where maps associated with corresponding parts of the overall period L are defined in a similar manner as the initial Poincaré map \mathcal{P} itself (2.2). Map \mathcal{P}_* maps a point (u_0, u'_0) to $(u(L_*), u'(L_*))$ where $u(x)$, $x \in [0; L_*]$ is a solution of Eq. (2.13) with initial conditions $u(0) = u_0$, $u'(0) = u'_0$. Similarly map \mathcal{P}_0 maps a point (u_0, u'_0) to $(u(L), u'(L))$ where $u(x)$, $x \in [L_*; L]$ is a solution of Eq. (2.14) with initial conditions $u(L_*) = u_0$, $u'(L_*) = u'_0$.

Note that \mathcal{P}_* is not defined in the whole \mathbb{R}^2 . We denote by $\mathcal{U}_{L_*}^+$ a domain of the map \mathcal{P}_* . Due to the fact that all solutions of equation (2.14) are regular, domain

of the map \mathcal{P} coincide with the domain of \mathcal{P}_* map, i.e.

$$\mathcal{U}_L^+ = \text{dom}(\mathcal{P}) = \text{dom}(\mathcal{P}_0 \mathcal{P}_*) = \text{dom}(\mathcal{P}_*) \equiv \mathcal{U}_{L_*}^+. \quad (2.19)$$

Since the phase portrait for Eq. (2.13) is symmetric with respect to the origin, $\mathcal{U}_{L_*}^+$ is also symmetric with respect to the origin (see how its computed in Figure 2.8). Two separatrices $\gamma_{1,2+}$ that correspond to the curve γ^+ enter zero equilibrium as $x \rightarrow +\infty$. It means that for any initial data posed at γ^+ and for any L_* the map \mathcal{P}_* is correctly defined, i.e. $\gamma^+ \in \mathcal{U}_{L_*}^+$. Another property of $\mathcal{U}_{L_*}^+$ directly follows from Proposition 4:

$$\mathcal{P}_*(\mathcal{U}_{L_*}^+) = I(\mathcal{U}_{L_*}^+) = \mathcal{U}_{L_*}^-. \quad (2.20)$$

Move on to the $\mathcal{U}_{L_*}^-$ set for equation (2.13). Since $\mathcal{U}_{L_*}^-$ is a reflection of $\mathcal{U}_{L_*}^+$ with respect to the u' axis, it inherits its symmetry properties. Set $\mathcal{U}_{L_*}^-$ also contains curve γ^- that corresponds to another two separatrices $\gamma_{1,2}^-$ of equation (2.13). Consider the second map \mathcal{P}_0 of the decomposition. As we mentioned above \mathcal{P}_0 is correctly defined on the whole $\mathcal{U}_{L_*}^-$. It turns out that the image $\mathcal{P}_0(\gamma^-)$ has a spiral-like structure and intersects the curve γ^+ infinitely many times. The following proposition is valid.

Proposition 6. *\mathcal{P}_0 -image of the curve γ^- intersects γ^+ infinitely many times at the points $\{0\} \cup u_{\pm n}$,*

$$u_{\pm n} = \pm \frac{2x_{n-1}}{\sqrt[4]{2} L_0} + \mathcal{O}\left(H_0^{-1/4}\right), \quad n \in \mathbb{N}, \quad (2.21)$$

as $H_0 \rightarrow \infty$, where

$$x_n = \text{cn}^{-1}\left(2^{-1/4}, k_0\right) + K(k_0)n. \quad (2.22)$$

Here $K(k)$ is the complete elliptic integral of the first kind, and $k_0 = 1/\sqrt{2}$.

Proof. First of all, the point $(0, 0)$ belongs to the intersection $\mathcal{P}_0(\gamma^-) \cap \gamma^+$ since it's a stable fixed point of equation (2.14) and the \mathcal{P}_0 map.

Next we note that all the intersections $\mathcal{P}_0(\gamma^-) \cap \gamma^+$ occur outside of the separatrix loops of (2.14) and correspond to zero mean solutions of (2.14). This obviously

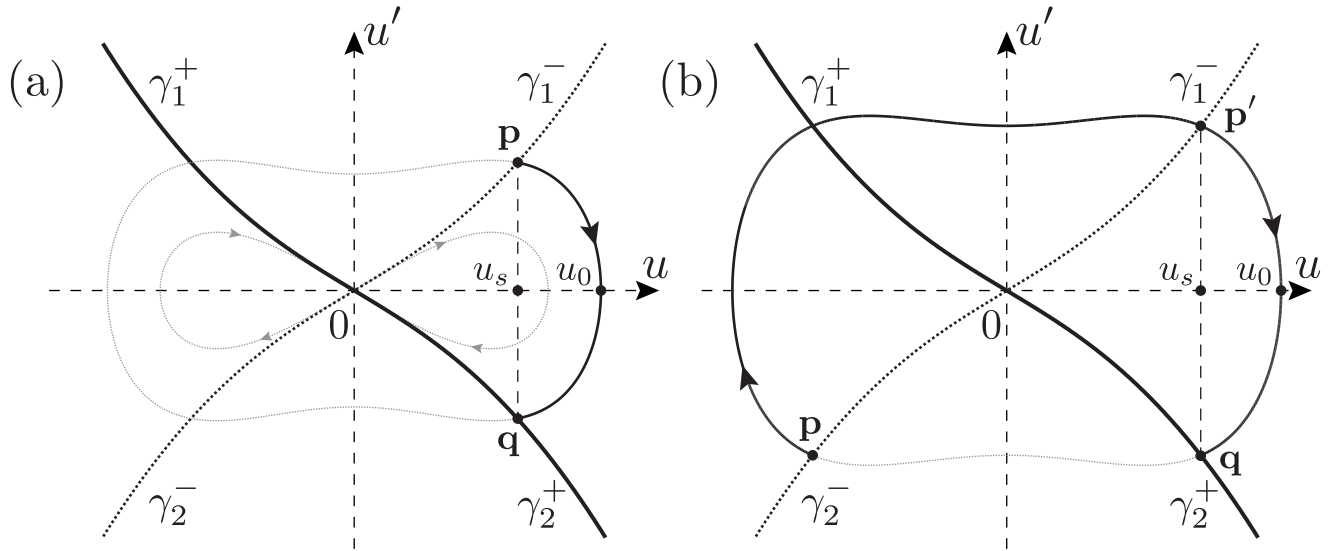


Figure 2.6. Illustration to the proof of Proposition 6.

follows from that fact that γ^+ lies outside of the loops both from left and right of u' axis (depicted in Fig. 2.6 (a)).

Prove the formula for the points from the right side of u' axis, u_{+n} . Such points corresponds to the γ_2^+ separatrix of equation (2.13), see Figure 2.6. Result points of intersections $\mathcal{P}_0(\gamma^-) \cap \gamma_2^+$ can be divided into two groups: $\mathcal{P}_0(\gamma_1^-) \cap \gamma_2^+$ and $\mathcal{P}_0(\gamma_2^-) \cap \gamma_2^+$.

Consider points from the first group. Let a point \mathbf{q} belong to the intersection $\mathcal{P}_0(\gamma_1^-) \cap \gamma_2^+$. Then there exists a point $\mathbf{p} = (u_s, u'_s) \in \gamma_1^-$ such that $\mathcal{P}_0(\mathbf{p}) \in \gamma_2^+$. Due to the symmetries of the phase portraits for equations (2.13) and (2.14), $\mathbf{q} = (u_s, -u'_s)$, see Figure 2.6 (a). Consider a phase trajectory of (2.14) that lies outside of separatrix loop and connects points \mathbf{p} and \mathbf{q} . According to Appendix B exact form of the solution is

$$u(x) = x_0 \operatorname{cn} \left(\sqrt{x_0^2 - 1} x + x_1, k \right), \quad (2.23)$$

where k is elliptic modulus,

$$k = \frac{1}{\sqrt{2}} \frac{x_0}{\sqrt{x_0^2 - 1}}, \quad (2.24)$$

and x_0, x_1 are constants that are determined by initial conditions $(u(0), u'(0)) = \mathbf{p}$.

Next let's introduce x variable shift $x \rightarrow x - L_0/2$. Equation (2.23) persists its form but now $u(0) = u_0$, $u_0 > 0$, and $u'(0) = 0$. That allows us to determine constants x_0, x_1 : $x_0 = u_0$, $x_1 = 0$. Solution (2.23) takes form

$$u(x) = u_0 \operatorname{cn} \left(\sqrt{u_0^2 - 1} x, k \right), \quad (2.25)$$

and for coordinates of the points \mathbf{p} and \mathbf{q} we have

$$\mathbf{p} = (u(-L_0/2), u'(-L_0/2)) = (u_s, u'_s); \quad (2.26)$$

$$\mathbf{q} = (u(L_0/2), u'(L_0/2)) = (u_s, -u'_s). \quad (2.27)$$

Since value of H_0 (2.17) conserves on the trajectory that connects point \mathbf{p} and the point $(u_0, 0)$ one can write

$$H_0 = -u_0^2 + \frac{u_0^4}{2} = (u'_s)^2 - u_s^2 + \frac{u_s^4}{2}. \quad (2.28)$$

On the other hand the point \mathbf{p} belong to the separatrix of (2.13) and its coordinates satisfy an equality

$$H_* = (u'_s)^2 - u_s^2 - \frac{u_s^4}{2} = 0. \quad (2.29)$$

Comparing (2.28) and (2.29) one can conclude that

$$u_s^4 = \frac{u_0^4}{2} - u_0^2. \quad (2.30)$$

At the point \mathbf{q} we have

$$u_s = u_0 \operatorname{cn} \left(\frac{\sqrt{u_0^2 - 1} L_0}{2}, k \right). \quad (2.31)$$

Substitute u_s from (2.30) into (2.31), divide both side of the equality by u_0 , and introduce $4v_0^2 = u_0^2 - 1$. Equation (2.31) takes form

$$\left(\frac{1}{2} - \frac{1}{4v_0^2 + 1} \right)^{1/4} = \operatorname{cn} (v_0 L_0, k), \quad k = \frac{1}{\sqrt{2}} \sqrt{1 + \frac{1}{4v_0^2}}. \quad (2.32)$$

Let us analyse the limit $v_0 \rightarrow \infty$. First of all consider k as a function of v_0 and expand it into the series:

$$k(v_0) = \frac{1}{\sqrt{2}} + \frac{1}{8\sqrt{2}} \frac{1}{v_0^2} - \frac{1}{32\sqrt{2}} \frac{1}{v_0^4} + \dots \quad (2.33)$$

Let $k_0 = 1/\sqrt{2}$. We introduce the remainder $\Delta k = k(v_0) - k_0$. Note that Δk has the main term of order v_0^{-2} as $v_0 \rightarrow \infty$. Denote $w_0 = v_0 L_0$, consider $\text{cn}(w_0, k)$ in the right side of (2.32) as a function of elliptic modulus k and expand it into the series in the vicinity of k_0 up to the second term:

$$\text{cn}(w_0, k_0 + \Delta k) = \text{cn}(w_0, k_0) + f(w_0, k_0)\Delta k + \mathcal{O}(w_0^{-1/4}). \quad (2.34)$$

Here $f(w_0, k_0)$ is the first derivative of elliptic cosine with respect to k at $k = k_0$:

$$f(w_0, k_0) = \frac{\text{sn}(w_0) \text{dn}(w_0)(w_0 - k_0 w_0 + k_0 \text{sn}(w_0) \text{cd}(w_0) - E(\phi(w_0)))}{2(k_0 - 1)k_0}. \quad (2.35)$$

Here $\phi(w, k)$ is the Jacobi amplitude and $E(\phi, k)$ is the incomplete elliptic integral of the second kind. All elliptic functions have the same modulus k_0 , we omit this parameter for the sake of brevity. This expression is quite tremendous, nevertheless, what interests us here is the orders of terms with respect to w_0 . It has a leading term of order w_0 as $w_0 \rightarrow \infty$. That allows us to conclude that the term $f(w_0, k_0)\Delta k$ of (2.34) in its turn has a leading term of order w_0^{-1} (or v_0^{-1}). Rewrite (2.32) in a form:

$$\left(\frac{1}{2} - \frac{1}{4v_0^2 + 1} \right)^{1/4} = \text{cn}(v_0 L_0, k_0) + \mathcal{O}(v_0^{-1}), \quad (2.36)$$

Using the same approach again we expand the left side of (2.36) into a series:

$$\left(\frac{1}{2} - \frac{1}{4v_0^2 + 1} \right)^{1/4} = \frac{1}{\sqrt[4]{2}} - \frac{1}{2\sqrt[4]{2}} \frac{1}{(4v_0^2 + 1)} + \mathcal{O}(v_0^{-4}). \quad (2.37)$$

Combining (2.37) with (2.36) and comparing the orders of terms we conclude that

$$\text{cn}(v_0 L_0, k_0) = \frac{1}{\sqrt[4]{2}} + \mathcal{O}(v_0^{-1}). \quad (2.38)$$

Let's express $v_0 L_0$ in the equation above

$$v_0 L_0 = \text{cn}^{-1} \left(\frac{1}{\sqrt[4]{2}} + \mathcal{O}(v_0^{-1}), k_0 \right) + 2K(k_0)n, \quad n \in \{0\} \cup \mathbb{N}. \quad (2.39)$$

Here $K(k)$ is the complete elliptic integral of the first kind. We left only positive roots since we are interested only in intersections $\mathcal{P}_0(\gamma_1^-) \cap \gamma_2^+$ where u_0 is positive

and we can write

$$v_0 = \frac{u_0}{2} \sqrt{1 - \frac{1}{u_0^2}} = \frac{u_0}{2} - \frac{1}{2u_0} + \mathcal{O}(u_0^{-3}). \quad (2.40)$$

We note that by definition of cn^{-1} function

$$\text{cn}^{-1} \left(2^{-1/4} + \mathcal{O}(v_0^{-1}) \right) = F \left(\arccos \left(2^{-1/4} + \mathcal{O}(v_0^{-1}) \right), k_0 \right), \quad (2.41)$$

where $F(\phi, k)$ is incomplete elliptic integral of the first kind. Consider series expansion of \arccos up to the main term:

$$\arccos \left(2^{-1/4} + \mathcal{O}(v_0^{-1}) \right) = \arccos \left(2^{-1/4} \right) + \mathcal{O}(v_0^{-1}). \quad (2.42)$$

Let's substitute (2.42) into (2.41), use additive property of integral, and apply integral mean value theorem to the second term:

$$\begin{aligned} \text{cn}^{-1} \left(2^{-1/4} + \mathcal{O}(v_0^{-1}) \right) &= F \left(\arccos \left(2^{-1/4} \right) + \mathcal{O}(v_0^{-1}), k_0 \right) = \\ &= F \left(\arccos \left(2^{-1/4} \right), k_0 \right) + F \left(\mathcal{O}(v_0^{-1}), k_0 \right) = \\ &= \text{cn}^{-1} \left(2^{-1/4}, k_0 \right) + \mathcal{O}(v_0^{-1}). \end{aligned} \quad (2.43)$$

Put (2.43) and (2.40) into (2.39), also note that according to (2.40) we can safely replace $\mathcal{O}(v_0^{-1})$ with $\mathcal{O}(u_0^{-1})$,

$$u_0 = \frac{2}{L_0} \left(\text{cn}^{-1} \left(2^{-1/4}, k_0 \right) + 2K(k_0)n \right) + \mathcal{O}(u_0^{-1}). \quad (2.44)$$

Finally let's get rid of u_0 in favor of u_s . For that purpose according to (2.28) we can write $\mathcal{O} \left(H_0^{-1/4} \right)$ instead of $\mathcal{O}(u_0^{-1})$, and it follows from (2.30) that

$$u_s = \frac{1}{\sqrt[4]{2}} u_0 + \mathcal{O}(u_0^{-1}). \quad (2.45)$$

Let's introduce the following denotation

$$x_n = \text{cn}^{-1} \left(2^{-1/4}, k_0 \right) + 2K(k_0)n. \quad (2.46)$$

Now combining the expressions above all together and replacing u_s with u_{+n} we get

$$u_{+n} = \frac{2x_{n-1}}{\sqrt[4]{2} L_0} + \mathcal{O} \left(H_0^{-1/4} \right), \quad n \in \mathbb{N}. \quad (2.47)$$

In order to get the final formula of the proposition for $\{u_{+n}\}$ we need to consider points of intersections from the second group $\mathcal{P}_0(\gamma_2^-) \cap \gamma_2^+$. We can easily reduce this task to the previous one. Let there exists a point of intersection $\mathbf{q} \in \gamma_2^+$. Consider point $\mathbf{p} \in \gamma_2^-$, such that $\mathcal{P}_0(\mathbf{p}) = \mathbf{q}$, see Fig. 2.6 (b). We note that there exists a point $\mathbf{p}' \in \gamma_1^-$, and the trajectory (2.23) goes from the point \mathbf{p} to \mathbf{p}' over a half of the period $2K(k)/\sqrt{x_0^2 - 1}$, and after that cross the u axis at the point u_0 . Then we introduce an x variable shift $x \rightarrow x - (L_0/2 + K(k)/\sqrt{x_0^2 - 1})$, so that $u(0) = u_0$, $u_0 > 0$, and $u'(0) = 0$, and can determine $x_0 = u_0$, $x_1 = 0$. Solution (2.23) takes form (2.25) again and for coordinates of the points \mathbf{p}' and \mathbf{q} we have

$$\mathbf{p}' = \left(u\left(-L_0/2 + \frac{K(k)}{\sqrt{u_0^2 - 1}}\right), u'\left(-L_0/2 + \frac{K(k)}{\sqrt{u_0^2 - 1}}\right) \right) = (u_s, u'_s); \quad (2.48)$$

$$\mathbf{q} = \left(u\left(L_0/2 - \frac{K(k)}{\sqrt{u_0^2 - 1}}\right), u'\left(L_0/2 - \frac{K(k)}{\sqrt{u_0^2 - 1}}\right) \right) = (u_s, -u'_s). \quad (2.49)$$

Now we can use relations (2.48), (2.49) instead of (2.26), (2.27), and repeat all the steps above. Difference in x variable shift results in the additional term $K(k)$ in (2.39) and (2.44). Finally we replace $K(k) = K(k_0 + \Delta k) = K(k_0) + \mathcal{O}(H_0^{-2/4})$, and get the following relation for x_n :

$$x_n = \operatorname{cn}^{-1} \left(2^{-1/4}, k_0 \right) + K(k_0)(2n + 1). \quad (2.50)$$

Relation (2.47) remains the same. Combining (2.46) with (2.50) we get the result for separatrix intersections points $\{u_{+n}\} \in \mathcal{P}(\gamma^-) \cap \gamma_2^+$:

$$u_{+n} = \frac{2x_{n-1}}{\sqrt[4]{2}L_0} + \mathcal{O} \left(H_0^{-1/4} \right), \quad n \in \mathbb{N}, \quad (2.51)$$

where x_n satisfies the relation

$$x_n = \operatorname{cn}^{-1} \left(2^{-1/4}, k_0 \right) + K(k_0)n. \quad (2.52)$$

Points $\{u_{-n}\}$, $n \in \mathbb{N}$ from the left side of u' axis, $u_{-n} \in \mathcal{P}_0(\gamma^-) \cap \gamma_1^+$, should be treated in a similar way, proposition is proven. \square

Propositions 6 says that the far we goes from the $(0, 0)$ point on the phase plane, the better the asymptotic relation (2.21) works. It turns out that formula

(2.21) works pretty well even for small number of n . See Figure 2.7 where we compare the predicted coordinates with actual intersections obtained by numerical computation of $\mathcal{P}_0(\gamma^-)$. Another interesting consequence of Proposition 6 is that set \mathcal{U}_L consists of infinitely many connected components. This obviously follows from that fact, that set $\mathcal{U}_{L_*}^-$ contains the entire curve γ^- and map \mathcal{P}_0 is continuous, so the image $\mathcal{P}_0(\mathcal{U}_{L_*}^-)$ cross \mathcal{U}_L^+ infinitely many times.

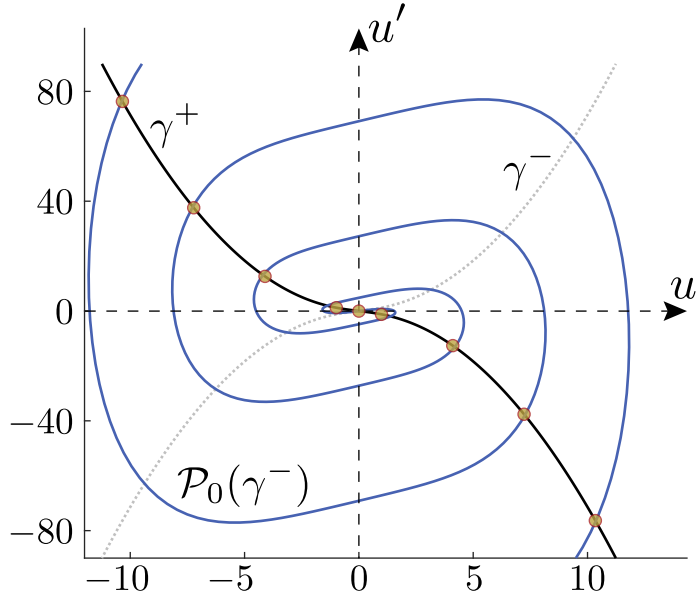


Figure 2.7. Comparison of asymptotic formula (2.21) with numerical computations for $L_0 = 1$. Curves γ^\pm are formed by the separatrices of (2.13), \mathcal{P}_0 -image of γ^- is a solid blue line computed numerically. Predicted points of intersections $u_{\pm n}$ from $\mathcal{P}_0(\gamma^-) \cap \gamma^+$ are marked with yellow dots. One can see that (2.21) predicts intersections quite precisely even for small number of n .

2.3.2. Construction of the Poincaré Map Domains

One of the possible way to construct \mathcal{U}_L^\pm sets for different maps associated with equation (2.1) is to use a numerical procedure called scanning of initial conditions plane (u, u') . That's how it works. At first ranges of scanning $u_{\min} \leq u \leq u_{\max}$, $u'_{\min} \leq u' \leq u'_{\max}$ are selected. Then the target segment of the initial conditions plane is covered by a uniform grid with small steps h and h' for each axis u and u' . Using Runge-Kutta 4th order method we solve differential equation in each node of the resulting grid. We use an interval $[0; L]$ for \mathcal{U}_L^+ where x changes in

forward direction from 0 to L , and an interval $[-L; 0]$ in order to get \mathcal{U}_L^- where x changes in backward direction from 0 to $-L$. If absolute value of a calculated solution does not exceed some predefined constant M that is large enough, we suppose that such solution is non-collapsing, and include corresponding node point into \mathcal{U}_L^\pm sets. Then we color nodes on the initial conditions plane that correspond to non-collapsing solutions to get the final picture of \mathcal{U}_L^\pm sets. In our experiments we used $M = 10^5$ and $M = 10^7$, and got consistent results. Such procedure is pretty straightforward and can be efficiently performed by a computer since it admits natural parallelization. Let's apply this procedure to equation (2.12).

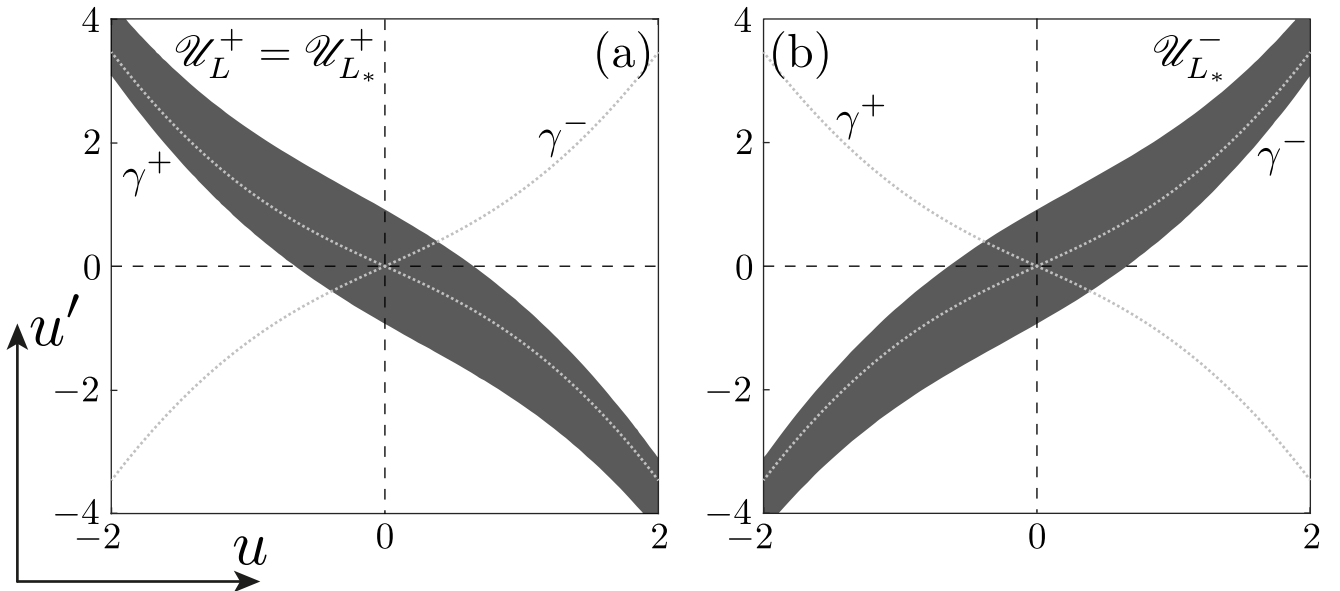


Figure 2.8. Sets \mathcal{U}_L^\pm for the equation (2.13) for the parameter $L_* = 2$. Panel (a) represents $\mathcal{U}_{L_*}^+$ set, it coincides with the set \mathcal{U}_L^+ for equation (2.12), since all solutions of the second equation (2.14) are regular. Panel (b) depicts $\mathcal{U}_{L_*}^-$ set, it's just a reflection of the set \mathcal{U}_L^+ from the right panel due to Proposition 4.

On Figure 2.8 (a) Poincaré map domain $\mathcal{U}_L^+ = \mathcal{U}_{L_*}^+$ for the parameters $(L_*, L_0) = (2, 1)$ is depicted. As we mentioned above it contains the curve γ^+ formed by separatrices of (2.13). Figure 2.8 (b) represents a \mathcal{P}_* -image of $\mathcal{U}_{L_*}^+$, $\mathcal{P}_*(\mathcal{U}_L^+) = \mathcal{U}_{L_*}^-$. According to Proposition 4 set $\mathcal{P}_*(\mathcal{U}_{L_*}^-)$ can be obtained by a reflection of the set $\mathcal{U}_{L_*}^+$, with respect to the u' axis. Set $\mathcal{U}_{L_*}^-$ in its turn contains curve γ^- .

Let's continue our scanning in order to get set \mathcal{U}_L^- and then intersect it with \mathcal{U}_L^+ . On Figure 2.9 (a) set \mathcal{U}_L^- and its intersection with \mathcal{U}_L^+ set are depicted

for values of parameters $(L_*, L_0) = (2, 1)$. From our numerical procedure we can conclude that intersection $\mathcal{U}_L = \mathcal{U}_L^+ \cap \mathcal{U}_L^-$ represents three connected components with monotonic borders. These components form a three-island set in the scanning area $-2 \leq u \leq 2$, $-4 \leq u' \leq 4$, denote them by D_i , $i \in \{-1, 0, +1\}$. Indeed, along with the monotonicity of the connected components borders we also know that two opposite borders of D_i , which entirely belong to the borders of the set \mathcal{U}_L^+ , consist of points that are mapped to infinity under action of \mathcal{P} (by construction of \mathcal{U}_L^+). On other hand borders of \mathcal{U}_L^- contain two other borders of each D_i , and they are mapped to infinity under action of \mathcal{P}^{-1} . Thereby the obtained structure satisfy all the conditions of island set from Definition 4. However set \mathcal{U}_L^- entirely contains an image of the curve γ^- . We know that according to Proposition 6 image $\mathcal{P}(\gamma^-)$ has infinitely many intersections with the curve γ^+ . That's why outside of the scanning area there exist many other intersections between sets \mathcal{U}_L^\pm , and they form infinitely many connected components in the result set \mathcal{U}_L . In a similar manner we denote those components by D_k , $k \in \{-1, -2, -3, \dots\}$ for the components on the left side of the u' axis and $k \in \{+1, +2, +3, \dots\}$ for the components on the right side. Due to monotonicity of \mathcal{U}_L^+ borders and general geometric properties of the spiral \mathcal{U}_L^- we can hypothesize that all the components D_k in \mathcal{U}_L set are also islands.

Our numerical studies shows that for equation (2.12) three central components of \mathcal{U}_L play a crucial role in an island set formation. For example in Figure 2.1 (b) geometry of the \mathcal{U}_L^- for parameters $(L_*, L_0) = (1.3, 1)$ does not allow to form an island around the center. Establishing a criteria for existence of the island set is a quite tricky task even for a simple form equation (2.12), and such criteria is out of scope for the current work. Our approach is based on scanning of a sufficiently large subset of initial conditions plane around the center $(u, u') = (0, 0)$. If the resulting subset of \mathcal{U}_L form an island set we just *make a hypothesis* that all other intersections and also islands.

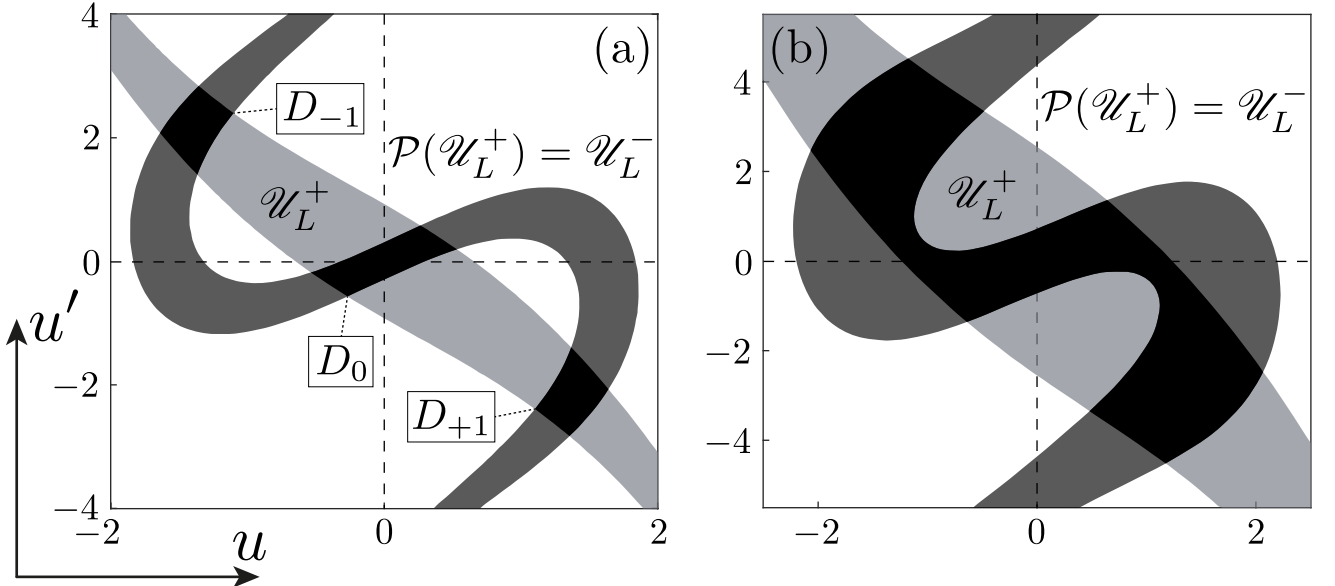


Figure 2.9. Sets \mathcal{U}_L^+ (light gray), \mathcal{U}_L^- (dark gray), and their intersection \mathcal{U}_L for two different sets of parameters. Panel (a) depict the case $(L_*, L_0) = (2, 1)$; three central connected components D_i form an island set. Panel (b) correspond to the case $(L_*, L_0) = (1.3, 1)$; geometry of the result sets does not allow to form islands.

2.3.3. Complete Island Set

Let \mathcal{U}_L represents an island set. It turns out that for Eq. (2.12) the property of “completeness” for an island set in a sense of Definition 8 naturally arises from its construction. Let’s demonstrate it in an heuristic manner. At first, upper boundary of the set $\mathcal{U}_L^+ = \mathcal{U}_{L_*}^+$ consists of such points that the corresponding solution to the Cauchy problem with initial conditions at these points tends to $+\infty$ exactly at the point $x = L_*$. Therefore, while point \mathbf{p} is approaching to the upper boundary of \mathcal{U}_L^+ it’s \mathcal{P} -image tends to $(+\infty, +\infty)$. On other hand lower boundary of \mathcal{U}_L^+ consists of points that the corresponding solution to the Cauchy problem with initial conditions at these points tends to $-\infty$. So, while point \mathbf{p} is approaching to the lower boundary of \mathcal{U}_L^+ it’s \mathcal{P} -image tends to $(-\infty, -\infty)$.

Let’s consider a curve Γ inside one of islands $D_i \in \mathcal{U}_L$ that connects opposite boundaries of the set \mathcal{U}_L^+ . Denote by Γ_* its \mathcal{P}_* -image, $\Gamma_* = \mathcal{P}_*(\Gamma)$. It’s clear that Γ_* belongs to $\mathcal{U}_{L_*}^-$, and it’s stretched out continuously from $-\infty$ to $+\infty$ by u inside $\mathcal{U}_{L_*}^-$. Now consider the second map \mathcal{P}_0 of the decomposition $\mathcal{P} = \mathcal{P}_0 \mathcal{P}_*$. We know

that this map curls the set $\mathcal{U}_{L_*}^-$ into a spiral (see Fig. 2.9 (a)). This spiral intersects \mathcal{U}_L^+ and form islands. So if we consider the \mathcal{P}_0 -image of Γ_* and take into account that the value of H_0 remains the same for all trajectories of (2.14) associated with \mathcal{P}_0 map, we can conclude that $\mathcal{P}_0(\Gamma_*)$ is stretched along the whole set \mathcal{U}_L^- and intersects each of the islands $D_i \in \mathcal{U}_L$ at least once. Such reasoning leads us to the conclusion that all islands in \mathcal{U}_L are forward-reachable. Similar consideration shows that islands from \mathcal{U}_L are also backward-reachable and the constructed island set is complete.

Let's illustrate this idea. For this purpose we construct \mathcal{P}_* and \mathcal{P} -images of islands from Figure 2.9 (a). Again we do this numerically with the scanning procedure described above. In Figure 2.10 (a) one can see the \mathcal{P}_* -image of islands D_i , $i \in \{-1, 0, +1\}$. As we have expected these images are infinite curvilinear strips stretched inside the \mathcal{P}_* -image of the \mathcal{U}_L^+ set. \mathcal{P} -images of the islands are depicted in Figure 2.10 (b). Images $\mathcal{P}(D_i)$ are infinite curvilinear strips curled up inside the \mathcal{U}_L^- set.

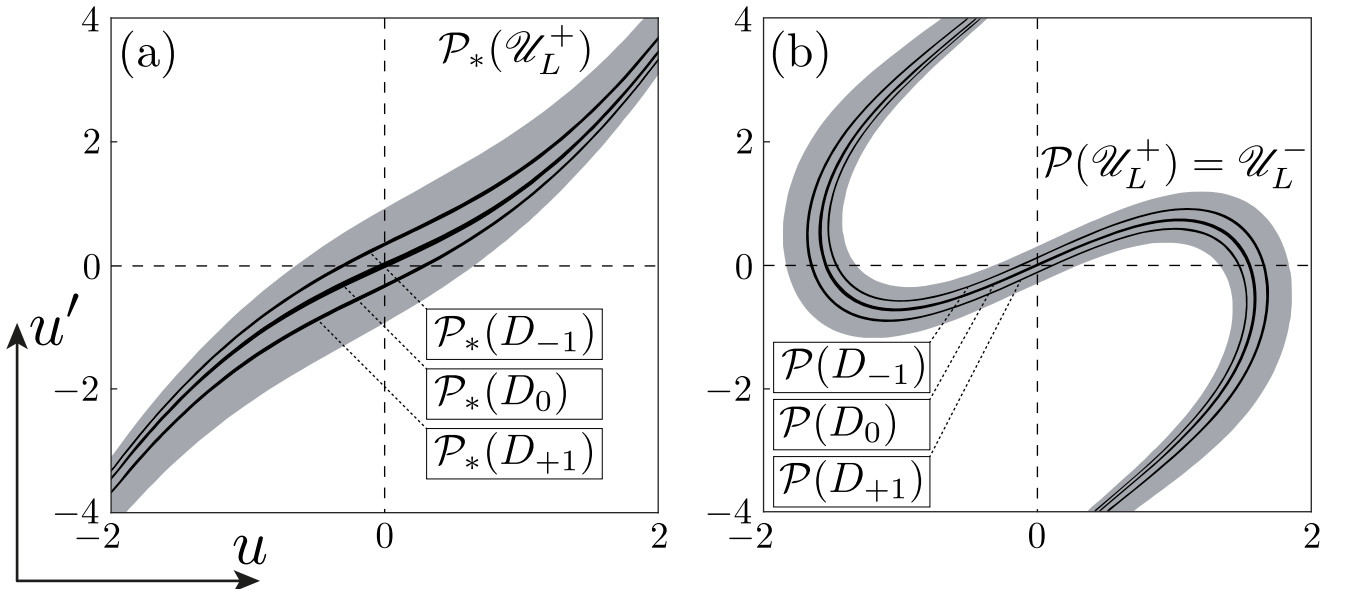


Figure 2.10. \mathcal{P}_* and \mathcal{P} -images of islands for Eq. (2.12) with parameters $(L_*, L_0) = (2, 1)$. Panel (a) represents their \mathcal{P}_* -images. Each image is a curvilinear strip stretched along the whole $\mathcal{P}_*(\mathcal{U}_L^+)$. Panel (b) represents \mathcal{P} -images.

The images $\mathcal{P}(D_i)$ resembles the image $\mathcal{P}_0(\gamma^-)$ of the separatrices γ^- . Each

of them intersects \mathcal{U}_L^+ infinitely many times and cross each island from \mathcal{U}_L . To illustrate this, we combined Figure 2.10 (b) with Figure 2.9 (a) in Figure 2.11 where the notation: $\mathcal{P}(D_i) \cap D_j = H_{ij}$ is introduced.

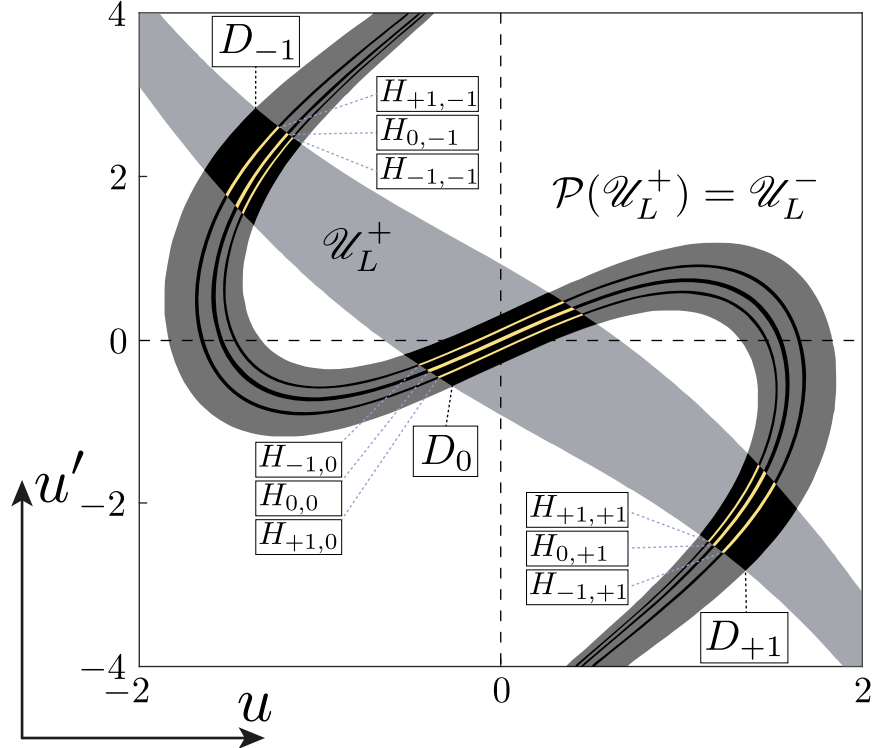


Figure 2.11. Island set $\mathcal{U}_L = \mathcal{U}_L^+ \cap \mathcal{U}_L^-$ and sets $H_{ij} = \mathcal{P}(D_i) \cap D_j$, $i, j \in \{-1, 0, +1\}$ for equation (2.12) with parameters $(L_*, L_0) = (2, 1)$. Island set $\mathcal{U}_L = \bigcup_{i \in S} D_i$ is forward-reachable, so \mathcal{P} -image of each island D_i intersects all other islands D_j , $j \in S$ including D_i itself.

The similar situation takes place for \mathcal{P}^{-1} map as well. Island set $\mathcal{U}_L = \bigcup_{i \in S} D_i$ for Eq. (2.12) is backward-reachable. It means that $V_{ij} = \mathcal{P}^{-1}(D_j) \cap D_i \neq \emptyset$ for each $i, j \in S$. In Figure 2.12 sets V_{ij} are depicted for $i, j \in \{-1, 0, +1\}$.

2.4. Symbolic Dynamics: Coding of Solutions

In this section we show how all the concepts introduced above can be used together to classify all bounded solutions of equation (2.1). Our classification is closely connected with the structure of the \mathcal{U}_L set. We demonstrate our approach for the previously considered piecewise pseudopotential equation (2.12). Let's introduce two sets.

Definition 12. Define set \mathcal{O} as a set of bi-infinite orbits of all regular solutions for equation (2.1), i.e. $\mathbf{r} \in \mathcal{O}$, $\mathbf{r} = \{\mathbf{p}_n\}$, $\mathcal{P}(\mathbf{p}_n) = \mathbf{p}_{n+1}$, $n \in \mathbb{Z}$.

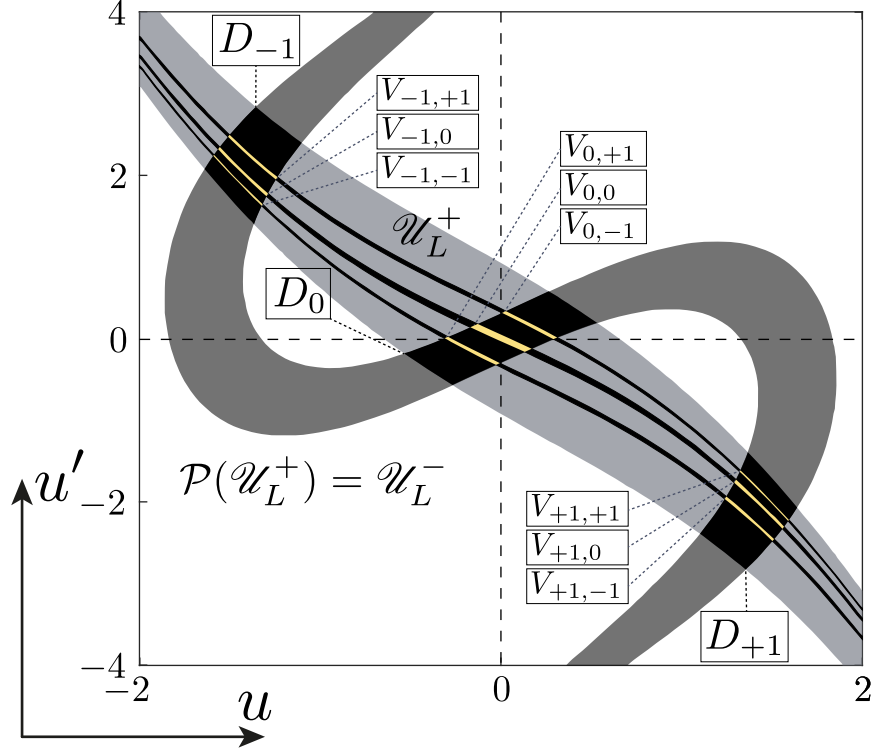


Figure 2.12. Island set $\mathcal{U}_L = \mathcal{U}_L^+ \cap \mathcal{U}_L^-$ and sets $V_{ij} = \mathcal{P}^{-1}(D_j) \cap D_i$, $i, j \in \{-1, 0, +1\}$ for equation (2.12) with parameters $(L_*, L_0) = (2, 1)$. Island set $\mathcal{U}_L = \bigcup_{i \in S} D_i$ is backward-reachable, so \mathcal{P} -pre-image of each island D_i intersects all other islands D_j , $j \in S$ including D_i itself.

Define a metric in \mathcal{O} as follows. Let $v, w \in \mathcal{O}$ be two orbits, $v = \{\mathbf{p}_n\}$, $\mathbf{p}_n = (\phi_n, \phi'_n)$, $w = \{\mathbf{q}_n\}$, $\mathbf{q}_n = (\psi_n, \psi'_n)$, then the distance $d_{\mathcal{O}}$ between orbits v and w is defined as a Euclidean distance between points \mathbf{p}_0 and \mathbf{q}_0 , i.e.

$$d_{\mathcal{O}}(v, w) = \|\mathbf{p}_0 - \mathbf{q}_0\| = \sqrt{(\phi_0 - \psi_0)^2 + (\phi'_0 - \psi'_0)^2}. \quad (2.53)$$

This implies that \mathcal{O} can be regarded as a topological space where neighbourhood $U_{\varepsilon}(u^*)$ of an element $u^* \in \mathcal{O}$ is defined as $U_{\varepsilon}(u^*) = \{u \mid d_{\mathcal{O}}(u^*, u) < \varepsilon\}$.

Definition 13. Define set \mathcal{S} as a set of bi-infinite sequences $\{\dots, i_{-1}, i_0, i_1, \dots\}$ over an alphabet where each symbol i_k , $k = 0, \pm 1, \dots$, corresponds to a connected component $D_k \in \mathcal{U}_L$.

We also write \mathcal{S}_N if the alphabet has N different symbols, and \mathcal{S}_∞ if the number of symbols is infinite (corresponds to the infinite number of connected components in \mathcal{U}_L). Set \mathcal{S} also can be regarded as a topological space where neighbourhood $W_k(\omega^*)$ of an element $\omega^* = \{\dots, i_{-1}^*, i_0^*, i_1^*, \dots\} \in \mathcal{S}$ is defined as $W_k(\omega^*) = \{\omega \mid i_s^* = i_s, |s| < k\}$.

What we are interested in is the connection between sets \mathcal{O} and \mathcal{S} . First of all the structure of island set \mathcal{U}_L can be easily used to assign symbolic sequences, also named codes, to the solutions, so the correspondence from \mathcal{O} to \mathcal{S} can be established. Let's demonstrate it with an example. Consider a localized solution $u(x)$ of Eq. (2.12) shown in the left panel of Figure 2.13. Construct the sequence of $(u(kL), u'(kL))$. On the plane (u, u') each of the points of this sequence is situated in some island D_i . In the point $x = 0$ value $u(0)$ and derivative $u'(0)$ match island D_{-1} . After that in the point $x = L$ our solution $u(x)$ cross the central islands D_0 and matches it again for $x = 2L$. In the point $x = 3L$ our solution came into the right island D_{+1} . That allows us to determine four central symbols of the result code: $\{-1, 0, 0, +1\}$, see Figure 2.13 (b). Moreover since our solution is localized all other points $(u(kL), u'(kL))$ correspond to the central component of \mathcal{U}_L and all the symbols from the left side of “ -1 ” and the right side of “ $+1$ ” are “ 0 ”. Thereby finally we obtain the result bi-infinite sequence $\{\dots, 0, -1, 0, 0, +1, 0, \dots\}$ for the localized solution $u(x)$ from Figure 2.13 (a). Obviously points of orbit of our solution cannot lie down outside of \mathcal{U}_L because the solution is regular and has bi-infinite orbit, so at each step we have exactly one symbol to choose and the overall process identifies the result bi-infinite sequence uniquely.

2.4.1. Uniqueness of Solutions Coding

The most intriguing question about coding is the following: when is the correspondence between solutions orbits \mathcal{O} and codes \mathcal{S} based on the \mathcal{U}_L set structure for Eq. (2.1) is bijective (one-to-one)? We can also formulate another question: when there exists a homeomorphism between two topological spaces \mathcal{O} and \mathcal{S} ? In this

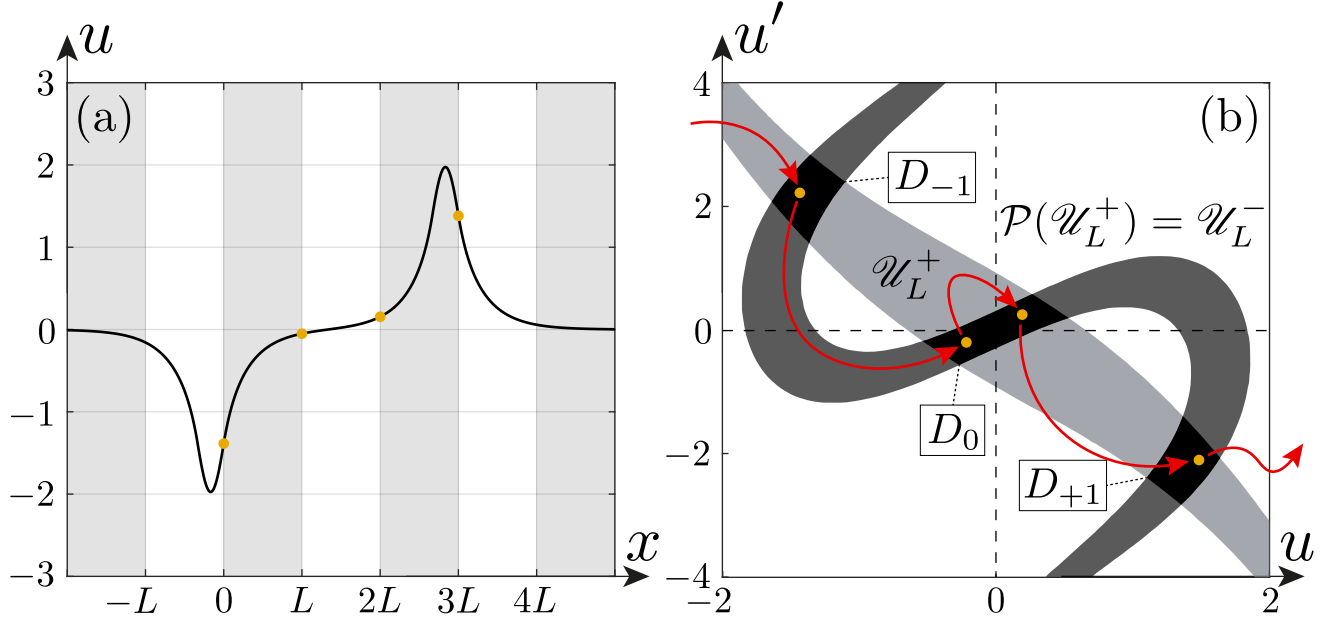


Figure 2.13. Illustration of the coding process. Panel (a) represents a localized solution for the Eq. (2.12) with parameters $(L_*, L_0) = (2, 1)$. This solution has been found numerically using the shooting method. Panel (b) represents a sketch of four points (yellow dots) of the solution orbit over the structure of the \mathcal{U}_L set. These points jump from island to island following the red arrows and determine the symbols of the result solution code: $\{\dots, 0, -1, 0, 0, +1, 0, \dots\}$.

section we determine sufficient conditions of existence of such correspondence.

One can reformulate one of the questions above as follows: could one find initial conditions for a Cauchy problem by a solution code? Let $\mathbf{s} = \{\dots, i_{-1}, i_0, i_1, \dots\}$ be a code derived from the structure of a complete island set \mathcal{U}_L . Consider its left part $\{\dots, i_{-2}, i_{-1}, i_0\}$. All the points from island D_{i_0} correspond to the symbol i_0 . Consider a set $H_{i_{-1}i_0} = \mathcal{P}(D_{i_{-1}}) \cap D_{i_0}$. The set $H_{i_{-1}i_0} \subset D_{i_0}$ consists of such points $\mathbf{p}_0 = (u_0, u'_0) \in D_{i_0}$ that the corresponding solution $u(x)$ to the Cauchy problem with initial conditions $u(0) = u_0, u'(0) = u'_0$ does not collapse at $[-L; 0]$, and $\mathbf{p}_{-1} = (u(-L), u'(-L)) \in D_{i_{-1}}$. Hence the code of solution with initial conditions taken from $H_{i_{-1}i_0}$ includes symbols $\{i_{-1}, i_0\}$. Continuing this process. Consider a set $H_{i_{-2}, i_{-1}, i_0} = \mathcal{P}(H_{i_{-2}, i_{-1}}) \cap D_{i_0}$, where $H_{i_{-2}, i_{-1}} = \mathcal{P}(D_{i_{-2}}) \cap D_{i_{-1}}$. The set $H_{i_{-2}, i_{-1}, i_0} \subset D_{i_0}$ consists of such points $\mathbf{p}_0 = (u_0, u'_0) \in D_{i_0}$ that the corresponding solution $u(x)$ to the Cauchy problem with initial conditions $u(0) = u_0, u'(0) = u'_0$ does not collapse at $[-2L; 0]$, and $\mathbf{p}_{-1} = (u(-L), u'(-L)) \in D_{i_{-1}}, \mathbf{p}_{-2} = (u(-2L), u'(-2L)) \in D_{i_{-2}}$.

That's why the code of solution with initial conditions taken from H_{i_{-2}, i_{-1}, i_0} includes symbols $\{i_{-2}, i_{-1}, i_0\}$.

In order to formalize this process we introduce an arrow operator $X \xrightarrow{\mathcal{P}} Y = \mathcal{P}(X) \cap Y$. This operator is not associative and should be applied strictly from left to right, i.e. $X \xrightarrow{\mathcal{P}} Y \xrightarrow{\mathcal{P}} Z = (\mathcal{P}(X) \cap Y) \xrightarrow{\mathcal{P}} Z$. Consider a sequence of nested sets:

$$\begin{aligned} D_{i_0} \supseteq H_{i_0} &= D_{i_0}; \\ D_{i_0} \supseteq H_{i_{-1}, i_0} &= D_{i_{-1}} \xrightarrow{\mathcal{P}} D_{i_0}; \\ D_{i_0} \supseteq H_{i_{-2}, i_{-1}, i_0} &= D_{i_{-2}} \xrightarrow{\mathcal{P}} D_{i_{-1}} \xrightarrow{\mathcal{P}} D_{i_0}; \\ D_{i_0} \supseteq H_{i_{-3}, i_{-2}, i_{-1}, i_0} &= D_{i_{-3}} \xrightarrow{\mathcal{P}} D_{i_{-2}} \xrightarrow{\mathcal{P}} D_{i_{-1}} \xrightarrow{\mathcal{P}} D_{i_0}; \\ &\dots \end{aligned} \tag{2.54}$$

All of them are situated inside the island D_{i_0} , moreover all of sets H_{i_{-k}, \dots, i_0} are non-empty due to completeness of the island set \mathcal{U}_L . Consider an intersection of these sets $H_\infty = \bigcap_{k=0}^{\infty} H_{i_{-k}, \dots, i_0}$. By the construction resulting set H_∞ , if non-empty, consists of such points that the corresponding solution with initial conditions $(u(0), u'(0))$ H_∞ exists on the interval $(-\infty; 0]$ and its code coincide with the left part of the initially considered sequence \mathbf{s} .

Let's do the similar operations with the right part of \mathbf{s} : $\{i_0, i_1, i_2, \dots\}$. Consider a sequence of nested sets:

$$\begin{aligned} D_{i_0} \supseteq V_{i_0} &= D_{i_0}; \\ D_{i_0} \supseteq V_{i_0, i_1} &= D_{i_1} \xrightarrow{\mathcal{P}^{-1}} D_{i_0}; \\ D_{i_0} \supseteq V_{i_0, i_1, i_2} &= D_{i_2} \xrightarrow{\mathcal{P}^{-1}} D_{i_1} \xrightarrow{\mathcal{P}^{-1}} D_{i_0}; \\ D_{i_0} \supseteq V_{i_0, i_1, i_2, i_3} &= D_{i_3} \xrightarrow{\mathcal{P}^{-1}} D_{i_2} \xrightarrow{\mathcal{P}^{-1}} D_{i_1} \xrightarrow{\mathcal{P}^{-1}} D_{i_0}; \\ &\dots \end{aligned}$$

All of these nested sets V_{i_0, \dots, i_k} are situated inside the island D_{i_0} and are non-empty. Consider an intersections $V_\infty = \bigcap_{k=0}^{\infty} V_{i_0, \dots, i_k}$. Set V_∞ , if non-empty, consists of such points that solution with initial conditions from V_∞ exists on the interval $[0; +\infty)$ and its code coincide with the right part of \mathbf{s} .

Intersection of these two sets $H_\infty \cap V_\infty$ consists of such points of initial conditions that gives the result regular solutions with the desired code \mathbf{s} . The geometry of $H_\infty \cap V_\infty$ can be quite complex. But if the intersection consists of just one point then we can say that the code identifies a solution uniquely.

Our goal is to formulate sufficient conditions that allows us to state that any bi-infinite code identify a regular solution uniquely. Again let \mathcal{U}_L represent a complete island set for equation of type (2.1). Consider the sequences of nested sets:

$$\mathcal{U}_L = \mathcal{H}_0 \supseteq \mathcal{H}_1 \supseteq \mathcal{H}_2 \supseteq \mathcal{H}_3 \supseteq \dots, \quad \mathcal{H}_i = \mathcal{P}(\mathcal{H}_{i-1}) \cap \mathcal{H}_0;$$

$$\mathcal{V}_L = \mathcal{V}_0 \supseteq \mathcal{V}_1 \supseteq \mathcal{V}_2 \supseteq \mathcal{V}_3 \supseteq \dots, \quad \mathcal{V}_i = \mathcal{P}^{-1}(\mathcal{V}_{i-1}) \cap \mathcal{V}_0.$$

Define the following sets as intersections of the sequences above:

$$\mathcal{H}_\infty = \mathcal{H}_0 \cap \mathcal{H}_1 \cap \mathcal{H}_2 \cap \mathcal{H}_3 \cap \dots;$$

$$\mathcal{V}_\infty = \mathcal{V}_0 \cap \mathcal{V}_1 \cap \mathcal{V}_2 \cap \mathcal{V}_3 \cap \dots.$$

By its construction their intersection $\mathcal{U}_\infty = \mathcal{H}_\infty \cap \mathcal{V}_\infty$ contains initial conditions for all regular solutions of equation (2.1). Set \mathcal{U}_∞ is a central object for describing of the set of regular solutions for equation of such type [7, 8, 10]. Its structure may be quite sophisticated having a form of a complex fractal set. One can have a nice illustration on how this set may look like for equation (2.12). For that purpose we combine Figure 2.11 and Figure 2.12 into a single plot.

In Figure 2.14 subsets of \mathcal{H}_1 (yellow) and \mathcal{V}_1 (blue) along with their intersection $\mathcal{H}_1 \cap \mathcal{V}_1$ (red) are presented. There exist other parts of \mathcal{H}_1 and \mathcal{V}_1 that can be obtained by considering \mathcal{P} and \mathcal{P}^{-1} -images of other islands lying outside of the scanning area, but we exclude them for the sake of clarity. One can see how the partitioning inside the \mathcal{U}_L occurs. Continuation of that process with higher orders of maps \mathcal{P} and \mathcal{P}^{-1} results in additional partitioning inside the set $\mathcal{H}_1 \cap \mathcal{V}_1$ and reveals the complex nature of the set \mathcal{U}_∞ . Eventually if for each code there exists exactly one point of initial conditions in the set \mathcal{U}_∞ then we can state the existence of one-to-one correspondence between regular solutions and symbolic sequences derived

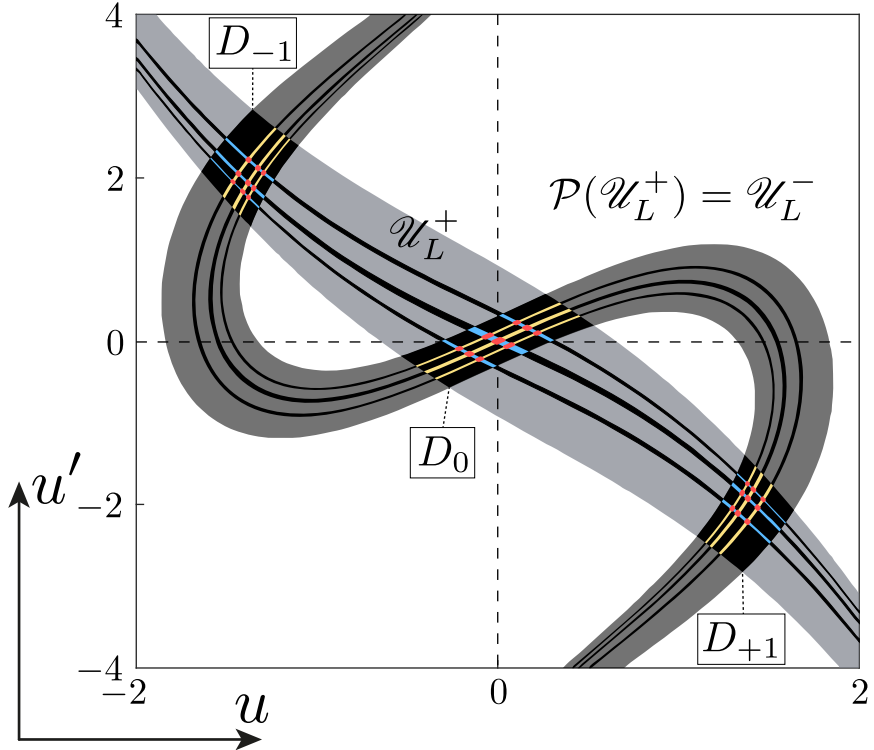


Figure 2.14. Subsets of \mathcal{H}_1 (yellow) and \mathcal{V}_1 (blue), and their intersection $\mathcal{H}_1 \cap \mathcal{V}_1$ (red). This figure give an illustration on how the partitioning inside the set \mathcal{U}_L (black) starts to occur while considering higher orders of \mathcal{P} and \mathcal{P}^{-1} .

from the structure of the set \mathcal{U}_L . Let's now formulate the sufficient conditions of that. We do this in a form of two hypotheses which are of the form of so-called Conley–Moser conditions [11, Chapter 25].

Hypothesis I. *For equation (2.1) with L -periodic functions $Q(x)$, $P(x)$ the set \mathcal{U}_L is a complete island set, $\mathcal{U}_L = \bigcup_{i \in S} D_i$, and there exist constants M, N such that $d_h(D_i) \leq M$ and $d_v(D_i) \leq N$ for any $i \in S$.*

Hypothesis II. *Let $\mathcal{U}_L = \bigcup_{i \in S} D_i$ be an island set. For each $i, j \in S$ there exist γ_{ij} such that for any h-strip $H \in D_i$ its \mathcal{P} -image $\tilde{H}_j = \mathcal{P}(H) \cap D_j$ is an $h_{\gamma_{ij}}$ -strip, and there exists $\mu > 1$ such that*

$$d_h(\tilde{H}_j) \leq (1/\mu)d_h(H). \quad (2.55)$$

For each $i, j \in S$ there exist δ_{ij} such that for any v-strip $V \in D_j$ its \mathcal{P} -pre-image $\tilde{V}_i = \mathcal{P}^{-1}(V) \cap D_i$ is a $v_{\delta_{ij}}$ -strip, and there exists $\nu > 1$ such that

$$d_v(\tilde{V}_i) \leq (1/\nu)d_v(V). \quad (2.56)$$

Two hypotheses introduced above allow us to formulate and prove the central theorem (Theorem 1) of our coding approach. This theorem partially reproduce the result initially proved in [8, Theorem 3.1]. However Theorem 1 turns out to be more suitable for further numerical analysis, since we excluded Hypothesis III from [8] and replaced it with modified version of Hypothesis II. Hypothesis III from [8] requires a sophisticated analyses of areas of sets D_i in plane which is hard to perform numerically.

Theorem 1. *Assume that Poincaré map associated with equation (2.1) satisfies Hypotheses I and II. Then there exists a homeomorphism of topological spaces* $\mathcal{C} : \mathcal{O} \rightarrow \mathcal{S}$, defined as follows: $\mathcal{C}(\mathbf{r}) = \mathbf{s}$, $\mathbf{r} \in \mathcal{O}$, $\mathbf{r} = \{\mathbf{p}_k\}$ and $\mathbf{s} \in \mathcal{S}$, $\mathbf{s} = \{i_k\}$, such that i_k is the number of the component $D_{i_k} \in \mathcal{U}_L$ where the point \mathbf{p}_k lies.*

Proof. Evidently, for each bi-infinite orbit $\mathbf{r} \in \mathcal{O}$ of regular solution the image $\mathbf{s} = \mathcal{C}(\mathbf{r})$, $\mathbf{s} \in \mathcal{S}$ is defined uniquely. Let's prove that for each sequence $\mathbf{s} \in \mathcal{S}$ there exist unique orbit $\mathbf{r} \in \mathcal{O}$ such that $\mathbf{s} = \mathcal{C}(\mathbf{r})$.

Consider a sequence $\mathbf{s} = \{\dots, i_{-1}, i_0, i_1, \dots\}$. Let's find a location of the points $\mathbf{p} \in D_{i_0}$ such that $\mathcal{P}^{-1}(\mathbf{p}) \in D_{i_{-1}}$, $\mathcal{P}^{-2}(\mathbf{p}) \in D_{i_{-2}}$, etc. First of all, D_{i_0} is a γ_{i_0} -island, then it's an $h_{\gamma_{i_0}}$ -strip. Define an $h_{\gamma_{i_0}}$ -strip $H_{i_0} = D_{i_0}$ as a base step. From Hypothesis I we conclude that

$$d_h(H_{i_0}) \leq M. \quad (2.57)$$

Points $\mathbf{p} \in D_{i_0}$ such that $\mathcal{P}^{-1}(\mathbf{p}) \in D_{i_{-1}}$ are situated in the set $H_{i_{-1}, i_0} = \mathcal{P}(D_{i_{-1}}) \cap D_{i_0}$. Due to Hypothesis II set H_{i_{-1}, i_0} is an $h_{\gamma_{i_0, i_{-1}}}$ -strip. Its thickness satisfies an inequality

$$d_h(H_{i_{-1}, i_0}) \leq \mu^{-1} d_h(H_{i_0}) \leq \mu^{-1} M. \quad (2.58)$$

For simplicity define $\gamma = \max\{\gamma_{i_0}, \gamma_{i_0, i_{-1}}\}$.

Points $\mathbf{p} \in D_{i_0}$ such that $\mathcal{P}^{-1}(\mathbf{p}) \in D_{i_{-1}}$, $\mathcal{P}^{-2}(\mathbf{p}) \in D_{i_{-2}}$ are situated in the set $H_{i_{-2}, i_{-1}, i_0} = \mathcal{P}(H_{i_{-2}, i_{-1}}) \cap D_{i_0}$ where $H_{i_{-2}, i_{-1}} = \mathcal{P}(D_{i_{-2}}) \cap D_{i_{-1}}$. By Hypothesis II set

*We use the symbol \mathcal{C} for the homeomorphism since it reminds the overall process as “coding”.

$H_{i_{-2}, i_{-1}}$ is an h-strip. Hence, set H_{i_{-2}, i_{-1}, i_0} is an h_γ -strip and its thickness satisfies an inequality

$$d_h(H_{i_{-2}, i_{-1}, i_0}) \leq \mu^{-1} d_h(H_{i_{-2}, i_{-1}}) \leq \mu^{-2} d_h(D_{i_{-2}}) \leq \mu^{-2} M. \quad (2.59)$$

Continuation of that process leads us to the sequence of nested h_γ -strips similar to what we had in (2.54):

$$D_{i_0} = H_{i_0} \supseteq H_{i_{-1}, i_0} \supseteq H_{i_{-2}, i_{-1}, i_0} \supseteq \dots \quad (2.60)$$

Let's show that the infinite intersection of the h_γ -strips (2.60) is an h_γ -curve. Sequence of their thicknesses is bounded from above with a decreasing sequence $\{\mu^{-n} M\}$, $n = 0, 1, 2, \dots$. Value $\mu > 1$, so the limit $\lim_{n \rightarrow \infty} \mu^{-n} M = 0$. Now consider boundaries of the strips (2.54) as a functions of u . All of them are γ -Lipschitz functions. Their domains are different, but all of them lie inside the domain Δ , defined as

$$\Delta = \text{dom}(\alpha_{i_0}^+) \cup \text{dom}(\alpha_{i_0}^-), \quad (2.61)$$

where $\alpha_{i_0}^\pm$ are opposite boundaries of the first strip H_{i_0} . We can continue each α^\pm boundary of h-strips (2.54) onto the whole Δ . Let $\alpha_{i_{-k}, \dots, i_0}^\pm$ be a boundaries of an h-strip H_{i_{-k}, \dots, i_0} . They can be considered as a functions of u , $u' = h_{i_{-k}, \dots, i_0}^\pm(u)$ with the domains $\Delta_{i_{-k}, \dots, i_0}^\pm = [a_{i_{-k}, \dots, i_0}^\pm; b_{i_{-k}, \dots, i_0}^\pm]$, and we can define new functions

$$\tilde{h}_{i_{-k}, \dots, i_0}^\pm(u) = \begin{cases} h_{i_{-k}, \dots, i_0}^\pm(a_{i_{-k}, \dots, i_0}^\pm) & u < a_{i_{-k}, \dots, i_0}^\pm; \\ h_{i_{-k}, \dots, i_0}^\pm(u) & u \in \Delta_{i_{-k}, \dots, i_0}^\pm; \\ h_{i_{-k}, \dots, i_0}^\pm(b_{i_{-k}, \dots, i_0}^\pm) & u > b_{i_{-k}, \dots, i_0}^\pm. \end{cases} \quad (2.62)$$

Such extension allows us to treat boundaries of H_{i_{-k}, \dots, i_0} as functions of u with the same domain and consider them as a part of the space $C_\gamma(\Delta)$ of γ -Lipschitz functions defined on the interval Δ . Definition of the h-strip thickness coincide with the metric defined by the maximum norm, and $C_\gamma(\Delta)$ is a complete metric space [12]. Now consider the sequence

$$\{\tilde{h}_{i_0}^+(u), \tilde{h}_{i_0}^-(u), \tilde{h}_{i_{-1}, i_0}^+, \tilde{h}_{i_{-1}, i_0}^-, \dots, \tilde{h}_{i_{-k}, \dots, i_0}^+, \tilde{h}_{i_{-k}, \dots, i_0}^-, \dots\}. \quad (2.63)$$

Since $H_{i_{-k}, \dots, i_0} \subseteq H_{i_{-k+1}, \dots, i_0}$ and $d_h(H_{i_{-k}, \dots, i_0}) \rightarrow 0$ as $k \rightarrow \infty$, sequence (2.63) is a Cauchy sequence. Therefore, since $C_\gamma(\Delta)$ is a complete metric space, the Cauchy sequence converges to a unique curve $\tilde{h}_\infty(u)$ which represents an h_γ -curve inside the island D_{i_0} . Since we extend h -strips boundaries onto the whole Δ there may be other parts of $\tilde{h}_\infty(u)$ lying outside of D_{i_0} . Denote by α_∞ a part of $\tilde{h}_\infty(u)$ that entirely belongs to D_{i_0} . This curve is the intersection of the h_γ -strips (2.60) and is an h_γ -curve.

In the same manner a sequence of nested v_δ -strips can be constructed,

$$D_{i_0} = V_{i_0} \supseteq V_{i_0, i_1} \supseteq V_{i_0, i_1, i_2} \supseteq \dots \quad (2.64)$$

Their thicknesses are bounded from above with a decreasing sequence $\{\nu^{-n}N\}$, $n = 0, 1, 2, \dots$ of a zero limit, $\lim_{n \rightarrow \infty} \nu^{-n}N = 0$. Considering a corresponding sequence of δ -Lipschitz functions we conclude that the intersection of the strips (2.64) exists and is a v_δ -curve. Denote this curve by β_∞ .

The orbit $\mathbf{r} \in \mathcal{O}$ corresponding to the bi-infinite sequence $\{\dots, i_{-1}, i_0, i_1, \dots\}$ is generated by \mathcal{P} and \mathcal{P}^{-1} -iterations of the intersection $\alpha_\infty \cap \beta_\infty$ which according to the definitions of h - and v -curves *consists of one point*. Therefore orbit \mathbf{r} exists and is unique.

The continuity of \mathcal{C} and \mathcal{C}^{-1} maps follows from an observation that follows below. Since \mathcal{P} is continuous, if $\mathbf{r}^{(1)}, \mathbf{r}^{(2)} \in \mathcal{O}$,

$$\begin{aligned} \mathbf{r}^{(1)} &= \{\dots, \mathbf{p}_{-1}^{(1)}, \mathbf{p}_0^{(1)}, \mathbf{p}_1^{(1)}, \dots\}, \\ \mathbf{r}^{(2)} &= \{\dots, \mathbf{p}_{-1}^{(2)}, \mathbf{p}_0^{(2)}, \mathbf{p}_1^{(2)}, \dots\}; \end{aligned}$$

are close enough in \mathcal{O} (i.e. points $\mathbf{p}_0^{(1)}$ and $\mathbf{p}_0^{(2)}$ are close in \mathbb{R}^2), then their \mathcal{C} -images share the same central block $|k| < n$ for some n . Therefore they are also close in \mathcal{S} -topology. If $\mathbf{s}^{(1)} = \mathcal{C}(\mathbf{p}^{(1)})$ and $\mathbf{s}^{(2)} = \mathcal{C}(\mathbf{p}^{(2)})$ share the same central block $|k| < n$ for some n then the points $\mathbf{p}_0^{(1)}$ and $\mathbf{p}_0^{(2)}$ are situated in the same area $H_{i_{-k}, \dots, i_0} \cap V_{i_0, \dots, i_k}$, so $\mathbf{p}_0^{(1)}$ and $\mathbf{p}_0^{(2)}$ are close in \mathcal{O} -topology. Theorem is proven. \square

In order to apply Theorem to equation (2.1) one should get a strong evidence

that Hypotheses I and II are valid. However it's rather difficult to obtain a rigorous mathematical proof of them even for the simplest form of the functions $Q(x)$, $P(x)$ in (2.1), so in our current work we rely on computing procedures that provide a numerical evidence.

Hypothesis I seems to be pretty straightforward to check in a finite domain, since we can apply the scanning procedure and get a picture of the set \mathcal{U}_L . There may be two scenarios. The first scenario is when we can prove that the set \mathcal{U}_L is bounded within a finite domain, like the authors of the work [8] did for $P(x) \equiv -1$. Then one can apply a scanning procedure to that domain and thus provide a numerical evidence that Hypothesis I holds. The second scenario is when we cannot prove any statement on the boundaries and structure of \mathcal{U}_L , or this set is infinite and unbounded. We saw previously that for equation (2.12) the set \mathcal{U}_L is unbounded, so the set \mathcal{S}_∞ may contain sequences over an alphabet of infinite number of symbols. In that case we still can scan only a finite subset of the initial conditions plane. If the finite subset represents an island set then we can reduce our consideration to the finite subset of symbols $\mathcal{S}_N \subset \mathcal{S}_\infty$ and, if the Hypothesis II is also valid for that subset of \mathcal{U}_L , establish a homeomorphism between a subset of regular solutions and sequences from \mathcal{S}_N .

Hypothesis II as it is does not seem to be easily verifiable numerically. However it can be reduced to another two statements which admit numerical verification. These statements called Strips Mapping Theorems are formulated and proved in Appendix C. Shortly speaking, in order to check Hypothesis II one should analyse linear operators $D\mathcal{P}_{\mathbf{p}}$, $D\mathcal{P}_{\mathbf{p}}^{-1}$, which are represented by the Jacobi matrices of \mathcal{P} and \mathcal{P}^{-1} ,

$$\mathcal{P}(\mathbf{q}) = \mathcal{P}(\mathbf{p}) + D\mathcal{P}_{\mathbf{p}}(\mathbf{q} - \mathbf{p}) + o(||\mathbf{q} - \mathbf{p}||); \quad (2.65)$$

$$\mathcal{P}^{-1}(\mathbf{q}) = \mathcal{P}^{-1}(\mathbf{p}) + D\mathcal{P}_{\mathbf{p}}^{-1}(\mathbf{q} - \mathbf{p}) + o(||\mathbf{q} - \mathbf{p}||). \quad (2.66)$$

Such linear operators can be constructed numerically. If for an island set $\mathcal{U}_L = \bigcup_{i \in S} D_i$ matrix of the linear operator $D\mathcal{P}_{\mathbf{p}}$ in each point $\mathbf{p} \in \mathcal{P}^{-1}(D_j) \cap D_i$ satisfies

a specific structure established in Theorem 2 of Appendix C then Hypothesis II is valid for h-strips. On other hand if matrix of the linear operator $D\mathcal{P}_{\mathbf{p}}^{-1}$ in each point $\mathbf{p} \in \mathcal{P}^{-1}(D_i) \cap D_j$ satisfies a specific structure established in Theorem 3 of Appendix C then Hypothesis II is also valid for v-strips. Again we cannot apply our analysis to an infinite set \mathcal{U}_L . But we can reduce the task to the finite subset of the island set, provide numerical evidence, and establish a homeomorphism between a subset of regular solutions and sequences from \mathcal{S}_N .

We applied both of the above mentioned techniques to Eq. (2.12) with the parameters $(L_*, L_0) = (2, 1)$. We restricted our consideration by the first five central components $D_i, i \in \{-2, -1, 0, +1, +2\}$ of the island set \mathcal{U}_L (see Figure 2.9). Our numerical analysis shown that both Hypothesis I and II are valid, so Theorem 1 allows us to conclude that there exists a homeomorphism between a subset of regular solutions and the set \mathcal{S}_5 .

Such correspondence allows us to make conclusion on different types of regular solutions that equation (2.12) has. For example, there exist periodic solutions of a period nL for any number $n \in \mathbb{N}$. Their symbolic codes have a periodic structure $\{\dots, i_0, \dots, i_n, i_0, \dots, i_n, \dots\}$. There also exist localized solutions of different shapes. Their symbolic codes have a central block of non-zero symbols, and all other symbols on the left and right sides of this block are “0”, $\{\dots, 0, 0, i_0, \dots, i_n, 0, 0, \dots\}$. Regular solution of the domain wall shapes can also be found. They are coded with sequences which has “0” symbols only on the left or on the right side, $\{\dots, 0, 0, i_0, i_1, \dots\}$, $\{\dots, i_{-1}, i_0, 0, 0 \dots\}$.

Several periodic and localized solutions are presented in Figure 2.15. Numerical computation of solution by its code in a general case is a separate complex task. Nevertheless localized solutions can be found by the shooting method, and periodic solutions of a period nL can be found by solving the nonlinear equation $\mathbf{p} - \mathcal{P}^n(\mathbf{p}) = 0$, $\mathbf{p} \in \mathbb{R}^2$, with properly chosen initial approximation which can be guessed from the \mathcal{U}_L structure. It’s worth to mention here the paper [10] where authors provide an algorithm which allows to reconstruct the profile of localized solution by its code

for equation (2.1) with $P(x) \equiv -1$. Presumably an analogous technique can be applied for a periodic pseudopotential $P(x)$.

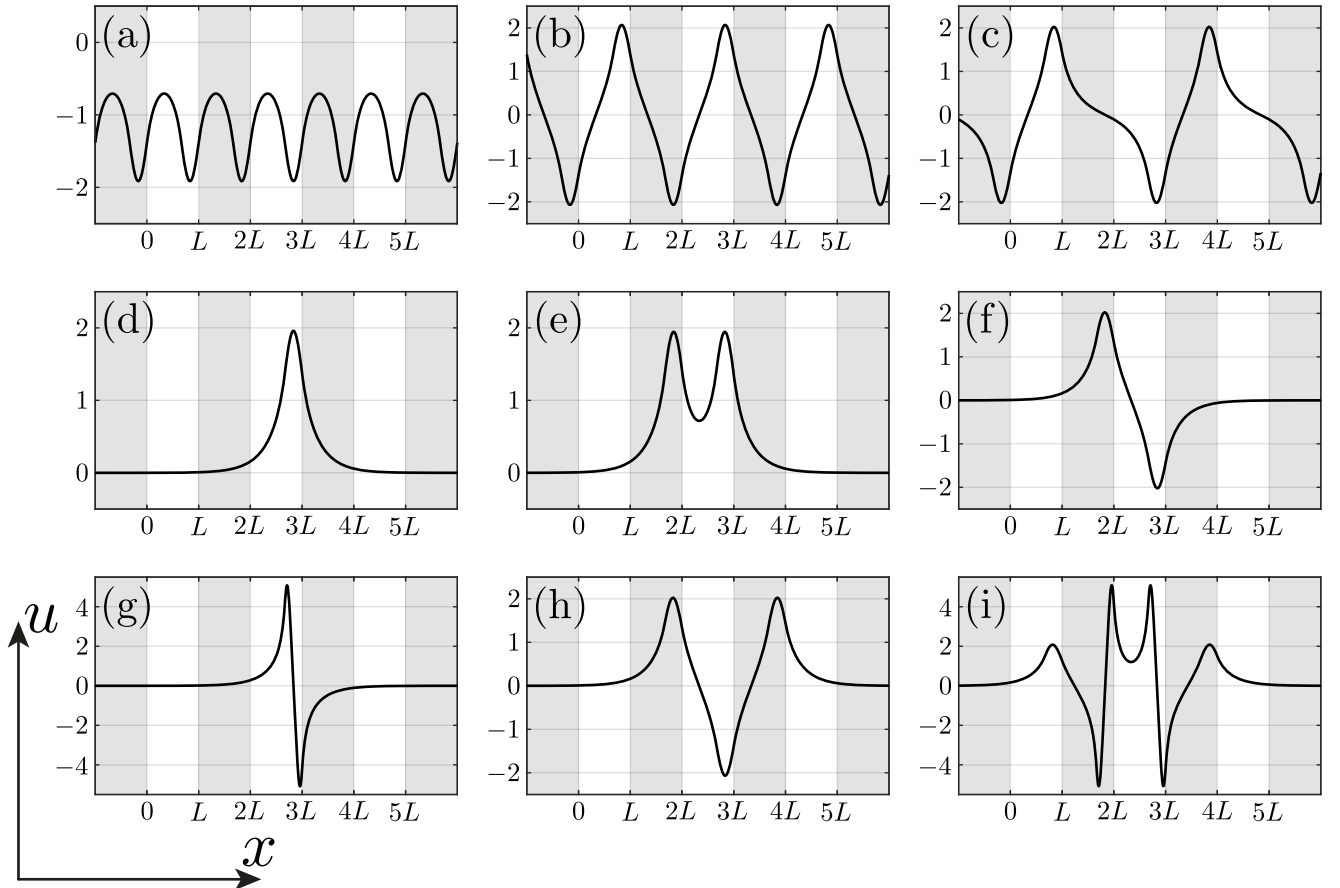


Figure 2.15. Different solutions for equation (2.12) with parameters $(L_*, L_0) = (2, 1)$. Each solution has a corresponding symbolic code, this code identify the solution uniquely. Gray strips divide the x axis according to the period L . First three panels represent periodic solutions, their codes have periodic structure: (a) L -periodic solution $\{\dots, -1, -1, -1, \dots\}$; (b) $2L$ -periodic solution $\{\dots, -1, +1, -1, +1 \dots\}$; (c) $3L$ -periodic solution $\{\dots, -1, +1, 0, -1, +1, 0 \dots\}$. Other six panels represent localized solutions, their codes have “0” symbol to the left and right of the central block: (d) $\{\dots, 0, 0, +1, 0, 0, \dots\}$; (e) $\{\dots, 0, 0, +1, +1, 0, 0, \dots\}$ (f) $\{\dots, 0, 0, +1, -1, 0, 0 \dots\}$ (g) $\{\dots, 0, 0, -2, 0, 0 \dots\}$ (h) $\{\dots, 0, 0, +1, -1, +1, 0, 0 \dots\}$ (i) $\{\dots, 0, 0, +1, +2, -2, +1, 0, 0 \dots\}$.

2.5. Summary

In this chapter the approach for classification of bounded solutions for equation (2.1) has been exposed. This approach is related to the analysis of the dynamics of Poincaré map \mathcal{P} on the set \mathcal{U}_L . It turns out that under some restrictions the

map \mathcal{P} is a horseshoe map with finite or infinite number of partitions. This allows us to establish a homeomorphism between orbits of regular solutions of (2.1) and symbolic sequences over some alphabet based on the structure of the set \mathcal{U}_L . We've formulated sufficient conditions for the existence of this homeomorphism in a form of two hypotheses. We've also shown how these hypotheses can be verified numerically and applied this approach to equation (2.12) with the simplest form of periodic pseudopotential $P(x)$.

On the example of equation (2.12) we show that the presence of sign-altering periodic pseudopotential results in the existence of a plethora of regular solutions. Such observation allows us to expect that similar variety of regular solutions is a common property for the overall class of equations (2.1).

Chapter 3

Localized Solutions of Gross-Pitaevskii Equation with Periodic Pseudopotential

3.1. Objectives

In this chapter we apply the coding approach to the Gross-Pitaevskii equation of the form

$$i\Psi_t + \Psi_{xx} - U(x)\Psi + P(x)|\Psi|^2\Psi = 0. \quad (3.1)$$

Here both potential $U(x)$ and pseudopotential $P(x)$ are periodic functions. Such equation occurs in physics of Bose-Einstein condensate (BEC) where periodical pseudopotential is achieved by means of the Feshbach resonance controlled by magnetic or optical fields [1–3]. Experimentally, the possibility of the periodic modulation of the nonlinearity was demonstrated in [13]. One can also find equation (3.1) in optics where spatial modulation of the Kerr coefficient can be achieved by means of inhomogeneous density of resonant nonlinearity-enhancing dopants implanted into the waveguide [4].

We are interested in stationary localized solutions of equation (3.1), also called as solitons in physical applications. Strictly speaking, the objects that we are going to study are not solitons in the mathematically rigorous meaning, but rather “solitary waves”, as they appear in a nonintegrable model. Nevertheless, the application of the word “soliton” to localized pulses in BECs is commonly adopted in physics literature, therefore we also use this word. Stationary solutions satisfy the ansatz $\Psi(t, x) = u(x)e^{i\omega t}$, where function $u(x)$ is a solution of equation

$$u_{xx} + Q(x)u + P(x)u^3 = 0, \quad Q(x) = -\omega - U(x). \quad (3.2)$$

Localized solutions satisfy the localization condition

$$\lim_{x \rightarrow \pm\infty} u(x) = 0, \quad (3.3)$$

which implies that the function $u(x)$ is real, see [14]. In what follows below we also assume that the potential $U(x)$ is absent, i.e. $U(x) \equiv 0$, so the effects produced by the periodic modulation of the nonlinearity are not obscured by the linear-lattice potential. Prototypical example of periodic pseudopotential is provided by a function

$$P(x) = \alpha + \cos 2x, \quad \alpha \in \mathbb{R}. \quad (3.4)$$

Resulting GPE equation takes form

$$i\Psi_t + \Psi_{xx} + (\alpha + \cos 2x)|\Psi|^2\Psi = 0, \quad (3.5)$$

where the period of pseudopotential function $P(x)$ is scaled to be $L = \pi$. Corresponding stationary state equation is

$$u_{xx} - \omega u + (\alpha + \cos 2x)u^3 = 0. \quad (3.6)$$

Equation (3.5) and (3.6) are the objects of our analysis during this chapter. The same model has been previously discussed in literature, see paper [15]. In [15] only single-peak localized solution, called *fundamental soliton* (FS), was studied in details. For that purpose authors used variational approximation method which requires initial guess of the solution shape. Such limitation does not allow to find more sophisticated localized solutions. By using of our coding technique we are going to reveal significantly wider class of stationary localized solutions of Eq. (3.5).

3.2. Coding of Solutions

Our approach requires the presence of singular solutions families. That's why according to Proposition 2 we assume that $\alpha \in (-1; 1)$, so that function $P(x)$ alternates its sign along the value x . We also assume that $\omega > 0$. This restriction comes from the obvious condition of the soliton localization, given by Eq.(3.3).

Let's introduce a Poincaré map $\mathcal{P} : \mathbb{R}^2 \rightarrow \mathbb{R}^2$ associate with equation (3.6) in the same way we did it before in (2.2) assuming $L = \pi$. Poincaré map \mathcal{P} and its

inverse \mathcal{P}^{-1} is not defined in the whole plane (u, u') of initial conditions. We can construct their domains using the scanning technique introduced in Chapter 2. Sets \mathcal{U}_π^+ and \mathcal{U}_π^- for different parameters (ω, α) are presented in Figure 3.1. Numerical results allow us to conclude that the sets \mathcal{U}_π^\pm are unbounded spirals with infinite number of rotations around the origin, similar to what we saw previously for equation (2.12). According to the Proposition 4 these sets are related with a reflection with respect to the u' axis, i.e. $\mathcal{U}_\pi^- = I\mathcal{U}_\pi^+$. Their thicknesses depend on the parameter α . If these sets are thin enough their intersection $\mathcal{U}_\pi = \mathcal{U}_\pi^+ \cap \mathcal{U}_\pi^-$ form an island set. In Figure 3.1 panels (a), (b), and (c) resulting set \mathcal{U}_π cannot be regarded as island set. In panel (d) \mathcal{U}_π is a seven-component island set in the scanning area.

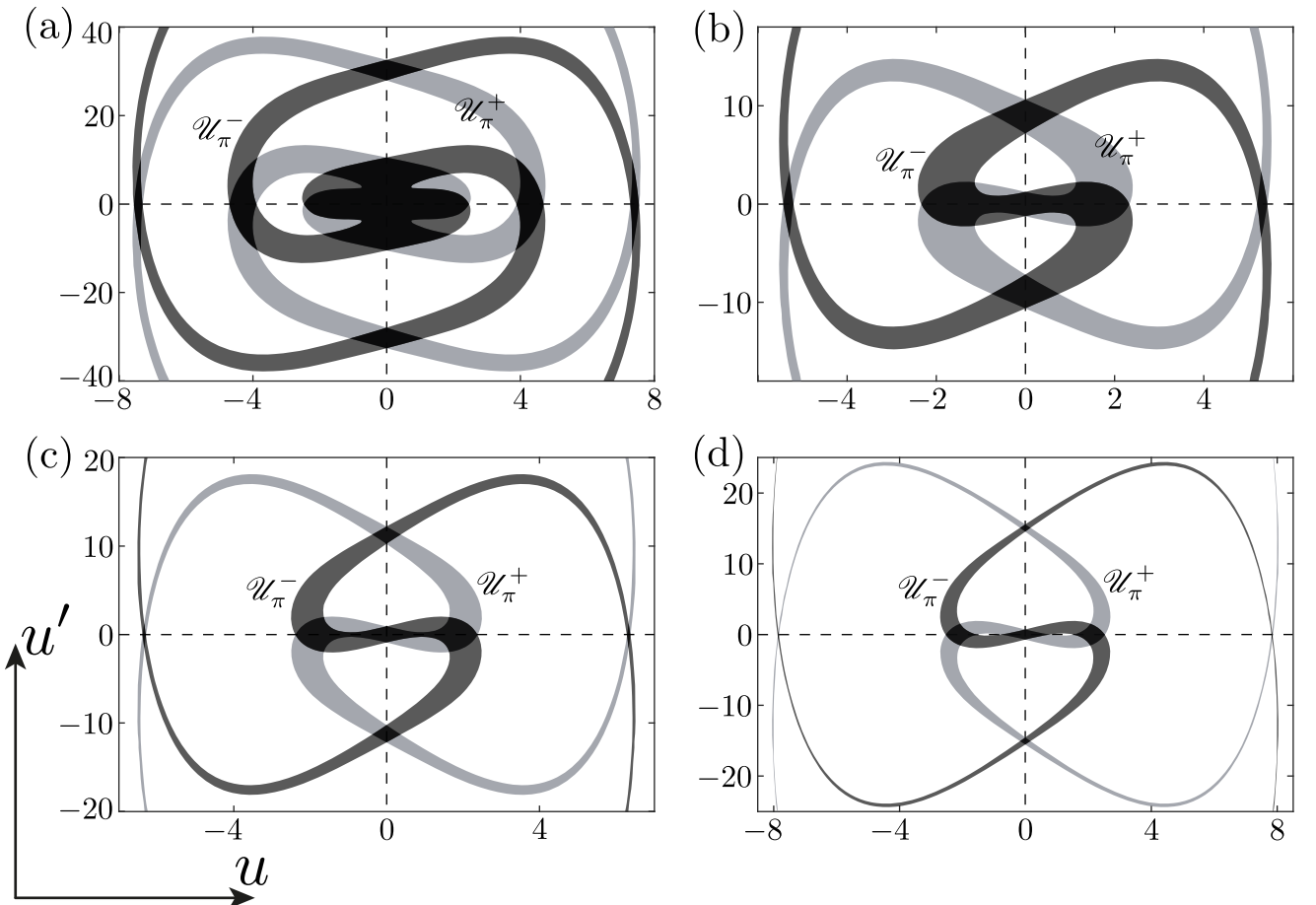


Figure 3.1. Sets \mathcal{U}_π^+ (light gray), \mathcal{U}_π^- (dark gray), and their intersection $\mathcal{U}_\pi = \mathcal{U}_\pi^+ \cap \mathcal{U}_\pi^-$ (black) for equation (3.6) with different parameters (ω, α) . Panel (a): $(\omega, \alpha) = (1, 0.6)$; panel (b): $(\omega, \alpha) = (1, 0.3)$; panel (c): $(\omega, \alpha) = (1, 0.1)$; panel (d): $(\omega, \alpha) = (1, -0.1)$. On panels (a), (b), and (c) intersection \mathcal{U}_π doesn't form an island set due to the central connected component. On panel (d) seven connected components of \mathcal{U}_π form an island set.

Presence of the island set structure is a first required step of our coding technique. In Chapter 2 we established two hypotheses which must be valid, so the conditions of Theorem 1 take place. Let's focus on the case $(\omega, \alpha) = (1.5, 0)$. We restrict the scanning area in plane (u, u') of initial conditions by seven components of \mathcal{U}_π . The set \mathcal{U}_π is depicted in Figure 3.2. From that picture we conclude that Hypothesis I holds since each connected component of \mathcal{U}_π represent a curvilinear quadrangle with monotonic boundaries, and each boundary satisfies the conditions from Definition 4. The connected components can be enumerated with symbols $\{D_k\}$, $k = \pm 1, \pm 2, \dots$ for the components along the u axis, and $k = \pm 1i, \pm 2i, \dots$ for the components along the u' axis. The central component is denoted by D_0 . Applying this notation for the seven-component island set from Figure 3.2 we have $\mathcal{U}_\pi = \bigcup_{k \in S_7} D_k$, $S_7 = \{-2, -1i, -1, 0, +1, +1i, +2\}$.

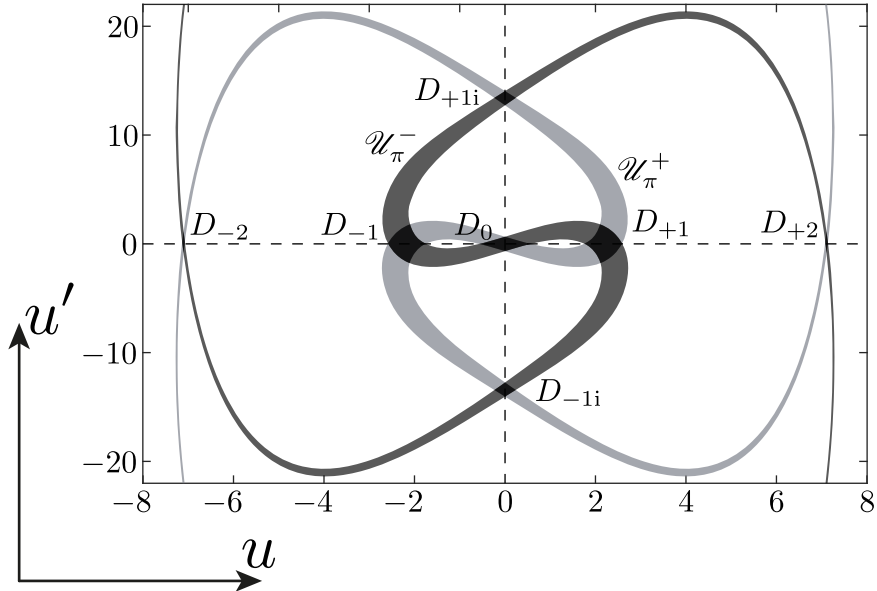


Figure 3.2. Seven-component island set $\mathcal{U}_\pi = \bigcup_{k \in S_7} D_k$ (black) formed by the intersection of \mathcal{U}_π^\pm for equation (3.6) with parameters $(\omega, \alpha) = (1.5, 0)$.

To check Hypothesis II we use the numerical procedure described in Chapter 2 which relies on Strips Mapping Theorems from Appendix C. Since set \mathcal{U}_π is symmetric with respect to the u and u' axis we can check Hypothesis II only for four islands: D_0 , D_{+1} , D_{+2} , and D_{+1i} . For each island D_k we introduce a grid of values for numerical computations like we do it during the scanning procedure. Using that

grid we compute sets $H_{i,k} = \mathcal{P}(D_i) \cap D_k$ and sets $V_{k,i} = \mathcal{P}^{-1}(D_i) \cap D_k$, where $i \in S_7$. In each point $\mathbf{p} \in V_{k,i}$ we construct a matrix of the 2-dimensional linear operator $D\mathcal{P}_{\mathbf{p}} = (a_{mn})$. Then we analyse signs of (a_{mn}) . For each set $V_{k,i}$ sings of (a_{mn}) must have exactly one configuration specified in Theorem 2. For each island D_k we also compute a numerical estimation of the lower boundary of $|a_{11}|$ values, denote it by μ_* . Corresponding histograms of $|a_{11}|$ values in logarithmic scale are presented in Figure 3.3 along with their lower boundary μ_* for each island. Value μ_* is the numerical estimation of the value μ from Theorem 2. If the signs of values (a_{mn}) computed for $V_{k,i}$ sets satisfy the conditions of Theorem 2 and the overall estimation $\mu_* > 1$ takes place, we conclude that Hypothesis II holds true for h-strips.

Similarly, for each set $H_{i,k}$ we construct a matrix of the linear operator $D\mathcal{P}_{\mathbf{p}}^{-1} = (b_{mn})$ in each point $\mathbf{p} \in H_{i,k}$. We perform an estimation of the lower boundary of the values $|b_{22}|$, denote the estimated value by ν_* . If $\nu_* > 1$ and the signs of values (b_{mn}) computed for $H_{i,k}$ sets satisfy the conditions of Theorem 3, we conclude that Hypothesis II holds true for v-strips as well.

Complete results of our numerical analysis are presented in Figure 3.3. Let's provide several examples on how this picture should be treated. Consider an island D_{+1} . Operator $D\mathcal{P}_{\mathbf{p}} = (a_{mn})$ is computed in each point of the set $V_{+1,0}$ and has signs configuration $(\begin{smallmatrix} - & + \\ + & - \end{smallmatrix})$ on the whole $V_{+1,0}$, i.e. $a_{11} < 0, a_{12} > 0, a_{21} < 0, a_{22} > 0$. Boundaries α_{+1}^{\pm} of the island D_{+1} are the parts of boundaries of \mathcal{U}_π^- and have the form of decreasing curves, see Figure 3.3 (b). Boundaries α_0^{\pm} of the island D_0 are increasing curves. It means that condition (2d) of Theorem 2 takes place for a pair of islands D_{+1} and D_0 . For the sets $V_{k,i}$ all the values $|a_{11}| \geq \mu_* > 1$. Thus, according to Theorem 2 we can conclude that for any h-strip $H \in D_{+1}$ its \mathcal{P} -image $\tilde{H}_0 = \mathcal{P}(H) \cap D_0$ is also as h-strip and $d_h(\tilde{H}_0) \leq (1/\mu_*)d_h(H)$.

For another example let's consider a pair of islands D_{+1i} and D_{+2} . Operator $D\mathcal{P}_{\mathbf{p}}^{-1} = (b_{mn})$ has sings configuration of the form $(\begin{smallmatrix} - & - \\ + & + \end{smallmatrix})$ for all $\mathbf{p} \in H_{+1i,+2}$. Boundaries β_{+1i}^{\pm} of the island D_{+1i} are decreasing curves, and boundaries β_{+2}^{\pm} of the island D_{+2} are increasing. Estimations $\nu_* > 1$ takes place for all the sets $H_{i,k}$. Thus, con-

dition (1d) of Theorem 3 is satisfied which implies that and for any v-strip $V \in D_{+2}$ its \mathcal{P} -pre-image $\tilde{V}_{+1i} = \mathcal{P}^{-1}(V) \cap D_{+1i}$ is also a v-strip and $d_v(\tilde{V}_{+1i}) \leq (1/\nu_*) d_v(V)$. Other sets $H_{i,k}$, $V_{k,i}$ are considered in a similar way. According to the numerical computations Theorems 2 and 3 are valid for all islands D_k , $k \in S_7$.

The procedure described above provides a numerical evidence for Hypotheses I and II. That allows us to apply Coding Theorem and conclude that for Eq. (3.6) there exists a homeomorphism $\mathcal{C} : \mathcal{O}_7 \rightarrow \mathcal{S}_7$ between a subset of orbits of bounded solutions, denoted by \mathcal{O}_7 , and a set \mathcal{S}_7 of bi-infinite sequences of symbols from alphabet $S_7 = \{-2, -1i, -1, 0, +1, +1i, +2\}$. Orbits of such solutions may visit only islands D_k , where $k \in S_7$. Moreover there is no any other bounded solution which orbit visits only these seven islands. The numerical results from above can be extended to a larger island set, although it requires significant computing capacities.

Existence of the homeomorphism allows to make a conclusion on the structure of bounded solutions of Eq. 3.6 For example Eq. 3.6 admits periodic solution of period $n\pi$ for any number $n \in \mathbb{N}$. Several periodic solutions are presented in Figure 3.4, π -periodic solution in panel (a), and 2π -periodic solutions in panels (b) and (c). There also exists a plethora of soliton solutions. The orbit corresponding to the soliton solution starts and ends in the central connected components; therefore, it has the code of the form $\{\dots, 0, 0, k_1, k_2, \dots, k_N, 0, 0, \dots\}$, where symbols k_1 and k_N are different from “0”. Some of the soliton solutions of (3.6) for $(\omega, \alpha) = (1.5, 0)$ are shown in Figure 3.4, panels (d) — (i). The soliton solution in panel (d) is the fundamental soliton (FS) that has been already studied in [15]. It has code $\{\dots, 0, +1, 0, \dots\}$, or $\{\dots, 0, -1, 0, \dots\}$ which is its symmetric counterpart.

Other types of localized solutions have been also found. For example, solution, shown in panel (e), represents a so-called *dipole soliton* (DS) [16], which is essentially confined to a single period of pseudopotential $P(x)$. This solution corresponds to code $\{\dots, 0, -1i, 0, \dots\}$, and its symmetric counterpart is $\{\dots, 0, +1i, 0, \dots\}$. DS is similar to *sub-fundamental solitons* (SFSs) reported in [17–20] in models with the linear lattice potential $U(x)$, as both soliton species feature the antisym-

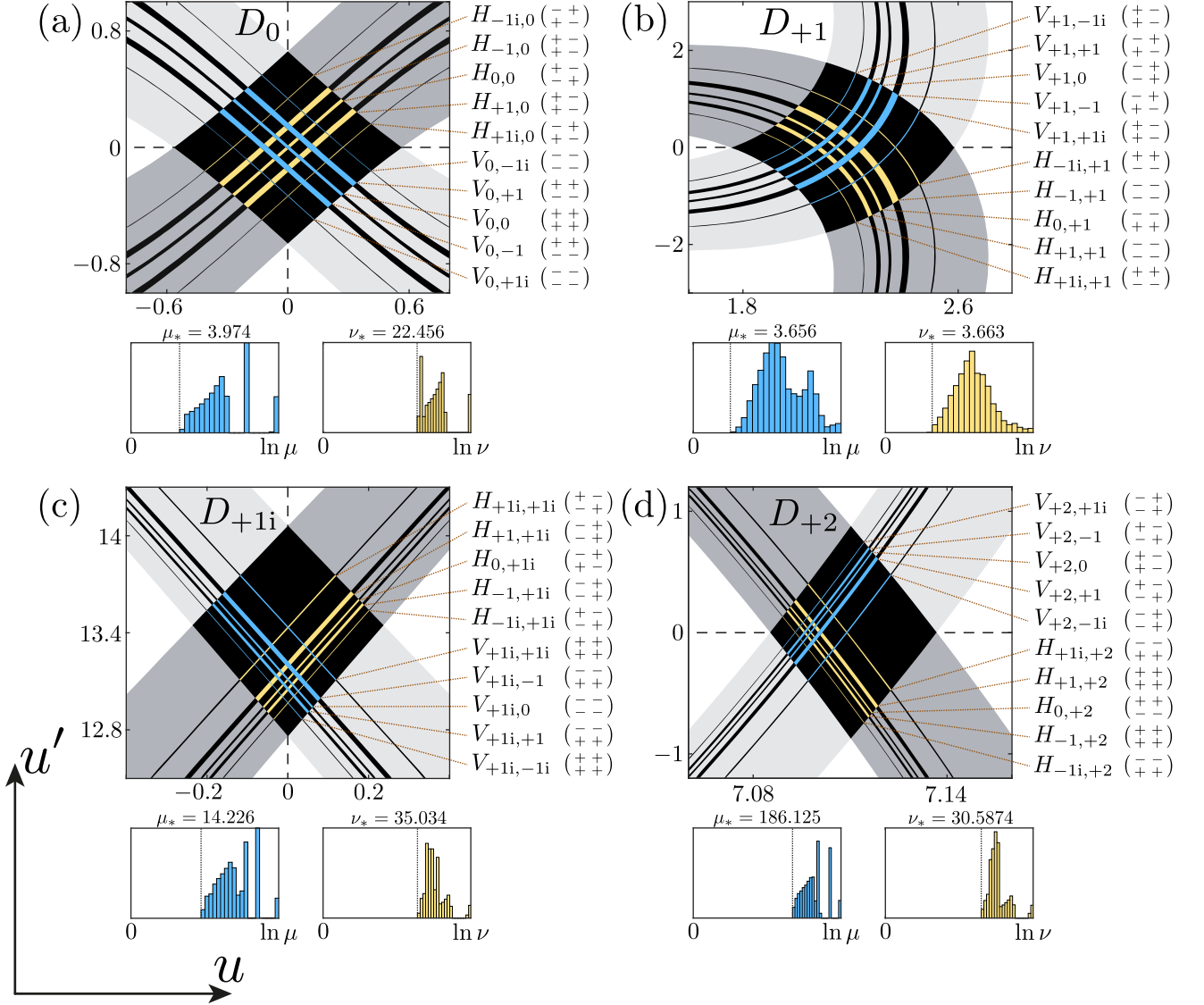


Figure 3.3. Illustration to Hypothesis II validation for equation (3.6) with parameters $(\omega, \alpha) = (1.5, 0)$. Islands D_k are black curvilinear quadrangles with monotonic boundaries. Boundaries of the set \mathcal{U}_π^+ (light gray) contains β_k^\pm boundaries for each island D_k ; boundaries of \mathcal{U}_π^- (dark gray) contains α_k^\pm boundaries correspondingly. Estimations of μ_* and ν_* values are shown with histograms below each island. Configuration of value signs in operators $D\mathcal{P}_{\mathbf{p}} = (a_{mn})$, $\mathbf{p} \in V_{k,i}$ (blue), and $D\mathcal{P}_{\mathbf{p}}^{-1} = (b_{mn})$, $\mathbf{p} \in H_{i,k}$ (yellow) are shown from the right side of each island D_k . All of them satisfy the conditions of Theorem 2 (On h-strip mapping) and Theorem 3 (On v-strips mapping) from Appendix C. Sets $H_{+2,k}$ and $V_{k,+2}$ are not depicted since they are too thin and barely visible at this scale, but all the computations have been also provided for them and the overall result satisfies the above mentioned theorems as well.

metric profile squeezed into a single cell of the underlying lattice potential (ordinary potential $U(x)$, in the case of SFS, and the pseudopotential $P(x)$, as concerns the DS). The area of the localization of the soliton corresponding to code

$\{\dots, 0, k_1, \dots, k_N, 0, \dots\}$, where the symbols k_1 and k_N are different from “0”, is $N\pi$, i.e. it extends over N periods of the underlying pseudopotential $P(x)$. In particular, the solitons with codes $\{\dots, 0, k, 0, \dots\}$, $k \neq 0$ (named *elementary solitons*), are localized, essentially, in one period of the pseudopotential.

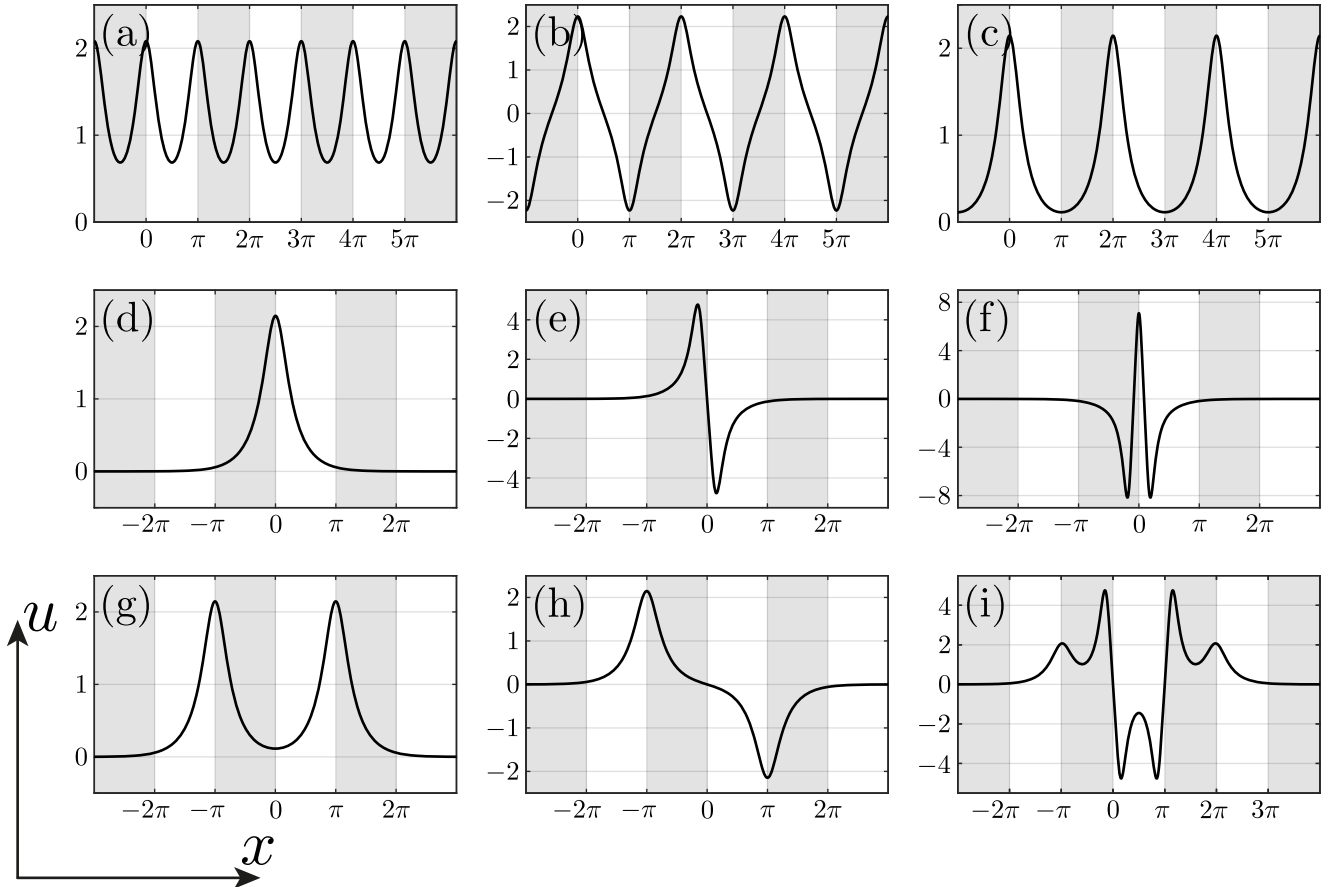


Figure 3.4. Different solutions for equation (3.6) with parameters $(\omega, \alpha) = (1.5, 0)$. Each solution has a corresponding symbolic code, this code identify the solution uniquely. Gray strips divide the x axis according to the period π . First three panels represent periodic solutions, their codes have periodic structure: (a) π -periodic solution $\{\dots, +1, +1, +1, \dots\}$; (b) 2π -periodic solution $\{\dots, +1, -1, +1, -1, \dots\}$; (c) 2π -periodic solution $\{\dots, +1, 0 + 1, 0, \dots\}$. Other six panels represent localized solutions, their codes have “0” symbol to the left and right of the central block: (d) fundamental soliton with code $\{\dots, 0, +1, 0, \dots\}$; (e) dipole soliton with code $\{\dots, 0, -1i, 0, \dots\}$ (f) elementary soliton with code $\{\dots, 0, +2, 0, \dots\}$ (g) $\{\dots, 0, +1, 0, +1, 0, \dots\}$ (h) $\{\dots, 0, +1, 0, -1, 0, \dots\}$ (i) $\{\dots, 0, +1, -1i, +1, \dots\}$.

3.3. Analysis of Stability

Stability is a critically important issue for stationary localized solutions. By stability of localized stationary solution we mean its resistance to small perturbations. From the perspective of real physical experiments only stable solutions can be obtained in a real experimental setup. Here we address the stability of stationary localized solutions produced by Eq. (3.5). Let $u(x)$ be a solution if Eq. (3.6). Following the well-established approach, see e.g. [21], let's consider small perturbations around a solution $u(x)$ of the form

$$\Psi(t, x) = \left(u(x) + \tilde{U}(t, x) \right) e^{i\omega t}; \quad |\tilde{U}(t, x)| \ll 1, \quad (3.7)$$

where $\tilde{U}(t, x)$ is a complex-valued function. Then the perturbation $\tilde{U}(t, x)$ satisfies the linear equation

$$i\tilde{U}_t + \tilde{U}_{xx} - \omega\tilde{U} + (\alpha + \cos 2x)u^2(2\tilde{U} + \tilde{U}^\dagger) = 0. \quad (3.8)$$

Here dagger “ \dagger ” means complex conjugate. Seeking solutions to (3.8) as

$$\tilde{U}(t, x) = (a(x) + w(x))e^{\lambda t} + (v^\dagger(x) - w^\dagger(x))e^{\lambda^\dagger t}; \quad \lambda \in \mathbb{C}, \quad (3.9)$$

we arrive at the eigenvalue problem

$$i \begin{pmatrix} 0 & \partial_{xx} + G_1(x) \\ \partial_{xx} + G_2(x) & 0 \end{pmatrix} \begin{pmatrix} v \\ w \end{pmatrix} = \lambda \begin{pmatrix} v \\ w \end{pmatrix}, \quad (3.10)$$

where

$$G_1(x) = -\omega + (\alpha + \cos 2x)u^2;$$

$$G_2(x) = -\omega + 3(\alpha + \cos 2x)u^2.$$

Equation (3.10) is the linear-stability eigenvalue problem for the soliton. Its λ -spectrum is called the linear-stability spectrum for this soliton. The soliton is linearly stable if the spectrum produced by Eq. (3.10) contains at least one eigenvalue λ with a non-zero real part, $\Re(\lambda) > 0$. Otherwise, the soliton is linearly unstable.

Equation (3.10) generates spectrum consisting of continuous and discrete parts. One can show, see e.g. [21], that the continuous spectrum is represented by two rays, $[i\omega; +i\infty)$ and $(-i\infty; -i\omega]$, if $\omega > 0$, and by the whole imaginary axis, if $\omega < 0$. The discrete spectrum includes zero eigenvalue $\lambda = 0$. It is easy to see that other eigenvalues of discrete spectrum of Eq. (3.10) have the following symmetry properties: if λ is an eigenvalue, then so are λ^\dagger , $-\lambda$, and $-\lambda^\dagger$. This means that these eigenvalues always appear in pairs or quadruples.

3.3.1. Fourier Collocation Method

To find discrete eigenvalues numerically we use so-called Fourier Collocation Method (FCM) described in [21]. This method is very efficient to find *exponential instabilities* that appear due to real eigenvalues. We also say that solution *oscillatory unstable* if the spectrum has quartets of complex with non-zero real parts.

To apply FCM, we first truncate the infinite x -axis into a finite interval into a finite interval $[-L/2; L/2]$, where L is the length of the interval. Length of the interval is considered to be large enough to cover soliton solution localization well. On this interval we expand the eigenfunctions $[v(x); w(x)]^T$ and functions G_1 , G_2 into Fourier series:

$$\begin{aligned} v(x) &= \sum_n a_n e^{ink_0 x}; & w(x) &= \sum_n b_n e^{ink_0 x}, \\ G_1 &= \sum_n c_n^{(1)} e^{ink_0 x}; & G_2 &= \sum_n c_n^{(2)} e^{ink_0 x}, \end{aligned}$$

where $k_0 = 2\pi/L$. After substitution of (3.11) and (3.11) into (3.10), we have the following eigenvalue system fro the coefficients a_j , b_j :

$$-(k_0 j)^2 b_j + \sum_n c_n^{(1)} b_{j-n} = -i\lambda a_j; \quad (3.11)$$

$$-(k_0 j)^2 a_j + \sum_n c_n^{(2)} a_{j-n} = -i\lambda b_j, \quad (3.12)$$

where $-\infty < j < +\infty$. Truncating the number of Fourier modes to $-N \leq j \leq N$, this infinite-dimensional eigenvalue problem can be reduced to the finite-dimensional

one:

$$i \begin{pmatrix} 0 & D + C_1 \\ D + C_2 & 0 \end{pmatrix} \begin{pmatrix} A \\ B \end{pmatrix} = \lambda \begin{pmatrix} A \\ B \end{pmatrix}, \quad (3.13)$$

where

$$D = (ik_0)^2 \text{diag}(-N, -N+1, \dots, N-1, N)^2;$$

$$A = (a_{-N}, a_{-N+1}, \dots, a_N)^T; \quad B = (b_{-N}, b_{-N+1}, \dots, b_N)^T,$$

and matrices C_1, C_2 are of the form of Toeplitz matrices

$$C_{1,2} = \begin{pmatrix} c_0^{(1,2)} & c_{-1}^{(1,2)} & \cdots & c_{-N}^{(1,2)} & 0 & \cdots & 0 \\ c_1^{(1,2)} & c_0^{(1,2)} & c_{-1}^{(1,2)} & \ddots & \ddots & \ddots & \vdots \\ \vdots & c_1^{(1,2)} & c_0^{(1,2)} & c_{-1}^{(1,2)} & \ddots & \ddots & 0 \\ c_N^{(1,2)} & \ddots & \ddots & \ddots & \ddots & \ddots & c_{-N}^{(1,2)} \\ 0 & c_N^{(1,2)} & \ddots & \ddots & \ddots & \ddots & \vdots \\ \vdots & \ddots & \ddots & \ddots & \ddots & \ddots & \vdots \\ 0 & \cdots & 0 & c_N^{(1,2)} & \cdots & c_1^{(1,2)} & c_0^{(1,2)} \end{pmatrix}. \quad (3.14)$$

The matrix eigenvalue problem (3.13) can be solved by any matrix eigenvalue problem solver. Solution of the eigenvalue problem gives $2N + 1$ eigenvalues. In our computations we used $N = 256$ and $N = 512$ and got nearly identical spectrums. From the practical point of view for the linear-stability analysis the number of Fourier modes can be relatively small, since eigenvalues for the higher modes have zero real part.

3.3.2. Evolutionary Simulation

To control linear-stability analysis and get additional confidence in stability of localized solutions we also performed a numerical simulation of their evolution. For that purpose Trofimov-Peskov finite-difference scheme [22] for numerical solution of the Gross-Pitaevskii (3.1) equation was used. The scheme preserves several

invariants of the problem: the norm of the solution

$$N = \int_{-\infty}^{+\infty} |u(x)|^2 dx, \quad (3.15)$$

and its energy

$$E = \int_{-\infty}^{+\infty} \left(|u'(x)|^2 + U(x)|u(x)| - \frac{1}{2}P(x)|u(x)|^4 \right) dx. \quad (3.16)$$

The scheme is implicit, its realization implying iterations for the calculation of values in each temporal layer, but it allows running computation with larger temporal step. In order to reveal instability (if it is), the soliton profile was perturbed at the initial moment with a small perturbation. A finite spatial domain $[-5\pi; 5\pi]$ was used, with reflection of radiation from boundaries eliminated by means of absorbing boundary conditions. During our analysis we got consistent results between the linear stability and evolutionary simulation.

3.3.3. Results of Linear Stability Analysis

With the help of FCM, a great number of localized stationary solutions of equation (3.5), represented by different codes, were analyzed. Due to the infinite number of essentially different solitons, it's not possible to perform a comprehensive stability analysis of all localized solutions. However, we observed that a majority of the solitons are linearly unstable, thus being physically irrelevant solutions. *Stable solitons* can be categorized as follows:

- (a) among the elementary solitons, it was found that FS and DS are *linearly stable*, under some restrictions on parameters ω and α , while other elementary solitons were found to be unstable;
- (b) there are stable localized solutions of the form of FS complexes — for instance, with codes $\{\dots, 0, +1, -1, +1, 0, \dots\}$ and $\{\dots, +1, 0, -1, 0, \dots\}$.

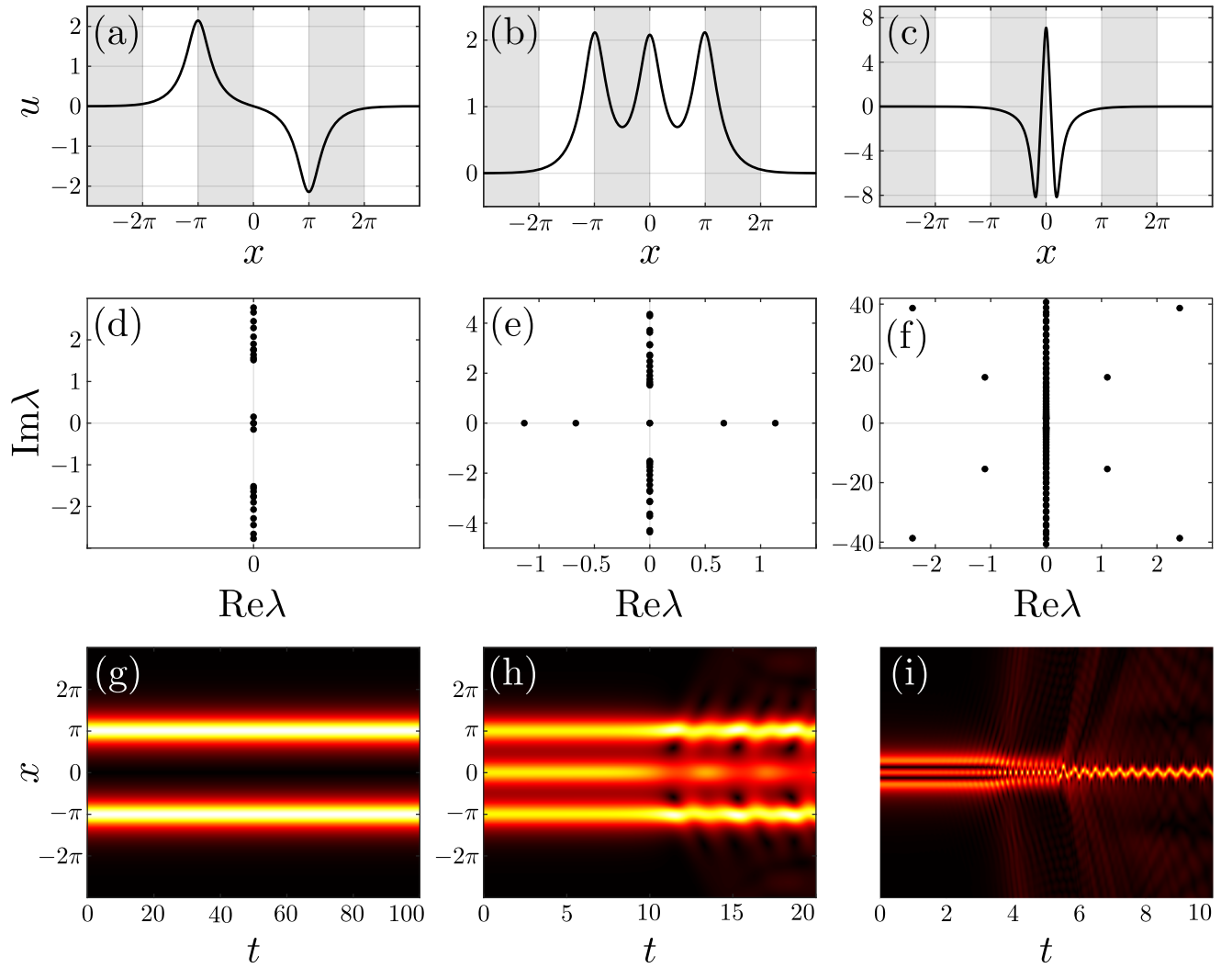


Figure 3.5. Examples of stability analysis for localized solutions of equation (3.5) with parameters $(\omega, \alpha) = (1.5, 0)$. First three panels represent profiles of solutions of different codes: (a) $\{\dots, 0, +1, 0, -1, 0, \dots\}$; (b) $\{\dots, 0, +1, +1, +1, 0, \dots\}$; (c) $\{\dots, 0, +2, 0, \dots\}$. Panels (d), (e), and (f) are the corresponding λ -spectrums for the solutions above. According to them, solution in panel (a) is linearly stable. Solution in panel (b) is exponentially unstable, while solution in panel (c) is oscillatory unstable. Linear-stability analysis match the results of evolutionary simulation presented in panel (g), (h), and (i).

Several localized solution, their linear-stability spectrums, and corresponding results of evolutionary simulation are in Figure 3.5. Panel (a) corresponds to a stable localized solution of code $\{\dots, 0, +1, 0, -1, 0, \dots\}$. Such solution can be considered as a combination of two FSs of codes $\{\dots, 0, +1, 0, \dots\}$ and $\{\dots, 0, -1, 0, \dots\}$. Another similar combination of code $\{\dots, 0, +1, +1, +1, 0, \dots\}$ in panel (b) is unstable. Elementary soliton of code $\{\dots, 0, +2, 0, \dots\}$ from panel (c) is unstable as

well as any other elementary solitons except of FS and DS. Other examples can be found in our work [16].

Combination of coding technique and linear-stability analysis together give a powerful tool of visualization of stationary localized solutions stability for equation of type (3.1) with periodic potential and pseudopotential. If it's possible to find such parameters that the Theorem 1 is applicable, then for these parameters we can apply coding and describe at least a huge subset of bounded solutions. After that one can vary one of the parameters using a numerical grid and perform a numerical continuation for the described solutions to the non-coding area of parameters. During the numerical continuation of solutions we can compute linear-stability spectrums in each point of the parameters grid. Then we can parametrized the obtained solutions, for example using their norm (3.15), plot the branches of different solution families and color the stability regions.

Illustration of the described idea for Eq. (3.5) is presented in Figure 3.6. In that figure several branches of solutions are depicted in (N, ω) axes, while parameter $\alpha = 0$. Regions of linear stability are marked with bold black lines. One can see that FS solution of code $\{\dots, 0, \pm 1, 0, \dots\}$, branch (I), and solution of code $\{\dots, 0, \pm 1, 0 \mp 1, 0, \dots\}$, branch (II), are mostly stable and loose their stability near the point $\omega = 0$. Dipole soliton, branch (IV), exists for $\omega > \omega^*$ and has an ω -region of stability. At $\omega^* \approx 0.265$, the DS family, coded by $\{\dots, 0, \pm 1i, 0, \dots\}$, undergoes a saddle-node bifurcation and annihilate with the family coded by $\{\dots, 0, \mp 1, \pm 1i, \pm 1, 0, \dots\}$.

Stable Dipole Soliton

As an outcome of our analysis for physical applications, the most significant finding is the existence of stable DS family, which was not previously considered in the setting of GPE with periodic pseudopotential. Existence of such family is also predicted by variational approximation method, [16]. The DS family may be parametrized by ω . The norm of the DS grows with the growth of ω . Although the DS is very similar, in its shape, to the sub-fundamental solitons in systems with

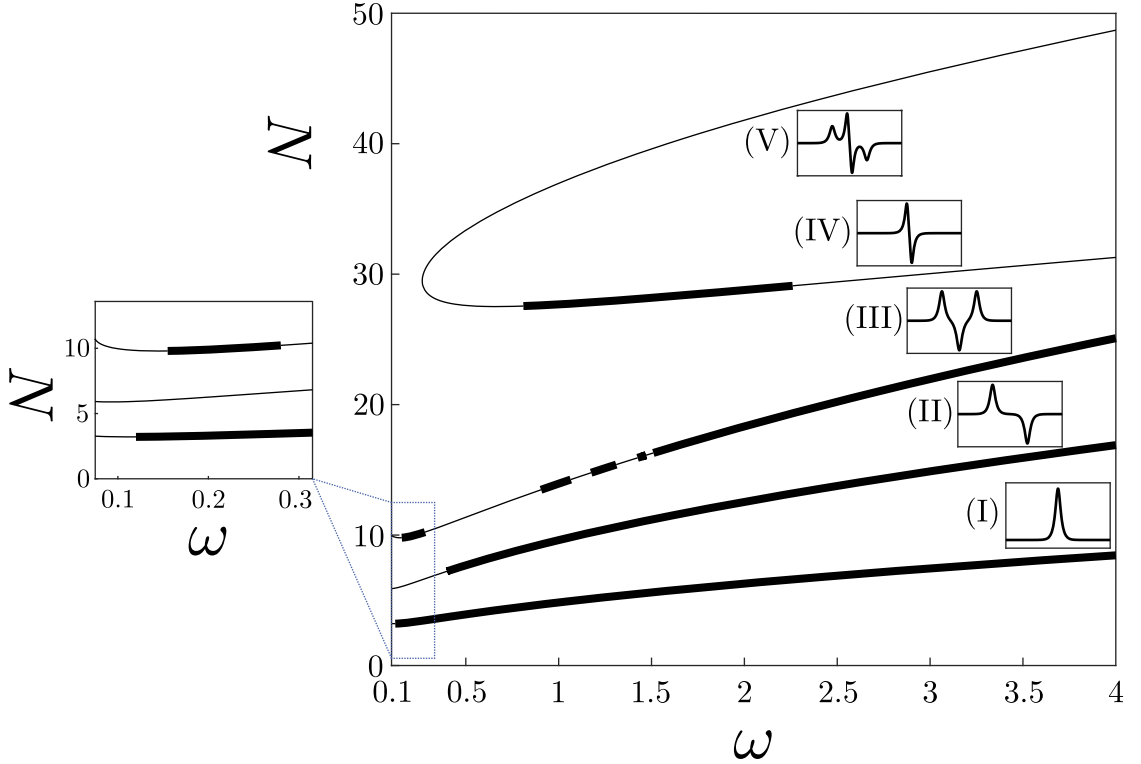


Figure 3.6. Branches of solutions for Eq. (3.5) and their linear stability. Branch (I) represent fundamental soliton family of code $\{\dots, 0, \pm 1, 0, \dots\}$. Branches (II) and (III) are FS complexes of codes $\{\dots, \pm 1, 0, \mp 1, 0, \dots\}$ and $\{\dots, \pm 1, \mp 1, \pm 1, 0, \dots\}$ correspondingly. Dipole soliton family of code $\{\dots, 0, \pm 1i, 0, \dots\}$ is presented by the branch (IV). It coalesces at $\omega = \omega^*$ with family $\{\dots, 0, \mp 1, \pm 1i, \pm 1, 0, \dots\}$ of branch (V). Linear stability regions are colored with bold black lines.

periodic potential, the DS in the present model is not sub-fundamental, as its norm is *higher* than that of the FS existing for the same ω , see Figure 3.6. Evolutionary simulation showed that if for some ω the DS is unstable, then it transforms into the FS after some time. An example of that is provided in Figure 3.7.

3.4. Summary

In this chapter we studied stationary solutions of Gross–Pitaevskii equation (3.1) with presence of periodic pseudopotential $P(x)$ of the cosine form (3.4), while potential $U(x)$ is absent. We focused on localized solutions as they are of particular interest for physical experiments. Periodicity of pseudopotential $P(x)$ allowed us to apply coding technique from Chapter 2. We provided a numerical evidence for Hy-

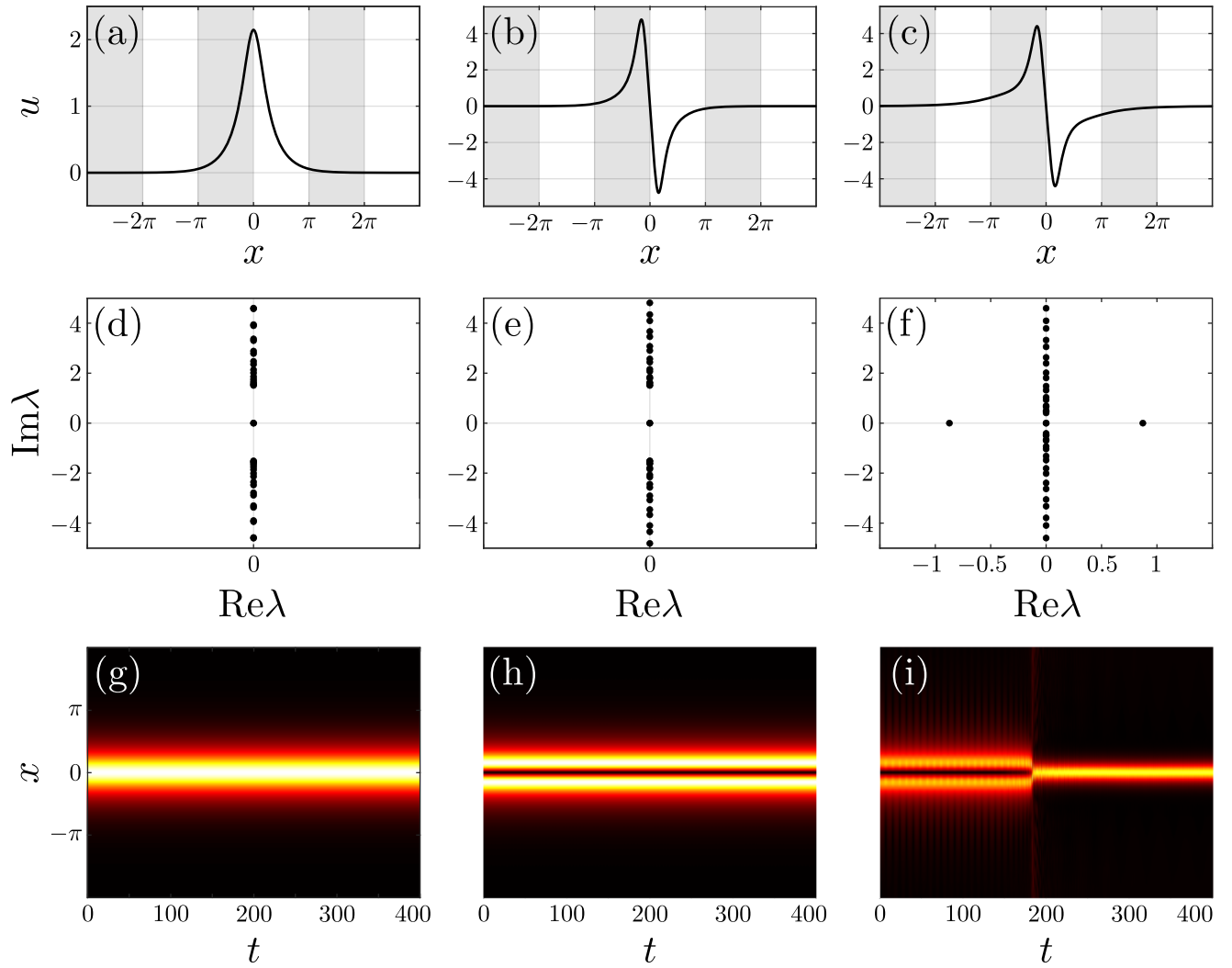


Figure 3.7. Stability of dipole soliton. Panel (a) represent a stable fundamental soliton (FS) for parameters $(\omega, \alpha) = (1.5, 0)$. Panel (b) corresponds to stable dipole soliton (DS) for $(\omega, \alpha) = (1.5, 0)$. Unstable DS is presented in panel (c) for parameters $(\omega, \alpha) = (0.4, 0)$. It's exponentially unstable and during our simulation at $t \approx 200$ transforms into a stable fundamental soliton.

potheses I and II, which allow to apply Theorem 1, and concluded that there exist a homeomorphism between a subset of bounded solutions and bi-infinite symbolic sequences from some alphabet. Existence of the homeomorphism reveal the complex nature of stationary solutions. Like we saw it in Chapter 2 presence of periodic pseudopotential that alters its sign along the period generates a great variety of different stationary solutions. We apply linear-stability analysis to identify physically relevant localized solutions among them. Outcome of our analysis is the existence of stable dipole soliton (DS) family previously not considered in this setting. Results of our finding were published in [16].

Chapter 4

• • •

Appendix A

Lemma on Bounded Solutions

Lemma (On bounded solutions). *Let $f(t, z)$ be a function that is continuous with respect to t and continuously differentiable with respect to z . Let $f(t, z)$ is defined for $t \geq t_0$, $|z| < +\infty$, and have the following properties:*

- (i) *for $|z| < \rho$, $\rho > 0$, the estimate $|f(t, z)| < \eta_\rho(t)|z|$ is valid, where $\eta_\rho(t) \in L_1(t_0; +\infty)$;*
- (ii) *for all z_1, z_2 such that $|z_{1,2}| < \rho$, $\rho > 0$, there exists function $\tilde{\eta}_\rho(t) \in L_1(t_0; +\infty)$, such that $|f(t, z_2) - f(t, z_1)| \leq \tilde{\eta}_\rho(t)|z_2 - z_1|$;*
- (iii) *for $|z| < \rho$, $\rho > 0$, the estimate $|f_z(t, z)| < \theta_\rho(t)|z|$ is valid, where $\theta_\rho \in L_1(t_0, +\infty)$;*
- (iv) *for all z_1, z_2 such that $z_{1,2} < \rho$, $\rho > 0$, there exists function $\tilde{\theta}_\rho \in L_1(t_0; +\infty)$, such that $|f_z(t, z_2) - f_z(t, z_1)| \leq \tilde{\theta}_\rho|z_2 - z_1|$.*

Then for the equation

$$z_{tt} - \alpha z_t + f(t, z) = 0, \quad \alpha > 0 \quad (\text{A.1})$$

the following statements are valid:

- (A) *for each solution $z(t)$ of the equation (A.1) that is bounded when $t \rightarrow +\infty$ there exists $C \in \mathbb{R}$ such that $z(t) \rightarrow C$ as $t \rightarrow +\infty$;*
- (B) *for each $C \in \mathbb{R}$ there exists unique solution $Z(t, C)$ of the equation (A.1), defined on a segment $(t_C; +\infty)$, such that*

$$Z(t, C) = C + o(1), \quad t \rightarrow +\infty; \quad (\text{A.2})$$

- (C) *family of solutions $Z(t, C)$ is C^1 -smooth with respect to the parameter C .*

Proof. Let us prove the statement (A) first. With the method of variation of parameters one can find that a solution of the equation (A.1) satisfies the equality:

$$z(t) = \varkappa_1 + \varkappa_2 e^{\alpha t} + \int_{t_0}^t e^{\alpha \eta} \left(\int_{\eta}^{+\infty} e^{-\alpha \xi} f(\xi, z(\xi)) d\xi \right) d\eta. \quad (\text{A.3})$$

It follows from the condition (i) that if $z(t)$ is bounded while $t \rightarrow +\infty$ then the integral

$$\int_{t_0}^{+\infty} e^{\alpha \eta} \left(\int_{\eta}^{+\infty} e^{-\alpha \xi} f(\xi, z(\xi)) d\xi \right) d\eta \quad (\text{A.4})$$

converges. Furthermore for all bounded solutions $\varkappa_2 = 0$, hence $z(t)$ tends to some constant for $t \rightarrow +\infty$. That proves the point (A).

Move on to the point (B). We make a variable change $u(t) = z(t) - C$, where C is an arbitrary number. Rewrite the equation (A.1) in the form of a system of equations

$$y_t = Ay + F(t, y), \quad (\text{A.5})$$

where

$$y = \begin{pmatrix} u \\ v \end{pmatrix}, \quad A = \begin{pmatrix} 0 & 1 \\ 0 & \alpha \end{pmatrix}, \quad F(t, y) = \begin{pmatrix} 0 \\ f(t, u + C) \end{pmatrix}.$$

Now we apply Theorem 9.1 from [23, Chapter XII] to the system (A.5). It states that the system (A.5) *has a solution which tends to zero at infinity* if the following conditions are satisfied:

- (1) function $F(t, y)$ is continuous and $\|F(t, y)\| \leq \lambda(t)$ for $t \in [t_0; +\infty)$, $\|y\| \leq \rho$, where $\lambda(t) \in L_1(t_0; +\infty)$;
- (2) for all $g(t) = \text{col}(g_1(t), g_2(t))$, $g(t) \in L_1(t_0; +\infty)$ there exists a solution $y(t) \in L_0^\infty(t_0; +\infty)$ of the inhomogeneous system

$$y_t = Ay + g(t); \quad (\text{A.6})$$

(hereinafter by the norm $\|\cdot\|$ we mean the Euclidean norm in \mathbb{R}).

At first, by the condition (i) if $|u| \leq \rho$ and $t > t_0$ relation $\|f(t, u, C)\| \leq \rho\eta_\rho(t)$ takes place, moreover $\eta_\rho \in L_1(t_0; +\infty)$, hence the condition (1) of the above-mentioned theorem is satisfied. At second, general solution of the inhomogeneous system of equations (A.6) can be written as:

$$u(t) = C_2 + \int_{t_0}^t \left(g_1(\eta) + e^{\alpha\eta} \left(C_1 - \int_{+\infty}^\eta e^{-\alpha\xi} g_2(\xi) d\xi \right) \right) d\eta; \quad (\text{A.7})$$

$$v(t) = u_t(t) - g_1(t). \quad (\text{A.8})$$

Since $g_{1,2}(t) \in L_1(t_0; +\infty)$ one can choose appropriate parameters C_1, C_2 in order to get a solution which tends to zero while $t \rightarrow +\infty$, so the condition (2) of the theorem is also met. Thereby both of the conditions for the applied theorem take place for the system (A.5). That implies existence of a solution $z(t)$ of (A.1) that approaches a given constant C while $t \rightarrow +\infty$ for all C .

Now we prove the uniqueness of such solution. Suppose that for the same C there exist two solutions $u_{1,2}(t)$ for equation

$$u_{tt} - \alpha u_t + f(t, u + C) = 0. \quad (\text{A.9})$$

Consider their difference $\Delta(t) = u_2(t) - u_1(t)$, it satisfies the equation

$$\Delta_{tt} - \alpha \Delta_t + R(t) \Delta = 0, \quad (\text{A.10})$$

and a boundary condition $\Delta \rightarrow 0$ as $t \rightarrow +\infty$ takes place. Here

$$R(t) \equiv \frac{f(t, u_2(t) + C) - f(t, u_1(t) + C)}{u_2(t) - u_1(t)}. \quad (\text{A.11})$$

By the condition (ii) we can apply Theorem 11 from [24, Chapter 3]. It states that there exists a homeomorphism between the bounded solutions of the equation (A.10) and solutions of equation

$$\Delta_{tt} - \alpha \Delta_t = 0, \quad (\text{A.12})$$

moreover (see a note to that theorem in [24]) this homeomorphism is a linear map. It means that only a zero solution of (A.10) satisfies the zero asymptotic at infinity,

i.e. $u_2(t) \equiv u_1(t)$. Thus we have proven the existence of the solutions family $Z(t, C)$ parametrised by $C \in \mathbb{R}$, statement (B) is proven.

To prove the statement (C) one can note that the derivative

$$\frac{\partial Z}{\partial C}(t, C) \equiv \Theta(t, C) \quad (\text{A.13})$$

satisfies the equation (A.9) after differentiation with respect to C , moreover $\Theta(t, C) \rightarrow 0$ as $t \rightarrow +\infty$. We have

$$\Theta_{tt} - \alpha \Theta_t + f_z(t, u + C)\Theta + f_z(t, u + C) = 0. \quad (\text{A.14})$$

Here we can use Theorem 11 from [24, Chapter 3] again, and using the condition (iii) we can conclude that there exists a solution of this equation $\Theta(t, C)$ such that $\Theta(t, C) \rightarrow 0$ as $t \rightarrow +\infty$, and function $\Theta(t, C)$ is continuous with respect to the parameter C . That proves the overall lemma. \square

Appendix B

Solutions of Duffing equations

Appendix C

Strips Mapping Theorems

Theorem 2 (On h-strips mapping). *Let Poincaré map \mathcal{P} and its inverse \mathcal{P}^{-1} are defined on a complete (see Definition 8) island set $\bigcup_{i \in S} D_i$, where S is a finite or countable set of indices. Let for all $i, j \in S$ set $V_{ij} = \mathcal{P}^{-1}(D_j) \cap D_i$ is non-empty, \mathcal{P} is defined on a closure $\overline{V_{ij}}$, and one of the following two conditions is met:*

(1) *borders α_i^\pm of an island D_i are increasing curves, $\forall \mathbf{p} \in \overline{V_{ij}}$ signs of values $\{a_{mn}\}$ in the matrix of the linear operator $D\mathcal{P}_{\mathbf{p}} = (a_{mn})$ have exactly one of the following configurations^{*}:*

$$(a) (+ +), \quad (b) (- -), \quad (c) (+ +), \quad (d) (- -);$$

and at the same time borders α_j^\pm of D_j are increasing curves for cases (a), (b), and decreasing curves for (c), (d);

(2) *borders α_i^\pm of an island D_i are decreasing curves, $\forall \mathbf{p} \in \overline{V_{ij}}$ signs of values $\{a_{mn}\}$ in the matrix of the linear operator $D\mathcal{P}_{\mathbf{p}} = (a_{mn})$ have exactly one of the following configurations:*

$$(a) (+ -), \quad (b) (- +), \quad (c) (+ -), \quad (d) (- +);$$

and at the same time borders α_j^\pm of D_j are decreasing curves for cases (a), (b), and increasing for (c), (d);

and moreover $\exists \mu > 1$ such that $\forall p \in \overline{V_{ij}}, |a_{11}| \geq \mu$, then for any h-strip $H \in D_i$, $\mathcal{P}(H) \cap D_j = \tilde{H}_j$ is also an h-strip, and $d_h(\tilde{H}_j) \leq (1/\mu)d_h(H)$ (here $d_h(\cdot)$ is an h-strip thickness in a sence of Definition 9).

*By “+” and “-” sign we mean strict inequalities $a_{mn} > 0, a_{mn} < 0$ to be held.

Proof. Let's fix indices i, j and prove the theorem for a pair of islands D_i, D_j . Mostly we consider the case (1a). Other cases The rest of the cases must be treated in a completely analogous way. Denote by $\mathbf{e}_1, \mathbf{e}_2$ basis vectors

$$\mathbf{e}_1 = \begin{pmatrix} 1 \\ 0 \end{pmatrix}; \quad \mathbf{e}_2 = \begin{pmatrix} 0 \\ 1 \end{pmatrix}. \quad (\text{C.1})$$

Define the following set of *cones*:

$$\begin{aligned} \mathbb{R}_{++}^2 &= \{\mathbf{v} \mid \mathbf{v} = x\mathbf{e}_1 + y\mathbf{e}_2, x > 0, y > 0\}; \\ \overline{\mathbb{R}}_{++}^2 &= \{\mathbf{v} \mid \mathbf{v} = x\mathbf{e}_1 + y\mathbf{e}_2, x \geq 0, y \geq 0\}; \\ \mathbb{R}_{+-}^2 &= \{\mathbf{v} \mid \mathbf{v} = x\mathbf{e}_1 + y\mathbf{e}_2, x > 0, y < 0\}; \\ \overline{\mathbb{R}}_{+-}^2 &= \{\mathbf{v} \mid \mathbf{v} = x\mathbf{e}_1 + y\mathbf{e}_2, x \geq 0, y \leq 0\}; \\ \mathbb{R}_{-+}^2 &= \{\mathbf{v} \mid \mathbf{v} = x\mathbf{e}_1 + y\mathbf{e}_2, x < 0, y > 0\}; \\ \overline{\mathbb{R}}_{-+}^2 &= \{\mathbf{v} \mid \mathbf{v} = x\mathbf{e}_1 + y\mathbf{e}_2, x \leq 0, y \geq 0\}; \\ \mathbb{R}_{--}^2 &= \{\mathbf{v} \mid \mathbf{v} = x\mathbf{e}_1 + y\mathbf{e}_2, x < 0, y < 0\}; \\ \overline{\mathbb{R}}_{--}^2 &= \{\mathbf{v} \mid \mathbf{v} = x\mathbf{e}_1 + y\mathbf{e}_2, x \leq 0, y \leq 0\}. \end{aligned}$$

As a first step in the proof, we show that values signs in the matrix of linear operator $D\mathcal{P}_{\mathbf{p}} = (a_{mn})$ uniquely determine the structure of cones mapping in each point \mathbf{p} of the set $\overline{V_{ij}}$. For the case (a) we have:

$$\forall \mathbf{v} = \begin{pmatrix} x \\ y \end{pmatrix} \in \overline{\mathbb{R}}_{++}^2, \quad D\mathcal{P}_{\mathbf{p}}(\mathbf{v}) = \begin{pmatrix} a_{11} & a_{12} \\ a_{21} & a_{22} \end{pmatrix} \begin{pmatrix} x \\ y \end{pmatrix} = \begin{pmatrix} \tilde{x} > 0 \\ \tilde{y} > 0 \end{pmatrix} \in \mathbb{R}_{++}^2.$$

It is easy to check that the complete scheme of the cones mapping for the case (1) of the theorem looks as follows:

- (a) $D\mathcal{P}_{\mathbf{p}}(\overline{\mathbb{R}}_{++}^2) \in \mathbb{R}_{++}^2, \quad D\mathcal{P}_{\mathbf{p}}(\overline{\mathbb{R}}_{--}^2) \in \mathbb{R}_{--}^2;$
- (b) $D\mathcal{P}_{\mathbf{p}}(\overline{\mathbb{R}}_{++}^2) \in \mathbb{R}_{--}^2, \quad D\mathcal{P}_{\mathbf{p}}(\overline{\mathbb{R}}_{--}^2) \in \mathbb{R}_{++}^2;$
- (c) $D\mathcal{P}_{\mathbf{p}}(\overline{\mathbb{R}}_{+-}^2) \in \mathbb{R}_{+-}^2, \quad D\mathcal{P}_{\mathbf{p}}(\overline{\mathbb{R}}_{-+}^2) \in \mathbb{R}_{-+}^2;$
- (d) $D\mathcal{P}_{\mathbf{p}}(\overline{\mathbb{R}}_{+-}^2) \in \mathbb{R}_{-+}^2, \quad D\mathcal{P}_{\mathbf{p}}(\overline{\mathbb{R}}_{-+}^2) \in \mathbb{R}_{+-}^2.$

Complete scheme for the case (2) have the following form correspondingly:

- (a) $D\mathcal{P}_{\mathbf{p}}(\bar{\mathbb{R}}_{-+}^2) \in \mathbb{R}_{-+}^2, D\mathcal{P}_{\mathbf{p}}(\bar{\mathbb{R}}_{+-}^2) \in \mathbb{R}_{+-}^2;$
- (b) $D\mathcal{P}_{\mathbf{p}}(\bar{\mathbb{R}}_{-+}^2) \in \mathbb{R}_{+-}^2, D\mathcal{P}_{\mathbf{p}}(\bar{\mathbb{R}}_{+-}^2) \in \mathbb{R}_{-+}^2;$
- (c) $D\mathcal{P}_{\mathbf{p}}(\bar{\mathbb{R}}_{--}^2) \in \mathbb{R}_{--}^2, D\mathcal{P}_{\mathbf{p}}(\bar{\mathbb{R}}_{++}^2) \in \mathbb{R}_{++}^2;$
- (d) $D\mathcal{P}_{\mathbf{p}}(\bar{\mathbb{R}}_{-+}^2) \in \mathbb{R}_{++}^2, D\mathcal{P}_{\mathbf{p}}(\bar{\mathbb{R}}_{+-}^2) \in \mathbb{R}_{--}^2.$

As a second step we show that such cones mapping preserve in some way Lipschitz constraints and monotonicity properties for curves from $\overline{V_{ij}}$ under the \mathcal{P} mapping. Show that for the case (1a). For that first of all we note that from compactness of $\overline{V_{ij}}$ the existence of the following supremum follows:

$$\tilde{\gamma}_{ij} = \sup \frac{y}{x}, \begin{pmatrix} x \\ y \end{pmatrix} = D\mathcal{P}_{\mathbf{p}}(\mathbf{v}), \mathbf{p} \in \overline{V_{ij}}, \mathbf{v} \in \bar{\mathbb{R}}_{++}^2.$$

Further, let there be two tow different points $\mathbf{p}_1, \mathbf{p}_2 \in \overline{V_{ij}}$, $\mathbf{p}_1 = (\psi_1, \psi'_1)$, $\mathbf{p}_2 = (\psi_2, \psi'_2)$, and besides $\psi_2 \geq \psi_1$, $\psi'_2 \geq \psi'_1$. Let points $\mathbf{q}_1, \mathbf{q}_2$ be the \mathcal{P} -images of the points $\mathbf{p}_1, \mathbf{p}_2$ correspondingly, $\mathcal{P}(\mathbf{p}_1) = \mathbf{q}_1 = (\phi_1, \phi'_1)$, $\mathcal{P}(\mathbf{p}_2) = \mathbf{q}_2 = (\phi_2, \phi'_2)$. Let $D\mathcal{P}_{\mathbf{p}_1}$ is a linearization of \mathcal{P} at the point \mathbf{p}_1 . Then the following expansion is valid:

$$\mathbf{q}_2 = \mathcal{P}(\mathbf{p}_2) = \mathbf{q}_1 + D\mathcal{P}_{\mathbf{p}_1}(\mathbf{p}_2 - \mathbf{p}_1) + r(||\mathbf{p}_2 - \mathbf{p}_1||), \quad (\text{C.2})$$

where $r(||\mathbf{p}_2 - \mathbf{p}_1||)/||\mathbf{p}_2 - \mathbf{p}_1|| \rightarrow 0$ as $||\mathbf{p}_2 - \mathbf{p}_1|| \rightarrow 0$ (here $||\cdot||$ is a Euclidean norm). Vector $\mathbf{p}_\Delta = \mathbf{p}_2 - \mathbf{p}_1 \in \bar{\mathbb{R}}_{++}^2$ which means that for its mapping by linearized operator we have $D\mathcal{P}_{\mathbf{p}_1}(\mathbf{p}_\Delta) = \mathbf{q}_\Delta \in \mathbb{R}_{++}^2$, and

$$\mathbf{q}_2 - \mathbf{q}_1 = \mathbf{q}_\Delta + r(||\mathbf{p}_2 - \mathbf{p}_1||). \quad (\text{C.3})$$

Expression above means that for “close enough” points $\mathbf{p}_1, \mathbf{p}_2$ their images satisfy the relationship $\mathbf{q}_2 - \mathbf{q}_1 \in \mathbb{R}_{++}^2$, i.e. $\phi_2 > \phi_1$, $\phi'_2 > \phi'_1$. Moreover one can choose a value $\gamma_{ij} > \widetilde{\gamma}_{ij}$ such that the following inequality is held:

$$0 < \phi'_2 - \phi'_1 < \gamma_{ij}(\phi_2 - \phi_1). \quad (\text{C.4})$$

This ordering is transitive, i.e. from the relation (C.4) and the second analogous relation for “close enough” point \mathbf{p}_2 , \mathbf{p}_3 ,

$$0 < \phi'_3 - \phi'_2 < \gamma_{ij}(\phi_3 - \phi_2), \quad (\text{C.5})$$

follow the analogous relation for the points \mathbf{p}_1 , \mathbf{p}_3 as well. That allows to spread the relation (C.4) over all points \mathbf{p}_1 , $\mathbf{p}_2 \in \overline{V_{ij}}$ that satisfies the conditions $\psi_2 \geq \psi_1$, $\psi'_2 \geq \psi'_1$. Other cases (1b)-(1d), (2a)-(2d) can be considered in a similar way.

Thus for the case (1) for all points \mathbf{p}_1 , $\mathbf{p}_2 \in \overline{V_{ij}}$, which coordinates satisfy the relations $\psi_2 \geq \psi_1$, $\psi'_2 \geq \psi'_1$, coordinates of their \mathcal{P} -images $\mathbf{q}_1 = (\phi_1, \phi'_1)$, $\mathbf{q}_2 = (\phi_2, \phi'_2)$ depending on signs of values in matrix of $D\mathcal{P}_{\mathbf{p}}$, $\mathbf{p} \in \overline{V_{ij}}$, met exactly one of the following inequalities ($\exists \gamma_{ij}$):

$$(a) \quad 0 < \phi'_2 - \phi'_1 < \gamma_{ij}(\phi_2 - \phi_1); \quad (\text{C.6a})$$

$$(b) \quad 0 < \phi'_1 - \phi'_2 < \gamma_{ij}(\phi_1 - \phi_2); \quad (\text{C.6b})$$

$$(c) \quad 0 < \phi'_1 - \phi'_2 < \gamma_{ij}(\phi_2 - \phi_1); \quad (\text{C.6c})$$

$$(d) \quad 0 < \phi'_2 - \phi'_1 < \gamma_{ij}(\phi_1 - \phi_2). \quad (\text{C.6d})$$

For the case (2) in its turn we have that for all points \mathbf{p}_1 , $\mathbf{p}_2 \in \overline{V_{ij}}$, which coordinates satisfy the relations $\psi_2 \leq \psi_1$, $\psi'_2 \geq \psi'_1$, exactly one of the following inequalities is met:

$$(a) \quad 0 < \phi'_2 - \phi'_1 < \gamma_{ij}(\phi_1 - \phi_2); \quad (\text{C.7a})$$

$$(b) \quad 0 < \phi'_1 - \phi'_2 < \gamma_{ij}(\phi_2 - \phi_1); \quad (\text{C.7b})$$

$$(c) \quad 0 < \phi'_1 - \phi'_2 < \gamma_{ij}(\phi_1 - \phi_2); \quad (\text{C.7c})$$

$$(d) \quad 0 < \phi'_2 - \phi'_1 < \gamma_{ij}(\phi_2 - \phi_1). \quad (\text{C.7d})$$

A third step we demonstrate how these inequalities above allow to conclude that for any h-strip $H \in D_i$ its image $\mathcal{P}H \cap D_j = \tilde{H}_j$ is also an h-strip. Let an h-strip $H \in D_i$ is placed between two monotonic h-curves $\tilde{\alpha}_i^\pm$. Endpoints of the $\tilde{\alpha}_i^\pm$ belong to the boundaries β_i^\pm of island D_i , so the H is a curvilinear quadrangle

bounded by curves $\tilde{\alpha}_i^\pm$ and segments of curves β_i^\pm . For the case (1a) of the theorem curves $\tilde{\alpha}_i^\pm$ are increasing. Let's consider an image of the curve $\tilde{\alpha}_i^+$. According to the definition of a complete island set $\mathcal{P}(\tilde{\alpha}_i^+)$ cross each of the boundaries β_j^\pm of island D_j at least once. At the same time $\mathcal{P}(\tilde{\alpha}_i^+)$ cannot cross boundaries α_j^\pm because they consist of points which tends to infinity under action of \mathcal{P}^{-1} .

Let $\mathcal{P}(\tilde{\alpha}_i^+)$ cross one of the boundaries β_j^\pm of the island D_j twice. Denote those intersection points by $\mathbf{q}_1 = \mathcal{P}(\mathbf{p}_1)$, $\mathbf{q}_2 = \mathcal{P}(\mathbf{p}_2)$. For the case (1a) boundaries α_j^\pm are increasing curves, and β_j^\pm are decreasing, hence the points \mathbf{q}_1 , \mathbf{q}_2 belong to a decreasing curve. From the other side points $\mathbf{p}_1, \mathbf{p}_2 \in \overline{V_{ij}}$ belong to increasing curve $\tilde{\alpha}_i^+$, and hence for their \mathcal{P} -image coordinates $\mathbf{q}_1 = (\phi_1, \phi'_1)$, $\mathbf{q}_2 = (\phi_2, \phi'_2)$ inequality (C.6a) must be held. This inequality means that points \mathbf{q}_1 , \mathbf{q}_2 cannot belong to a decreasing curve, and $\mathcal{P}(\tilde{\alpha}_i^+)$ cross each boundary β_j^\pm only once. Similar statement is valid also for the $\mathcal{P}(\tilde{\alpha}_i^-)$. Thereby $\mathcal{P}(\tilde{\alpha}_i^\pm) \cap D_j$ are monotonic curves. Their type of monotonicity coincide with the monotonicity type of corresponding boundaries of the island D_j , moreover these curves bound the set $\mathcal{P}H \cap D_j$, hence $\mathcal{P}H \cap D_j = \tilde{H}_j$ is an h-strip. Other cases can be considered in a similar way using the corresponding inequalities (C.6b) – (C.6d), (C.7a) – (C.7d).

Finally, in a fourth step of this proof we show that under the introduced constrain on $|a_{11}|$ value of linearized operator, for all h-strip $H \in D_i$, $\rho(\tilde{H}_j) \leq \mu\rho(H)$, so that thickness of an h-strip \mathcal{P} -image within island D_j is less than thickness of an original h-strip inside island D_i . To prove that first assume that h-strips H and \tilde{H}_j are well-measured in a sense on Definition 10. Let the thickness of the h-strip \tilde{H}_j can be measured along the vertical curve connecting points $\mathbf{q}_1 = (\phi_1, \phi'_1)$, $\mathbf{q}_2 = (\phi_2, \phi'_2)$, $\phi'_1 < \phi'_2$. Consider a parametrization of that curve $\mathbf{q}(t) = (0, \phi'(t))$, where

$$\phi'(t) = t\phi'_2 + (1-t)\phi'_1, \quad 0 \leq t \leq 1. \quad (\text{C.8})$$

Strip \tilde{H}_j is well-measurable, so the curve $\mathbf{q}(t)$ entirely belongs to \tilde{H}_j . Since $\tilde{H}_j = \mathcal{P}H \cap D_j$ there exists a pre-image $\mathbf{p}(t) = \mathcal{P}^{-1}(\mathbf{q}(t)) = (\psi(t), \psi'(t))$, $\mathbf{p}(t) \subset H$ and $\mathbf{q}(t) = \mathcal{P}(\mathbf{p}(t))$. For the case (1a) let's demonstrate that $\mathbf{p}(t)$ is a decreasing curve

connecting point from the opposite boundaries $\tilde{\alpha}_i^\pm$ of the strip H inside D_i . Remark, here by “decreasing” we mean that the curve is a graph of decreasing function in (u, u') coordinates, not as a function of t . The curve $\mathbf{q}(t)$ belongs to some set which is a \mathcal{P} -image of a part of the set $\overline{V_{ij}}$. The signs of values in the matrix of $D\mathcal{P}_{\mathbf{p}}$, $\mathbf{p} \in \overline{V_{ij}}$ have the form $(\begin{smallmatrix} + & + \\ + & + \end{smallmatrix})$, so the signs of values for the linearized inverse map $D\mathcal{P}_{\mathbf{q}}^{-1}$ have a configuration $(\begin{smallmatrix} + & - \\ - & + \end{smallmatrix})$ on the curve $\mathbf{q}(t)$. This allows to conclude the corresponding cones mapping:

$$D\mathcal{P}_{\mathbf{q}(t)}^{-1}(\overline{\mathbb{R}}_{-+}^2) \in \mathbb{R}_{-+}^2, \quad D\mathcal{P}_{\mathbf{q}(t)}^{-1}(\overline{\mathbb{R}}_{+-}^2) \in \mathbb{R}_{+-}^2. \quad (\text{C.9})$$

Therefore the corresponding monotonicity property (C.7a) takes place. It immediately follows from (C.7a) that the vertical curve $\mathbf{q}(t)$ is mapped to the decreasing curve $\mathbf{p}(t)$ (decreasing in (u, u') coordinates). Moreover the inequality $\phi'_1 < \phi'_2$ provides that $\psi'(t) > 0$.

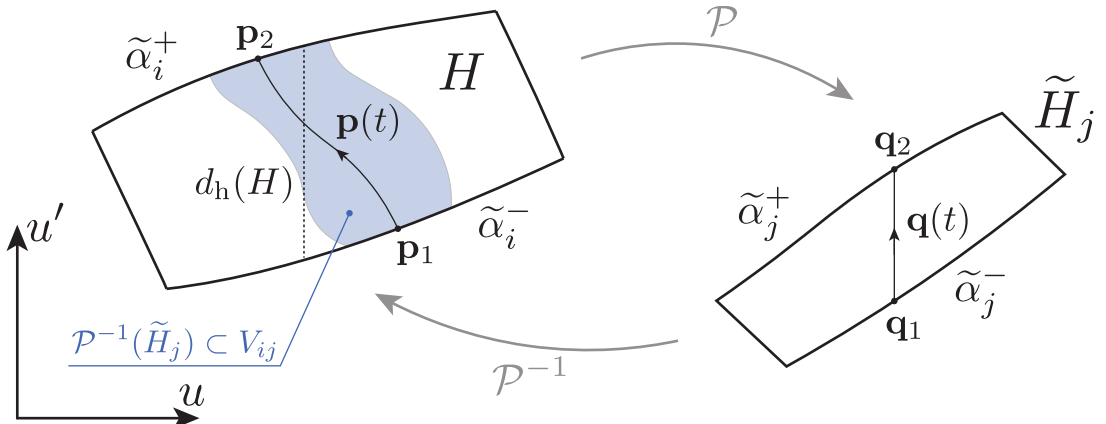


Figure C.1. Illustration for the proof of the h-strips thickness decrease for the case when both h-strips H and \tilde{H}_j are well-measurable. Thickness of H is measured along the vertical dotted line, thickness of \tilde{H}_j is measured along the vertical line $\mathbf{q}(t)$. Arrows indicate curves traverse directions while t changes from 0 to 1. Pre-image of \tilde{H}_j strip is colored with gray.

Consider tangent vectors to $\mathbf{p}(t)$ and $\mathbf{q}(t)$ (upper dot means the derivative with respect to t):

$$\dot{\mathbf{p}}(t) = (\dot{\psi}(t), \dot{\psi}'(t)); \quad (\text{C.10})$$

$$\dot{\mathbf{q}}(t) = (0, \dot{\phi}'(t)). \quad (\text{C.11})$$

In each point t they are connected by the $D\mathcal{P}_{\mathbf{p}(t)}$ operator

$$\dot{\mathbf{q}}(t) = D\mathcal{P}_{\mathbf{p}(t)}(\dot{\mathbf{p}}(t)). \quad (\text{C.12})$$

Rewrite this relation in a matrix form:

$$\begin{pmatrix} a_{11}(t) & a_{12}(t) \\ a_{21}(t) & a_{22}(t) \end{pmatrix} \begin{pmatrix} \dot{\psi}(t) \\ \dot{\psi}'(t) \end{pmatrix} = \begin{pmatrix} 0 \\ \dot{\phi}'(t) \end{pmatrix}. \quad (\text{C.13})$$

We take into account that matrix (a_{mn}) is a linearization of Poincaré map to conclude that its determinant $a_{11}(t)a_{22}(t) - a_{12}(t)a_{21}(t) = 1$ in each point t . From the relations above and the theorem condition on values of $a_{11}(t)$ follows

$$\dot{\phi}'(t) = \frac{1}{a_{11}(t)}\dot{\psi}'(t) \leq \frac{1}{\mu}\dot{\psi}'(t). \quad (\text{C.14})$$

Integration of (C.14) with limits $0 \leq t \leq 1$ gives:

$$d_h(\tilde{H}_j) = \phi'_2 - \phi'_1 = \int_0^1 \dot{\phi}'(t)dt \leq \frac{1}{\mu} \int_0^1 \dot{\psi}'(t)dt = \frac{1}{\mu}(\psi'_2 - \psi'_1). \quad (\text{C.15})$$

Curve $\mathbf{p}(t)$ is decreasing and boundaries of H are increasing curves, so it follows from general geometric considerations that $\psi'_2 - \psi'_1 \leq d_h(H)$, i.e. $d_h(\tilde{H}_j) \leq (1/\mu)d_h(H)$. That gives the final statement of the theorem for well-measurable strips.

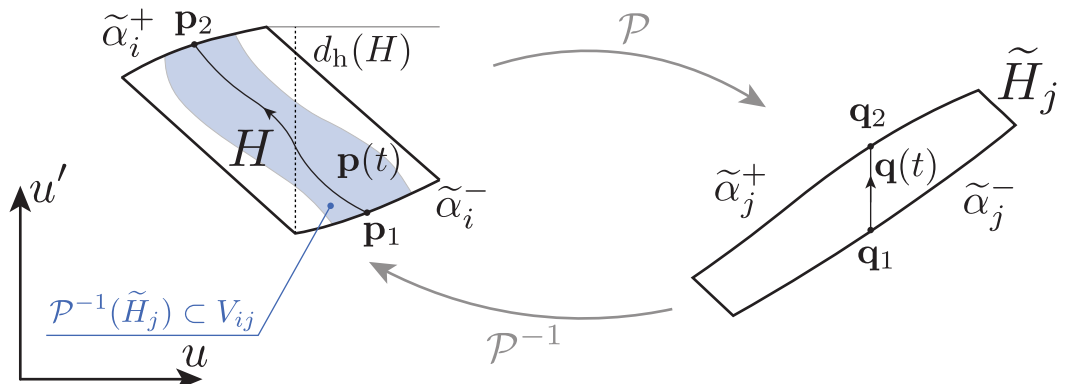


Figure C.2. Illustration for the proof of the h-strips thickness decrease for the case when strip H is not well-measurable. Its thickness is measured along the vertical dotted line. One endpoint of that line does not belong to the strip boundary $\tilde{\alpha}_i^+$. Pre-image of \tilde{H}_j strip is colored with gray.

The proof above can be easily generalized to the cases when h-strips H and \tilde{H}_j are not well-measurable. If strip H is not well-measurable, the inequality $\psi'_2 - \psi'_1 \leq$

$d_h(H)$ in (C.15) takes place anyway. This fact is illustrated on Figure C.2. Vertical distance between points $\mathbf{p}_1, \mathbf{p}_2$ turns out to be certainly less than the width of H strip.

In the case when h-strip \tilde{H}_j is not well-measurable, one should choose corner points $\mathbf{q}_1, \mathbf{q}_2$ in a such way that the vertical distance between them equals the thickness of \tilde{H}_j , and then connect $\mathbf{q}_1, \mathbf{q}_2$ with a monotonic decreasing curve $\mathbf{q}(t)$, see Fig. C.3. This is always possible due to the geometric properties of not well-measurable h-strip. According to the choice of points $\mathbf{q}_1, \mathbf{q}_2$, $d_h(\tilde{H}_j) = \phi_2 - \phi_1$, and all the steps above remain valid since the corresponding cones mapping with all the consequences can be also applied for the decreasing curves $\mathbf{p}(t)$ and $\mathbf{q}(t)$.

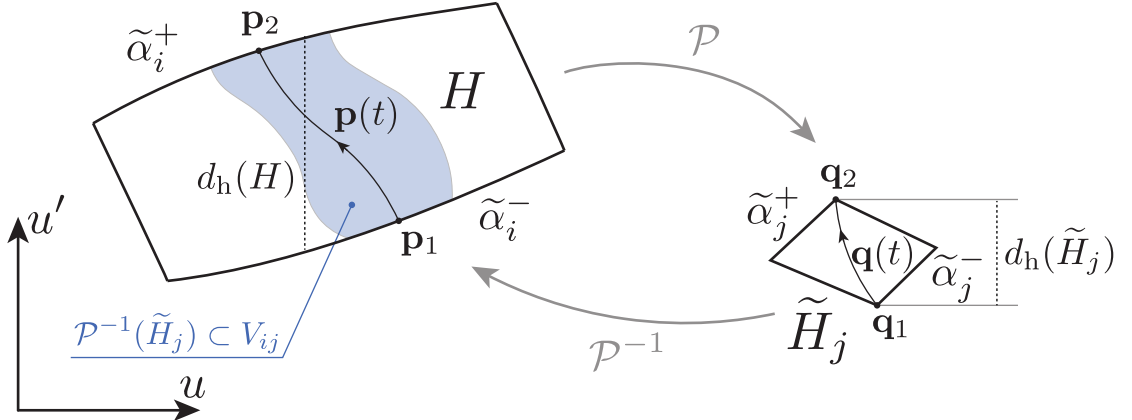


Figure C.3. Illustration for the proof of the h-strips thickness decrease for the case when strip \tilde{H}_j is not well-measurable. Thickness of H and \tilde{H}_j are measured along the dotted lines. Pre-image of \tilde{H}_j strip is colored with gray.

If both h-strips H and \tilde{H}_j are not well-measurable then two above mentioned technics should be combined together. During the consideration of all other cases of the theorem only type of curves monotonicity is changed, but the overall approach remains the same and can be applied with just minor adjustments. Theorem is proven. \square

Theorem 3 (On v-strips mapping). *Let Poincaré map \mathcal{P} and its inverse \mathcal{P}^{-1} are defined on a complete (see Definition 8) island set $\bigcup_{i \in S} D_i$, where S is a finite or countable set of indices. Let for all $i, j \in S$ set $H_{ij} = \mathcal{P}(D_i) \cap D_j$ is non-empty, \mathcal{P}^{-1} is defined on a closure $\overline{H_{ij}}$, and one of the following two conditions is met:*

(1) *borders β_j^\pm of an island D_j are increasing curves, $\forall \mathbf{q} \in \overline{H_{ij}}$ signs of values $\{b_{mn}\}$ in the matrix of the linear operator $D\mathcal{P}_{\mathbf{q}}^{-1} = (b_{mn})$ have exactly one of the following configurations:*

$$(a) (+ +), \quad (b) (- -), \quad (c) (+ -), \quad (d) (- +);$$

and at the same time borders β_i^\pm of D_i are increasing curves for cases (a), (b), and decreasing curves for (c), (d);

(2) *borders β_j^\pm of an island D_j are decreasing curves, $\forall \mathbf{q} \in \overline{H_{ij}}$ signs of values $\{b_{mn}\}$ in the matrix of the linear operator $D\mathcal{P}_{\mathbf{q}}^{-1} = (b_{mn})$ have exactly one of the following configurations:*

$$(a) (+ -), \quad (b) (- +), \quad (c) (+ -), \quad (d) (- +);$$

and at the same time borders β_i^\pm of D_i are decreasing curves for cases (a), (b), and increasing for (c), (d);

and moreover $\exists \nu > 1$ such that $\forall q \in \overline{H_{ij}}, |b_{22}| \geq \nu$, then for any v-strip $V \in D_j$, $\mathcal{P}^{-1}(V) \cap D_i = \tilde{V}_i$ is also a v-strip, and $d_v(\tilde{V}_i) \leq (1/\nu)d_v(V)$ (here $d_v(\cdot)$ is an v-strip thickness in a sence of Definition 11).

Proof. Completely analogous to the proof of the h-strips mapping theorem. \square

Bibliography

1. Extreme Tunability of Interactions in a ${}^7\text{Li}$ Bose-Einstein Condensate / S. E. Pollack [et al.] // Phys. Rev. Lett. — 2009. — Mar. — Vol. 102, issue 9. — P. 090402.
2. Feshbach resonances in ultracold gases / C. Chin [et al.] // Rev. Mod. Phys. — 2010. — Apr. — Vol. 82, issue 2. — P. 1225–1286.
3. Combination of a magnetic Feshbach resonance and an optical bound-to-bound transition / D. M. Bauer [et al.] // Phys. Rev. A. — 2009. — June. — Vol. 79, issue 6. — P. 062713.
4. *Hukriede J., Runde D., Kip D.* Fabrication and application of holographic Bragg gratings in lithium niobate channel waveguides. — 01/2003.
5. *Pachpatte B. G.* Inequalities for Differential and Integral Equations. Vol. 197. — Mathematics in Science, Engineering, 1998.
6. *Alfimov G. L., Zezyulin D. A.* Nonlinear modes for the Gross–Pitaevskii equation with periodic potential // Nonlinearity. — 2007. — No. 20. — P. 2075–2092.
7. *Alfimov G. L., Lebedev M. E.* On Regular and Singular Solutions for Equation $u_{xx} + Q(x)u + P(x)u^3$ // Ufa Mathematical Journal. — 2015. — Vol. 7, no. 2. — P. 3–16.
8. *Alfimov G. L., Avramenko A. I.* Coding of nonlinear states for the Gross–Pitaevskii equation with periodic potential // Physica D: Nonlinear Phenomena. — 2013. — Vol. 254. — P. 29–45. — ISSN 0167-2789.
9. *Guckenheimer J., Holmes P.* Nonlinear Oscillations, Dynamical Systems, and Bifurcations of Vector Fields. Vol. 42. — Springer-Verlag New York, 1983. — (Applied Mathematical Sciences).

10. *Alfimov G. L., Kizin P. P., Zezyulin D. A.* Gap solitons for the repulsive Gross-Pitaevskii equation with periodic potential: Coding and method for computation // Discrete & Continuous Dynamical Systems - B. — 2017. — Vol. 22, no. 4. — P. 1207–1229.
11. *Wiggins S.* Introduction To Applied Nonlinear Dynamical Systems And Chaos. Vol. 4. — 2003. — ISBN 0-387-00177-8.
12. *Arnold V. I.* Ordinary Differential Equations. — Springer Berlin Heidelberg, 1992. — (Springer Textbook).
13. Submicron Spatial Modulation of an Interatomic Interaction in a Bose-Einstein Condensate / R. Yamazaki [et al.] // Phys. Rev. Lett. — 2010. — July. — Vol. 105, issue 5. — P. 050405.
14. *Alfimov G. L., Konotop V. V., Salerno M.* Matter solitons in Bose-Einstein condensates with optical lattices // Europhys. Lett. — 2002. — Vol. 58, no. 1. — P. 7–13.
15. *Sakaguchi H., Malomed B. A.* Matter-wave solitons in nonlinear optical lattices // Phys. Rev. E. — 2005. — Oct. — Vol. 72, issue 4. — P. 046610.
16. *Lebedev M. E., Alfimov G. L., Malomed B.* Stable dipole solitons and soliton complexes in the nonlinear Schrödinger equation with periodically modulated nonlinearity // Chaos. — 2016. — Vol. 26. — P. 073110.
17. *Mayteevarunyoo T., Malomed B. A.* Stability limits for gap solitons in a Bose-Einstein condensate trapped in a time-modulated optical lattice // Phys. Rev. A. — 2006. — Sept. — Vol. 74, issue 3. — P. 033616.
18. *Wang D. L., Yan X. H., Liu W. M.* Localized gap-soliton trains of Bose-Einstein condensates in an optical lattice // Phys. Rev. E. — 2008. — Aug. — Vol. 78, issue 2. — P. 026606.

19. Matter-wave vortices and solitons in anisotropic optical lattices / T. Mayteevarunyoo [et al.] // Physica D: Nonlinear Phenomena. — 2009. — Vol. 238. — P. 1439–1448.
20. Solitons in quasi-one-dimensional Bose-Einstein condensates with competing dipolar and local interactions / J. Cuevas [et al.] // Phys. Rev. A. — 2009. — May. — Vol. 79, issue 5. — P. 053608.
21. Yang J. Nonlinear Waves in Integrable and Nonintegrable Systems. Vol. 16. — SIAM, 2010. — (Mathematical modeling and computation).
22. Trofimov V., Peskov N. Comparison of finite-difference schemes for the Gross-Pitaevskii equation // Mathematical Modelling and Analysis. — 2009. — Mar. — Vol. 14. — P. 109–126.
23. Hartman P. Ordinary Differential Equations. — New York: John Wiley, Sons, 1964.
24. Coppel W. A. Stability and Asymptotic Behaviour of Differential Equations. — Boston: Heath, Co., 1965.